Uncovering pathogenesis of the DNAJ-PKAc fusion in fibrolamellar carcinoma

Rigney E Turnham

A dissertation

submitted in partial fulfillment of the

requirements for the degree of

Doctor of Philosophy

University of Washington

2018

Reading Committee:

John D Scott, Chair

G Stanley McKnight

Shao-En Ong

Raymond S Yeung

Program Authorized to Offer Degree:

Department of Pharmacology

University of Washington

Abstract

Uncovering pathogenesis of the DNAJ-PKAc fusion in fibrolamellar carcinoma

Rigney E Turnham

Chair of the Supervisory Committee:

John D Scott

Department of Pharmacology

Fibrolamellar carcinoma (FLC) is a rare liver cancer that occurs in healthy adolescents and young adults. FLCs uniquely produce DNAJ-PKAc, a *de novo* chimeric enzyme consisting of a chaperonin-binding domain fused to the Cα subunit of protein kinase A. FLC patients do not consistently respond to conventional chemotherapy, or to any directed agents that have been tested to date; the search for new therapies for these patients is hindered by the limited availability of clinical samples and a lack of disease relevant cell lines or viable animal models that faithfully recapitulate the pathogenesis of FLC. We performed gene-editing on non-transformed mouse hepatocytes to generate disease-relevant cell lines (AML12$^{DNAJ\text{-}PKAc}$ cells). Biochemical analyses of clinical samples and disease-relevant cell lines reveal that a unique property of DNAJ-PKAc is its ability to recruit and bind heat shock protein 70 (Hsp70). Drug screening reveals that Hsp70 and MEK kinase inhibitor combinations that selectively block proliferation of AML12$^{DNAJ\text{-}PKAc}$ cells. Further analyses indicate that the proto-oncogene A-kinase anchoring protein (AKAP)-Lbc is up-regulated in FLC and functions to cluster DNAJ-PKAc/Hsp70 sub-complexes with a RAF-MEK-ERK kinase module. Phosphoproteomic profiling

of AML12$^{DNAJ\text{-}PKAc}$ cells demonstrates that DNAJ-PKAc biases the signaling landscape toward ERK activation, and mobilizes other downstream kinase cascades. Thus we propose the oncogenic action of DNAJ-PKAc proceeds through an acquired scaffolding function that permits recruitment of Hsp70 and local ERK signaling.

List of Figures

Table of Contents

Glossary

Abbreviation	Full Name
AKAP	A-Kinase anchoring protein
AML12	Alpha mouse liver 12 cell line
ATP	Adenosine triphosphate
AURKA	Aurora kinase A
Bad	Bcl-2 antagonist of cell death
BrdU	Bromodeoxyuridine
cAMP	Cyclic adenosine monophosphate
CCCP	Carbonyl cyanide m−chlorophenylhydrazone
CNC	Carney complex
CPS1	Carbamoyl phosphate synthetase I
CRISPR	Clustered Regularly Interspaced Short Palindromic Repeats
DAPI	4′,6-diamidino-2-phenylindole
DNAJ	J-domain of Hsp40
DNAJ-PKAc	Protein product resultant from *DNAJB1-PRKACA* fusion found in fibrolamellar carcinoma
DNAJB1	DnaJ Heat Shock Protein Family (Hsp40) Member B1
Drp1	Dynamin-related protein 1
ECAR	Extracellular acidification rate
ERK	Extracellular-signal-regulated kinase
FADH2	Flavin adenine dinucleotide
FCCP	Carbonyl cyanide-4-(trifluoromethoxy)phenylhydrazone
FLC	Fibrolamellar carcinoma
GO	Gene ontology
Grp75	Mitochondrial-localized Hsp70
GSVA	Gene set enrichment analysis
HCC	Hepatocellular carcinoma
HSP	Heat shock protein
IC50	Half maximal inhibitory concentration
KiR	Kinase Inhibitor Regularization
KSR-1	Kinase suppressor of Ras
MAPK	Mitogen activated protein kinase
MEK	Mitogen activated protein kinase kinase
MKT-077	Cationic dye; an allosteric Hsp70 inhibitor
MOMP	Mitochondrial outermembrane permeabilization
MSigDB	Molecular Signatures Database, Broad Institute

Glossary, continued

Abbreviation	Full Name
mTOR	Mammalian target of rapamycin
MTS	(3-(4,5-dimethylthiazol-2-yl)-5-(3-carboxymethoxyphenyl)-2-(4-sulfophenyl)-2H-tetrazolium)
NADH	Nicotinamide adenine dinucleotide
OCR	Oxygen consumption rates
OTC	Ornithine transcarbamoylase
PDX	Patient-derived xenograft
PKAc	Catalytic subunit of protein kinase A
PLA	Proximity ligation assay
PRKACA	Catalytic alpha subunit of protein kinase A (PKA)
RAF	Rapidly Accelerated Fibrosarcoma; participates in MAPK signaling
RI and RII	Regulatory subunits of PKA
RNAi	RNA interference
RPPA	Reverse-phase protein array
STS	Staurosporine
TMRM	Tetramethylrhodamine
Ver-155008	ATP-competitive inhibitor of Hsp70
$\Delta\psi_m$	mitochondrial membrane potential
μm	micrometer
nm	nanometer

Acknowledgements

I would like to acknowledge my mentor, John, for providing guidance throughout graduate school. I not only learned about cellular signaling, but how to present my science and really tell a story about my work. That is a skill that I will carry with me the rest of my career.

I also want to thank Ray Yeung for helping shape this project to be truly translational. Because of Ray, I learned more about the clinical side of liver cancer and had many experiences that no amount of studying this disease solely at the benchside could ever compare to. Working with Ray both in the lab and in the clinic has undoubtedly made me a better scientist. I also thank Kim Riehle, who is instrumental in the fibrolamellar project, and would edit anything I gave her. She is one of the busiest people I know, but she always has time to edit a paper or listen to a talk, and that kind of support is really remarkable.

I thank my thesis committee members, Shao-En Ong, Dusty Maly, and Stan McKnight, who each provided helpful advice and support throughout graduate school. I also thank my collaborators who have been great to work with; David Hockenbery, Andrew Shieh, Taran Gujral, and John Gordan were all instrumental for the completion of the fibrolamellar project as it stands. I also thank the department of Pharmacology, especially Diane, Debbie, and Jenny.

I thank my lab mates for all of their help and influence over the years. I've had thoughtful discussions from everyone who has come through our doors. What I always found remarkable is the willingness for experimental assistance from my colleagues, no matter what was on their plate for the day. In particular, I thank Emily, Jennifer, Wilfred, Donelson, Mitch, Paula, Laura, Stacey, Irvin, and Derek. I also thank Heidi, Kevin Two, Kevin Three, and Renay in the Yeung lab for all their expertise, discussions, and for their senses of humor. I would like to thank Mel for our morning talks, and for always putting a smile on my face with your thoughtfulness. Katherine, thank you for all the behind-the-scenes work that you do for us.

I next want to thank my classmates Eedann, Emily, Kristine, Sabrina, Samara, and Stacey. I couldn't have asked for a better group of smart women to enter graduate school with. Emily, I couldn’t have asked for a better partner throughout graduate school. You made this journey enjoyable, and you have taught me so much. I am so grateful to have your friendship, and I can’t wait to see all the amazing things you do. Get it, babygirl.

Finally, I thank my family. To my mother Kathy and my father Dan, thank you for always encouraging me to follow my dreams and nurturing my curiosity. Kira, my sister and my best friend, I am so lucky to live life with you. I am forever proud and lucky to be your big sister. To my aunts and uncles Kim, Karla, Lucy, Jim, Dave, John, Bruce, and Kenny, I thank you for your continued support. I thank my late Grandpa Tom and Oma Ruth; I think about you often and I know you would be so proud. I miss you everyday. To Grandma Betty and Grandaddy Jim, I love you very much, thank you for your support in my time in Seattle.

Preface

Portions of the text and data presented in this dissertation are published in the following manuscripts:

Turnham RE and Scott JD. Protein kinase A catalytic subunit isoform *PRKACA*; history, function and physiology. *Gene*. 2016 Feb 15; 577(2): 101–108.

Turnham RE, Kenerson HL, Smith FD, Golkowski M, Garcia I, Bauer R, Lau HT, Sullivan KM, Langeberg LK, Ong SE, Riehle KJ, Yeung RS, and Scott JD. An acquired scaffolding function of the DNAJ-PKAc fusion enhances oncogenesis in fibrolamellar carcinoma. 2018. *In review.*

Chapter 1: Introduction

Fibrolamellar hepatocellular carcinoma (FLC) is a distinct and unique form of liver cancer that primarily affects young adults with no prior history of liver disease or cirrhosis[1]. First described in 1956, FLC is characterized by a central scar on cross-sectional imaging, and is typically diagnosed based on its histological features; large eosinophilic and mitochondria-rich cells with large nucleoli, fibrous bands interspersed between clusters of tumor cells, and CK7 and CD68 stain immunopositivity[2-5]. FLC is rare, as it represents between 1-8% of all hepatocellular carcinomas (HCCs)[1]. Clinically, FLC patients present with a palpable mass, normal levels of serum tumor markers (e.g. αFP), vague symptoms, and no known risk factors, all of which makes FLC difficult to diagnose[1]. There seems to be no bias based on gender, ethnic background, or geographical regions[1,6]. Presently, surgery is the only effective treatment for these patients; the high rate of recurrence presents a major clinical challenge[7]. Lymph node metastasis, the most common site of spread, significantly reduces survival[8]. If amenable to resection and without metastasis, overall survival rate is very good. However, if the tumor is unresectable, the median 5-year survival rate is less than 5%[9]. FLC patients rarely respond to conventional chemotherapy or to any targeted therapies that have been tested to date[1], but several clinical trials are ongoing. Administration of an Aurora A kinase inhibitor, ENDM-2076, was used in a phase II clinical trials that just completed in June 2018 (NCT02234986). Another ongoing clinical trial includes inhibition of the mammalian target of rapamycin (mTOR), estrogen depravation (gonadotropin-releasing hormone agonist and an aromatase inhibitor) or combination of the two in unresectable FLC (NCT01642186). Patients with unresectable disease confined to the liver can be considered for liver transplantation. The overall survival for FLC patients undergoing transplantation is comparable to that of other HCC patients, with a 5-year survival rate 68% for FLC and 50% for HCC[10]. Of late, immunotherapy has significantly advanced the treatment of many cancers[11]. PD1 and PDL1 inhibitors have been used

anecdotally in FLC patients, without consistent response. A number of recent investigations aim to understand the immune landscape in FLC, and to activate an anti-tumoral immune response.

Efforts to identify genetic drivers of oncogenesis in FLC induced many genome- and transcriptome- wide studies. It was through one of these efforts that a breakthrough discovery was made: a 400-kb deletion in chromosome 19 that occurred in 15/15 FLCs sequenced[12]. This deletion is only found on one allele, and leads to a loss of 7 genes and a mircoRNA. These genes include: *ASF1B*, the histone H3-H4 chaperone anti-silencing function 1; *LPHN1*, the adhesion G protein-coupled receptor L1; *ADGRE5*, another adhesion G protein-coupled receptor E5; *DDX39*, a putative RNA helicase; *PKN1*, the protein kinase N1 (part of the protein kinase C superfamily); *PTGER1*, the prostaglandin E receptor 1; and *GIPC1*, a cytoplasmic scaffolding protein; and microRNA *miR639*. This genetic mutation also leads to translation of a *de novo* chimeric gene product wherein the first exon of *DNAJB1* (and in a few cases, part of exon 2) is fused with exons 2-10 of *PRKACA*[12]. *DNAJB1* encodes a member of the heat shock protein 40 (Hsp40) family, while *PRKACA* encodes the catalytic (Cα) subunit of protein kinase A (PKA). The detection of this deletion and subsequent fusion protein has only been reported in FLC, is the only consistent mutation found in FLC, and has been confirmed by multiple investigators[13-20]. Mutations in other genes have been identified, without any consistency between patients. For example, a translocation between chromosome 5 and chromosome 9 was found in a single FLC, resulting in a fusion transcript containing the N-terminus of Cleft Lip and Palate Transmembrane 1-like protein (*CLPTM1L*) to part of the DNA-binding domain of *GLIS3*[17]. A second fusion protein, *GOLTIA-KISS1* was found in 14/26 FLCs but also in 2/9 normal livers sequenced[15]. Mutations in 71 commonly deleted miRNAs have been identified in FLC, 5 of which target *IFG2BP1*[15]. Another study identified mutations in the Breast Cancer susceptibility gene (*BRCA*) in 4.2% of patients, along with Cub and Sushi Multiple Domains 2 (*CSMD2*), Armadillo Repeat Containing X-Linked 1 (*ARMCX1*) and Collagen Type VI Alpha 6

Chain (*COL6A6*)[16]. One sequencing study found mutations in *MUC4* in 4 tumors sequenced, mutations in *GOLGA6L2, DSPP, FOXO6, PCSK5, and HLA-DRB1* in 3 patients, and *FER1L6, CPS1, TENM4, NEFH*, *and* lincRNA *FAM186A* mutations in 2 patients[13]. FLCs have also been evaluated for gene expression changes. The neuroendocrine markers *NTS*, *CALCA, PCSK1,* and *DNER* are overexpressed in FLC identified by many independent studies[14-18,21-23] which correlates with clinical features, as elevated serum neurotensin is often detected in these patients[24-27]. One study identified altered PKA-associated pathways; *AKAP12* (Gravin), *PRKAR2A*, and *AKAP13* (AKAP-Lbc) were increased in FLCs, while expression levels of *PRKAR2B*, *AKAP3* and *AKAP1* were decreased[14]. *CREB3L1* was found to be up-regulated in FLC by three independent studies[14,15,18]; however there was only slight enrichment of CREB target genes. Epidermal growth factor receptor (EGFR) and Erb-B2 receptor tyrosine kinase 2 pathways are also activated in FLC[14,15,20,21]. The Wnt signaling pathway has increased, activity in FLC, along with cell cycle genes like AURKA, cyclins and cyclin-dependent pathways. In fact, identification of increased AURKA expression prompted the clinical trial mentioned above[14]. Another analysis of 32 patient samples found p53 pathway inactivation in these tumors, along with increased Notch, NRAS, and RB1 signaling pathways in FLC as compared to normal liver[15]. Overexpression of RAS/MAPK and PI3K pathways were described in FLC[22] along with the mammalian target of rapamycin complex 1 (mTORC1) pathway[16,28].

Overall, these studies demonstrated: 1) FLC is a unique subtype of HCC, as the pattern of genetic alterations vastly differs from that of classical HCC, and 2) the deletion of 400-kb in chromosome 19 and the fusion between *DNAJB1* and *PRKACA* is the only consistent genetic alteration in over 90% of FLC patients sequenced. One hypothesis as to why the prevalence of the fusion is not 100% in FLC patients is the historic difficulty in distinguishing FLC from other HCCs, in part due to a lack of a biomarker. Thus some patients have been misdiagnosed with

FLC and historic data are difficult to interpret[21]. The identification of this chimeric protein has led to the current overarching hypothesis that the DNAJ-PKAc fusion protein is the driver mutation in FLC.

1.1 Heat shock protein 40

DNAJB1, the gene that encodes heat shock protein 40 (Hsp40), is located on human chromosome 19 and has 3 exons that ultimately produce a 240 amino acid protein (40kDa, also its namesake). The Hsp40 family of proteins is important for regulating protein translation, folding/unfolding, translocation, and degradation[29]. Hsp40 proteins act by stimulating the ATPase activity of their co-chaperone, heat shock protein 70 (Hsp70)[30]. Hsp40 regulates and stabilizes Hsp70s interaction with client proteins, and together, Hsp40/Hsp70 work together to facilitate the correct folding of proteins[31]. Hsp40s are defined by the presence of the J domain, a motif conserved from *E. coli*[32] to mammals. This J-domain is thought to be the binding site for interaction with Hsp70 proteins, and it is this J-domain in its entirety that is fused to PKAc in FLC[33,12]. Structurally, the J domain contains four alpha-helices with a loop region containing three highly conserved amino acids[34]. This is known as the histidine, proline, and aspartic acid (HDP) motif, and is present in all known J-domains. It is these three amino acids that are required for complementation with Hsp70; a single mutation in this motif abolishes Hsp70 binding, for instance, mutation of histidine to glutamine in heat shock protein 40 position 33 inhibits complementation with Hsp70[35,33]. Hsp40s are divided into three groups; DNAJA, DNAJB, and DnaJC[36]. Each family has the conserved J domain and a zinc-finger domain, while DNAJA and DNAJB also have a glycine/phenylalanine-rich domain and a cysteine-rich region[36]. DNAJA and DNAJB proteins are thought to be more general co-chaperones that interact with unfolded, misfolded or aggregated proteins, and transfer them to Hsp70, while DNAJC proteins are thought to bind a narrower group of substrates[36]. A recent crystal structure of DNAJ in complex with Hsp70 highlights the role of the J-domain in stimulating ATP hydrolysis of Hsp70

and increases Hsp70s affinity for substrates[37].

1.2 Heat shock proteins in disease

In normal cells, HSPs are up-regulated in response to stress. However, dysregulated expression of HSPs can contribute to diseases, including Parkinsons, Alzheimers, ataxia, autoimmune diseases, and cancer[29,38-41]. Hsp40 family members are overexpressed in gastric, colorectal, cervical and lung cancers[41-44], and *DNAJA1* has been used as a biomarker in acute lymphoblastic leukemia (ALL)[45]. Conversely, a few family members including *DNAJA3* and *DNAJB6* are thought of as tumor suppressors; overexpression of these proteins is associated with less cell growth and invasion in head and neck carcinoma and breast cancer, respectively[46,47]. In liver cancer, *DNAJC25* expression is reduced; overexpression in a model of HCC led to an increase in apoptosis[48]. Hsp70 overexpression is associated with poor prognosis in many different cancers, including HCC, cholangiocarcinoma, colon, melanoma, breast, colorectal, lung and cervical cancers[29,49]. HSPA9, also known as mortalin or GRP75, has been detected in liver and breast cancers, and is associated with tumor progression and poor prognosis[50,51]. For this reason, Hsp70 has been of recent interest as a target for cancer therapy, however a small molecule inhibitor has yet to succeed. The only Hsp70 inhibitor that has made it to clinical trials was MKT-077, a cationic rhodacyanine dye that disrupts the ATPase activity of Hsp70[52], unfortunately the trial was halted due to nephrotoxic side effects.

1.3 Protein kinase A

The gene to which the 5' end of *DNAJB1* is fused in FLC is *PRKACA*. The human *PRKACA* gene is located on chromosome 19 and encodes the PKA catalytic subunit alpha (Cα) isoform. *PRKACA* has 10 exons that ultimately produce a 351 amino acid protein[53,54]. PKA is a serine/threonine kinase that is responsible for phosphorylating a broad array of downstream

substrates, the extent of which depends on cellular localization[55,56]. Not surprisingly PKA is considered an essential regulator of many cell-signaling events[57,58]. Inactive PKA exists as a holoenzyme, comprised of two regulatory (R) subunits and two catalytic (C) subunits[59]. In the presence of cAMP, the holoenzyme becomes active by binding two cAMP molecules cooperatively to each R subunit, resulting in a conformational change in the R subunits, thus releasing the two C subunits to phosphorylate downstream targets (**Fig. 1.1**)[60]. There are two distinct types of R subunits, RI and RII, of which there are two isoforms of each type, RIα, RIβ, RIIα, and RIIβ. PKA holoenzymes that contain either RI or RII are termed PKA type I or type II, respectively. The RI and RII isoforms differ in their localization and expression levels, and are believed by some to have differential sensitivities for cAMP[61-63]. More recently, it has been realized that the differential localization of the type I and type II PKA holoenzymes is an important determining factor that dictates their physiological roles[55,56,64].

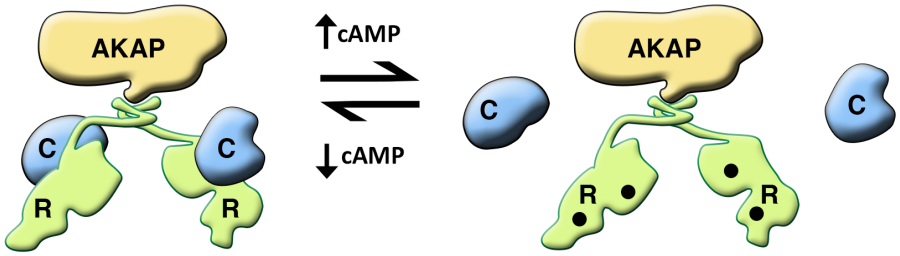

Fig. 1.1. The anchored PKA holoenzyme. This schematic representation of the protein components of an anchored PKA holoenzyme shows the C subunits (blue) and the R subunit dimer (green) in complex with an A-kinase anchoring protein (AKAP, yellow). Following stimulation of cAMP synthesis, this second messenger (cAMP, black) binds to the R subunits in a manner that releases the C subunits to phosphorylate target substrates.

Specificity of PKA signaling is attained through the binding of the R subunits to scaffolding proteins called A-kinase anchoring proteins, or AKAPs[65]. AKAPs are a diverse family of about 50 proteins that vary in localization and structure, and all share the ability to bind the R subunits of PKA[58,66]. The trademark feature in all AKAPs is the amphipathic helix that binds with high affinity to the R subunits[67]. AKAPs target the PKA holoenzyme to different subcellular locations in proximity to other proteins to optimize signal transduction. This process allows for local

cAMP-responsive events to occur within specific compartments of the cell[68]. Recently, AKAP-PKA complexes were evaluated with electron microscopy and a three-dimensional reconstruction of the holoenzyme revealed that the AKAP-PKA complex has some flexibility, which might further allow PKA to adopt the optimal conformation for substrate phosphorylation[69]. Although the majority of AKAPs preferentially associate with the RII subunit, there is reason to believe that RI subunits can also be compartmentalized though interaction with anchoring proteins[70,71]. In addition there are a few RI selective anchoring proteins that only compartmentalize the type I PKA[72,73]. Perhaps the most biologically relevant feature of AKAPs is their ability to cluster PKA with other classes of signaling enzyme[55,74-77]. By constraining broad specificity enzymes such as PKA, PKC, and the protein phosphatases PP1 and PP2B in customized macromolecular units, AKAP complexes allow cells to efficiently and accurately respond to the transient production of diffusible second messenger signals. This concept was first proposed in 1995 when it was shown that the anchoring protein AKAP79/150 not only compartmentalized PKA, but also sequestered the protein phosphatase PP2B[78]. As a result, the opposing actions of a protein kinase and a protein phosphatase were constrained within the confines of the same macromolecular complex[78]. It was subsequently shown that the proximity of both enzymes to phosphoprotein substrates such as ion channels and cytoskeletal components enhanced the bi-directional control of neuronal events that underlie synaptic transmission, glucose homeostasis, cardiac transcriptional regulation and higher-order cognitive function in genetically modified mice[79-85].

1.4 PKA in disease

Somatic mutations in *PRKACA* can result in Cushing's syndrome. Cushing's syndrome is a disease caused by excess glucocorticoid production as a result of adrenocortical (AC) and ACTH-producing pituitary tumors[86]. These tumors include adrenocortical adenomas (ACA), adrenocortical carcinomas (ACC) and bilateral adrenal hyperplasia (BAH). Overproduction of

glucocorticoids in Cushing's syndrome can result in other disorders, like hypertension, osteoporosis, diabetes as well as interfering with hormone production from the pituitary. Recently several groups have independently reported that whole-exome sequencing of cortisol-producing ACTs resulted in the identification of T617G heterozygous mutation that results in an amino acid substitution, Leu206Arg[87-90]. This mutation was only found in ACAs, with a varying frequency of approximately 20% to 70% depending on the study. This mutation L206R is found in the p+1 loop of PKA, and interferes with binding between the catalytic subunit and the R subunits of PKA in the presence of cAMP. Further studies have confirmed this mutation in *PRKACA*, and concluded that the Leu206Arg mutation of PKA results in higher basal PKA activity[87,91].

Three mutations have been found in patients with adrenocortical adenomas; c.595_596insCAC that results in an insertion of a tryptophan (Leu199_Cys200insTrp), c.600_601insGTG that results in a insertion of valine (p.Cys200_Gly201insVal), and a missense mutation, c.639C>G that changes Ser213 to Arg while inserting four amino acids[91,92]. This mutation is found in a highly conserved region of the catalytic subunit of PKA, and is thought to elevate basal activity of PKA. In contrast, the Leu206Arg, Leu199_Cys200insTrp, and the Cys200_Gly201insVal mutations are all found near the autoinhibitory sequence of the regulatory subunit[91]. The autoinhibitory sequence is involved in keeping the catalytic subunit inactive by blocking the active site in the absence of cAMP[91], this mutations in this region may lead to increased PKA activity. Collectively, these findings provide further evidence that disruption of this conserved structure of the catalytic subunit of PKA can lead to aberrant and unregulated kinase activity[93]. Germline gene amplification of *PRKACA* has also been recently reported in Cushing's syndrome patients that resulted in bilateral adrenal hyperplasia. Interestingly, exome sequencing revealed that none of these patients harbored mutations in the *PRKACA* gene, but rather exhibited increased copy numbers of *PRKACA* transcript[94,95].

Carney complex (CNC) is another disease of the adrenal gland, which presents as somatotroph-pituitary adenomas, testicular Sertoli cell calcified tumors, benign thyroid nodules, differentiated thyroid cancer, and most commonly, primary pigmented nodular adrenocortical disease[96]. Inactivating mutations in the gene that encodes RIα (*PRKAR1A*) have been identified in over 60% of patients with CNC[92,97,98]. While the exact mutations differ from family to family, these mutations usually lead to a premature stop codon and the RNA gets promptly degraded. One molecular explanation is that a decrease in the cellular RIα pool allows the catalytic subunit to roam unregulated and increases the kinase activity in tissues. Interestingly, 3 patients with a history of Carney complex were reviewed for liver tumors and found to display the typical morphology of FLCs, but were negative for the *DNAJB1-PRKACA* fusion[99].

Although PKA is not traditionally considered to be an oncogene, there is a growing body of literature that suggests this kinase may contribute in some ways to the progression of cancer. For example, extracellular PKA catalytic subunit has been detected in the serum of a variety of cancer patients, including colon, renal, rectal, prostate, lung, adrenal carcinomas and lymphomas[100-102]. Increased *PRKACA* transcripts have also been observed in breast cancer, specifically in patients that are resistant to trastuzumab, which is a common treatment for HER2 positive breast cancer[103]. In these instances, *PRKACA* can be used as a biomarker for cancer as well as a prognostic tool[103].

1.5 Current FLC models

Progress towards a cure for FLC has been hindered by a lack of *in vitro* or *in vivo* models. The chronic difficulty in culturing human hepatocytes has limited the availability of useful cell lines, and culturing primary FLCs has been unreliable. One group developed a human FLC patient-derived xenograft (PDX) model that shows enrichment of cancer stem cells, specifically

hepatobiliary stem cells, and can be propagated in mice[23]. This model is limited in recapitulating carcinogenesis in FLC, however, as it was generated from a patient with malignant ascites, a very rare event even in advanced FLC. Given this rare phenotype, we suspect that these cells have acquired mutations beyond the *DNAJB1-PRKACA* fusion, and thus may be suboptimal for studies of tumor initiation in FLC. More recently, two independent groups used CRISPR/Cas9 methodology to introduce the FLC deletion into mouse livers by tail vein injection; these animals developed liver tumors that resemble human FLC[104,105]. Specifically, it was shown that just expressing the *DNAJB1-PRKACA* cDNA in mouse livers is sufficient to drive tumorigenesis in mice[104]. Interestingly, when a kinase dead *DNAJB1-PRKACA* mutant (equivalent to K72H[106]) cDNA was introduced in trans, the mice did not develop tumors, suggesting that the kinase activity of the fusion protein is at least necessary for tumor initiation. One major disadvantage of the mouse model developed by both groups is that without also administering a hepatotoxin, mice took more than 14 months to develop tumors, limiting their utility in therapeutic testing. Since FLC patients do not have underlying liver injury, combining liver injury with introduction of the *DNAJB1-PRKACA* mutation would not be a faithful representation of FLC in humans.

In summary, recent genome sequencing of FLCs, has led to the discovery of a deletion in chromosome 19 and subsequent fusion transcript in these tumors, *DNABJ1-PRKACA*. This novel gene product translates to a chimeric protein that has been confirmed in almost every FLC examined, and is specific for FLC. The DNAJ-PKAc fusion protein has been the target of many drug discovery efforts, and work is underway to understand the molecular consequence of expression of the chimeric protein and the dysregulated pathways downstream. In this study, we developed a reliable and sustainable model of FLC using genetic engineering of non-transformed mouse hepatocytes to better understand tumor initiation. This cell line, named AML12$^{DNAJ\text{-}PKAc}$, grows faster than its parent cells, and has a distinct molecular signature, thus recapitulating some aspects of human FLC. This renewable cell line is amenable to a wide

variety of manipulations, and here we describe the first combination drug screen on an FLC model. These experiments have led to the hypothesis that DNAJ-PKAc functions as a scaffolding protein, assembling additional signaling elements that contribute to the pathogenesis of this cancer. More specifically, we show that the chaperonin-binding domain of the FLC-specific fusion enzyme supports recruitment of Hsp70, creating a unique molecular context in which the DNAJ-PKAc chimera acts in FLCs.

Chapter 2: Development and characterization of an *in vitro* model of fibrolamellar carcinoma using CRISPR

Fibrolamellar carcinoma (FLC) is a rare variant of hepatocellular carcinoma that is characterized by thick, fibrous lamellae in the liver in affected adolescents and young adults[1]. A recent breakthrough has come from whole-genome sequencing of FLC, demonstrating a 400 kilobase deletion in chromosome 19 that creates an in-frame fusion of two well known genes[12]: the first exon of *DNAJB1* (which encodes the heat shock protein 40) is fused to *PRKACA* (the gene which encodes the catalytic subunit alpha of PKA). The search for new therapies for these patents is hindered by the limited availability of clinical samples and a lack of disease relevant cell lines or viable animal models that faithfully recapitulate the pathogenesis of FLC[23,104,105]. To this end, we sought to develop a model focusing on disease initiation that is easy to maintain and manipulate. Herein we describe the generation of an *in vitro* model of FLC using CRISPR-Cas9 gene editing in non-transformed mouse hepatocytes (AML12). Using this system, we have recapitulated the genomic 400kb deletion seen in FLC, and the resultant DNAJ-PKAc fusion. These cells proliferate faster than their wild type counterparts, and have elevated PKA activity, as do FLCs[107]. We can now use these cells to better understand how the DNAJ-PKAc fusion drives the development of cancer in healthy young people, with the ultimate goal of developing effective therapeutics for these patients.

2 Results

2.1 Development of an *in vitro* model of FLC

Since human FLCs develop in healthy, non-injured livers, we chose a non-transformed mouse cell line (AML12) in order to understand the early stages of transformation in this disease. AML12 cells were established from a 5-month old male CD1 mouse that was transgenic for human TGF alpha[108]; wild type AML12 cells do not lead to the development of tumors when

implanted in immunocompromised mice, nor do they display other characteristics of cancer cells. On mouse chromosome 8, *Dnajb1*, *Prkaca*, and their intervening genes are syntenic to human chromosome 19, where *DNAJB1* and *PRKACA* are located[12,104]. Therefore, we employed CRISPR/Cas9 gene editing of mouse chromosome 8 in AML12 cells to generate sustainable and homogenous cell lines. Using this system, a 400kb region was excised between intron 1 of the gene for Hsp40 (*Dnajb1*) and intron 1 of the gene for PKAc (*Prkaca*; **Fig. 2.1a**). We estimate the frequency of the resultant rearrangement in AML12 cells was 1/100 (data not shown). Initial characterization by genomic DNA PCR shows the presence of a *Dnajb1-Prkaca* fusion in 5 clones; clone 2, clone 4, clone 5, clone 10 and clone 14 (**Fig. 2.1b**). Sequencing of *Dnajb1-Prkaca* genomic PCR product (**Fig. 2.1b**) confirmed the Cas9 cut site and non-homologous end joining of *Dnajb1* and *Prkaca* in each of the 5 clones, similar to the predicted cut site (**Fig. 2.1c**). Genomic DNA of intervening genes (*Gipc1*, *Ddx39* and *Lphn1*) located at the 5', middle and 3' end of the non-engineered strand of chromosome 8 were also detected, confirming a heterozygous deletion (**Fig. 2.1d**). Quantitative PCR was used to measure mRNA transcripts for native *Dnajb1* and *Prkaca* in wild type AML12 and five gene-edited AML12$^{DNAJ-PKAc}$ cell lines (**Fig. 2.1e & f**). Different levels of both transcripts were detected each AML12$^{DNAJ-PKAc}$ cell line (**Fig. 2.1e & f**). Likewise, differential production of the *Dnajb1-Prkaca* fusion transcript was measured in each clonal cell line (**Fig. 2.1g**). The total amount of PKAc message (wild type plus fusion) was also quantified by measuring from the 3' end of *Prkaca* in AML12 cells and the 5 clones (**Fig. 2.1h**). Endogenous mRNA sequencing confirms the in-frame fusion of exon 1 of *Dnajb1* to exons 2-10 of *Prkaca* in clone 14 AML12$^{DNAJ-PKAc}$ cells (**Fig. 2.1i**). Western blot analysis using an antibody recognizing the C terminus of PKAc confirmed the presence of a slower migrating band in AML12$^{DNAJ-PKAc}$ cells, corresponding to the DNAJ-PKAc fusion protein (**Fig. 2.1j**). In 4 of 5 of our clones, DNAJ-PKAc is expressed at higher levels than wild type PKAc, similar to the pattern seen in human FLCs[107]. Clone 14 was selected for further characterization (herein called AML12$^{DNAJ-PKAc}$ cells) due to expression levels of wild type

Dnajb1 and *Prkaca* that are similar to wild type AML12 cells (**Fig. 2.1e & f**) and because expression levels of wild type PKAc compared to DNAJ-PKAc are similar to that seen in human FLCs (**Fig. 2.1j**). Clone 10 was also further characterized for select experiments, as it seemed to be a homozygous knockout of *Dnajb1* and *Prkaca* genes, despite still expressing genes in-between (**Fig. 2.1e & f, j**).

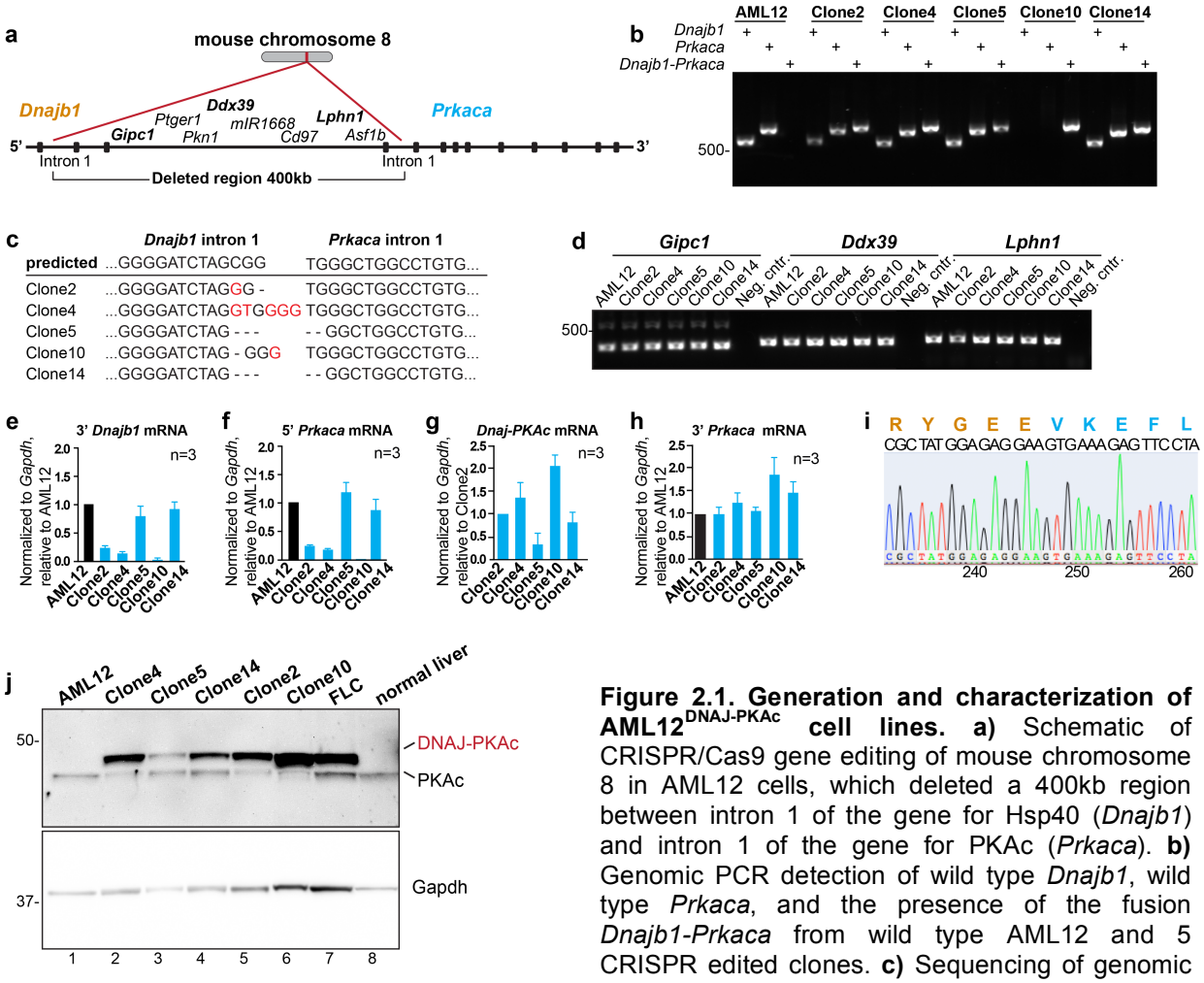

Figure 2.1. Generation and characterization of AML12$^{DNAJ-PKAc}$ cell lines. a) Schematic of CRISPR/Cas9 gene editing of mouse chromosome 8 in AML12 cells, which deleted a 400kb region between intron 1 of the gene for Hsp40 (*Dnajb1*) and intron 1 of the gene for PKAc (*Prkaca*). **b)** Genomic PCR detection of wild type *Dnajb1*, wild type *Prkaca*, and the presence of the fusion *Dnajb1-Prkaca* from wild type AML12 and 5 CRISPR edited clones. **c)** Sequencing of genomic DNA from *Dnajb1-Prkaca* transcripts from each of the 5 clones against the predicted fusion in intron 1 for both *Dnajb1* and *Prkaca*. **d)** Genomic DNA transcripts for *Gipc1, Ddx39* and *Lphn1* genes encoded on the non-engineered strand of mouse chromosome 8. **e-h)** Quantitative PCR detection of native mRNA transcripts in (**black**) AML12 and (**blue**) gene-edited cell lines. **e)** Detection of native *Dnajb1* mRNA transcripts, **f)** *Prkaca* transcripts, **g)** *Dnajb1-Prkaca* mRNA transcripts, and **h)** total Prkaca transcripts. Data (n=3) is normalized to Gapdh (**e-h**) and normalized wild type AML12 control (**e, f, h**) or clone 2 (**g**). **i)** Amino acid sequence from clone 14 of the fusion protein DNAJ-PKAc is shown orange and blue. Codon sequence of the fusion gene from AML12 clone 14 is shown below. **j)** Immunoblot detection of both native and mutant PKAc in five clonal AML12$^{DNAJ-PKAc}$ cell lines and FLC and normal adjacent liver. **Bottom panel**) Gapdh loading control.

2.2 Characterization of the *in vitro* FLC model and molecular consequence of DNAJ-PKAc expression

Given that accelerated cell proliferation is a key feature of carcinogenesis[109], we measured proliferation and cell viability in AML12$^{DNAJ\text{-}PKAc}$ cells compared to wild type AML12 cells by various techniques. Cells were cultured over time and underwent serial measurements of proliferation by MTS ((3-(4,5-dimethylthiazol-2-yl)-5-(3-carboxymethoxyphenyl)-2-(4-sulfophenyl)-2H-tetrazolium) assay. Amalgamated data show that the proliferation rate of AML12$^{DNAJ\text{-}PKAc}$ cells is higher than wild type AML12 cells (**Fig. 2.2a**). Parallel immunohistochemical analyses of *in situ* incorporation of BrdU confirmed increased DNA synthesis (82 ± 2% vs 36 ± 5%, **Fig. 2.2b**). Thus AML12$^{DNAJ\text{-}PKAc}$ cells proliferate more rapidly than their wild type counterparts. However, these cells do not acquire enhanced migratory or transmigratory properties as measured by scratch wound assay (**Appendix I, supplemental Fig. S1**). McKnight and colleagues have shown that changes in PKAc usually result in respective changes in the PKA regulatory (R) subunits[110,111]. We then investigated the expression of the PKA R subunits by western blot (**Fig. 2.2c**) and found that coincident with increased expression of PKAc, our mutant clones have increased RIα expression, as seen in FLC[107]. To determine if the mutant kinase is enzymatically active, radioactive kinase assays were performed, revealing that AML12$^{DNAJ\text{-}PKAc}$ cells have similar basal PKA activity compared to wild type AML12 cells. AML12$^{DNAJ\text{-}PKAc}$ cells have a sight increase in cAMP-stimulated PKA activity, however (**Fig. 2.2d**). This finding mirrors the elevation in cAMP-driven PKA activity seen in human FLCs[107], and is consistent with the notion that DNAJ-PKAc is still regulated by the R subunits of PKA[112]. The intrinsic kinase activities of wild type PKAc and DNAJ-PKAc were also measured using recombinant protein with Kemptide as a substrate. Kinase activities of purified PKAc and DNAJ-PKAc were similar, and both enzymes are inhibited by PKI (**Fig. 2.2e**). Given these data and the recently solved crystal structure that confirms no changes in active site

structure of DNAJ-PKAc[112], we surmised that the oncogenic nature of DNAJ-PKAc might be due to changes in binding partners rather than a change in intrinsic kinase activity.

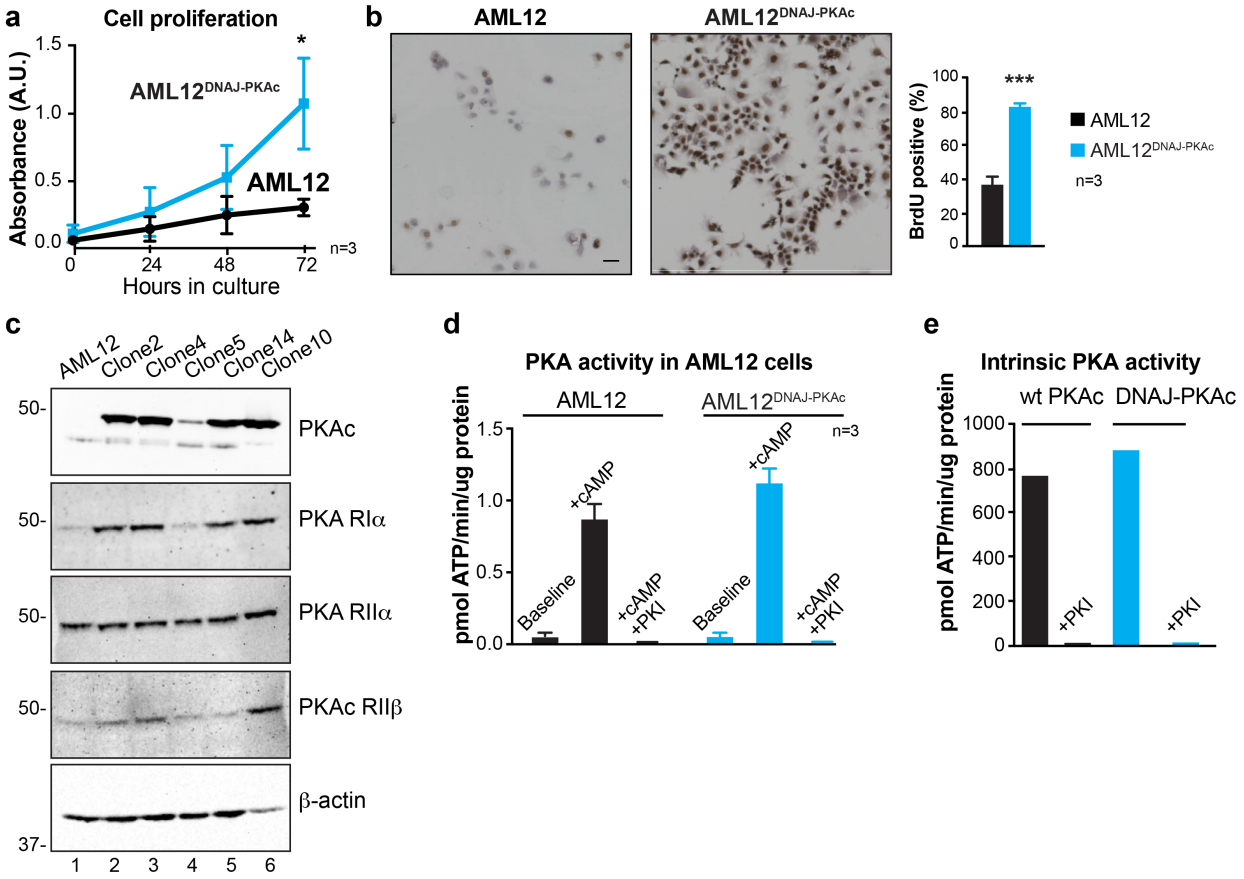

Figure 2.2. Cell proliferation analyses and kinase activity of AML12$^{DNAJ-PKAc}$ cells. a) Cell growth of wild type AML12 (**black**) and clone 14 AML12$^{DNAJ-PKAc}$ (**blue**) cells was measured by MTS assay. Absorbance (AU) was measured over a time course of 72h. Amalgamated data from three independent experiments is presented. **b)** *In situ* incorporation of BrdU as an independent means of assessing cell proliferation. Representative panels of wild type AML12 (**left**) and clone 14 AML12$^{DNAJ-PKAc}$ cells (**right**), with quantification of n=3 data (bar graphs). **c)** Immunoblot detection of PKA regulatory (R) subunits RIα, RIIα, RIIβ in 5 clones, with wild type AML12 cells as the control (top panel). β-actin served as the loading control (bottom panel). **d-e)** Specific activity (pmol/μg/min) of basal PKA activity in **d)** wild type AML12 (**black**) and clone 14 AML12$^{DNAJ-PKAc}$ (**blue**) and **e)** purified PKAc (**black**) and DNAJ-PKAc (**blue**) was measured by radioactive kinase assay using Kemptide as a substrate. **d)** cAMP-responsive PKA activity was measured in wild type AML12 (**black**) and AML12$^{DNAJ-PKAc}$ (**blue**). **d & e)** treatment with PKI inhibitor peptide specifically blocked PKA activity.

To determine the molecular consequences of DNAJ-PKAc expression in hepatocytes, we performed RNA sequencing on clone 14 AML12$^{DNAJ-PKAc}$ and wild type AML12 cells in collaboration with the Gujral lab, and assessed differential expression with the DESeq2 analysis package[113]. Using a false discovery rate (FDR) of 0.02 and a fold-change threshold of 1, we

detected 1,134 differentially expressed genes in AML12$^{DNAJ\text{-}PKAc}$ versus AML12 cells (842 down-regulated genes and 242 up-regulated genes, **Fig. 2.3a**). A list of the 50 most dysregulated genes in AML12$^{DNAJ\text{-}PKAc}$ cells is listed in **supplemental table S1**. Gene set enrichment analysis (GSEA) was used to identify significantly enriched pathway gene sets[114]. From the "canonical pathways" collection from the Molecular Signatures Database (MSigDB, Broad Institute, c2.cp), 37 pathways were differentially enriched in AML12$^{DNAJ\text{-}PKAc}$ cells. Three of the 37 enriched pathways were E2F targets, and 4 other pathways were involved in cell replication and mitosis. The whole list can be found in **Appendix I, supplemental table S2**. From the "hallmark" gene collection in the MSigDB, three pathways were enriched in AML12$^{DNAJ\text{-}PKAc}$ versus AML12 cells; they corresponded to E2F targets, oxidative phosphorylation, and G2M checkpoint pathways. A heatmap of the significantly enriched genes that correspond to the hallmark E2F targets as well as the oxidative phosphorylation can be found in **figures 2.3 b & c**, respectively. Of the "gene ontology" (GO) gene set (c5), gene sets that are involved in DNA replication comprised over 50% of the significantly upregulated pathways; these included centromere complex assembly, sister chromatid cohesion, condensed chromosome centromeric region, sister chromatid segregation, chromosome centromeric region, kinetochore, and mitotic nuclear division. Among the other 14 differentially regulated gene sets, 4 pathways corresponded to mitochondrial function: inner mitochondrial membrane protein complex, mitochondrial respiratory chain complex, oxidative phosphorylation, and mitochondrial protein complex were all upregulated in AML12$^{DNAJ\text{-}PKAc}$ cells versus AML12 cells. A heat map of the significantly enriched genes in AML12$^{DNAJ\text{-}PKAc}$ cells that correspond to the GO mitochondrial protein complex data set is presented in **Fig. 2.3d**. Interestingly, there is a decrease in liver-specific genes in AML12$^{DNAJ\text{-}PKAc}$ cells versus wild type cells (from the "canonical pathways" data set, MSigDB, **Fig. 2.3e**).

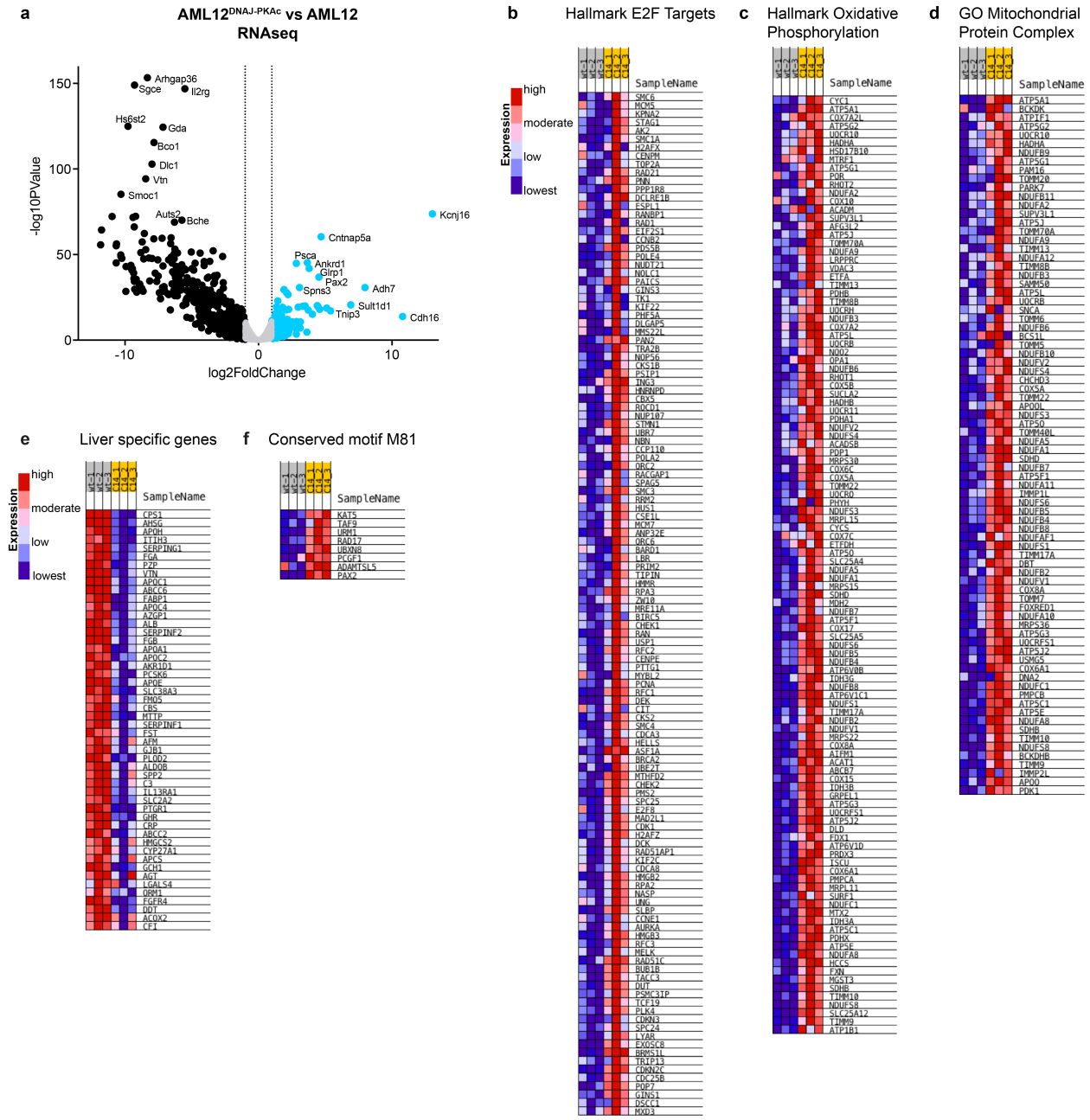

Figure 2.3. RNA sequencing and pathway analysis of AML12 and AML12$^{DNAJ-PKAc}$ cells.
a) Volcano plot of RNAseq results of RNAs found in clone 14 AML12$^{DNAJ-PKAc}$ versus AML12 cells. RNAs found significantly increased in AML12$^{DNAJ-PKAc}$ cells are depicted in blue; RNAs found significantly decreased in AML12$^{DNAJ-PKAc}$ cells depicted in black. Log2FoldChange cutoff =1. **b-f)** Heatmap from the Molecular Signatures Database (MSigDB, Broad Institute) depicting differentially expressed genes found in clone 14 AML12$^{DNAJ-PKAc}$ cells. Relative expression enrichment scores indicate up-regulated (**red**) and down-regulated (**blue**) genes across samples. FDR < 0.02. **b)** Heatmap of E2F Hallmark gene sets depicting differentially expressed genes; gene set is from Hallmark_E2F_Targets. **c)** Heatmap of Oxidative Phosphorylation gene set showing differentially expressed genes; gene set is from Hallmark_Oxidative_Phosphorylation. **d)** Heatmap of Mitochondrial Protein Complex gene set from Gene Ontology (GO) gene set from MSigDB; gene set is GO_Mitochondrial_Protein_Complex (C5.cc). **e)** Heatmap of Liver specific gene set from Canonical Pathways from MSigDB; gene set is Hsiao_Liver_Specific_Genes (c2.cgp). **f)** Heatmap from the highly conserved M81 motif from the Motif gene set; gene set name is CGGAARNGGCNG_Unknown (c3.tft).

We next compared our RNAseq data to published datasets from FLCs to identify oncogenic pathways that may be a direct consequence of the DNAJ-PKAc fusion. Sorenson *et.al*'s list of top 100 dysregulated genes in FLC[15] contained 12 genes that were also dysregulated in AML12$^{DNAJ-PKAc}$ cells (**Table 2.1**). Of these 12, expression of 9 genes decreased in FLCs and AML12$^{DNAJ-PKAc}$ cells (*Auts2, Abca6, Xdh, Sox5, Slc3a1, Gbp7, Slc2a2, Afm,* and *Adra1a*). Three genes were increased in both FLCs and AML12$^{DNAJ-PKAc}$ cells (*Iqgap3, Nox4,* and *Ttc39a*). From the canonical pathways data set, there were 2 pathways increased in both FLCs and AML12$^{DNAJ-PKAc}$ cells; these included cell cycle RB1 targets, and cell cycle targets of TP53 and TP57. Oikawa *et.al* also had limited data to analyze, but in the list of 9 genes with increased expression in their model of FLC[23], 2 genes (*Wnt7B* and *Krt20*) are increased in AML12$^{DNAJ-PKAc}$ cells. In the "motif gene sets" (c3, MSigDB), one gene set in AML12$^{DNAJ-PKAc}$ cells correlated with that of FLCs, known as the CGGAARNGGCNG_UNKNOWN, or M81 motif, gene set. The genes found in this set in AML12$^{DNAJ-PKAc}$ cells are shown in **figure 2.3f**. Due to limited available human data, only a few studies were available for analysis; more bioinformatics are needed to compare human FLC gene changes with AML12$^{DNAJ-PKAc}$ cells to better understand the effects of the fusion protein DNAJ-PKAc.

		AML12 cells				Human tissue[15]			
Gene	**Description**	**FC**	**adj. p-value**	**Mean expression WT AML12**	**Mean expression AML12$^{DNAJ-PKAc}$**	**FC 2**	**adj. p-value2**	**Mean Expression Normal Liver**	**Mean Expression FLC**
TTC39A	tetratricopeptide repeat domain 39A	1.45	3.15E-07	2.58	7.07	20	9.60E-34	39	782
NOX4	NADPH oxidase 4	1.44	3.63E-11	54.81	148.31	21	3.60E-32	18	365
IQGAP3	IQ motif containing GTPase activating protein 3	1.08	0.0012	32.29	68.30	21	1.60E-26	49	1015
ADRA1A	adrenergic receptor, alpha 1a	-1.39	1.23E-05	2.77	1.05	-54	1.10E-55	2766	52
AFM	afamin	-2.00	0.0053	8.26	2.05	-13	5.50E-26	32339	2410
SLC2A2	solute carrier family member 2	-2.17	2.02E-18	301.16	66.76	-15	3.40E-26	26002	1741
GBP7	guanylate binding protein 7	-2.20	1.09E-07	11.75	2.56	-15	1.80E-28	3012	199
SLC3A1	solute carrier family 3, member 1	-2.44	7.61E-06	50.26	9.24	-37	1.90E-35	1250	34
SOX5	SRY (sex determining region Y)-box 5	-3.27	3.11E-07	3.23	0.33	-13	4.60E-29	881	68
XDH	xanthine dehydrogenase	-3.53	4.56E-08	69.58	6.02	-14	3.80E-28	6640	483
ABCA6	ATP-binding cassette, sub-family A (ABC1), member 6	-3.93	1.83E-23	18.21	1.19	-10	2.60E-26	6930	704
AUTS2	autism susceptibility candidate 2	-6.29	1.11E-69	19.87	0.25	-11	8.40E-30	4211	392

Table 2.1. Genes found dysregulated in AML12$^{DNAJ-PKAc}$ cells and FLCs[15]. Available data matched 12 dysregulated genes similar in both AML12$^{DNAJ-PKAc}$ cells and FLCs; 9 genes were decreased in both AML12$^{DNAJ-PKAc}$ cells and FLCs, and 3 genes were increased in AML12$^{DNAJ-PKAc}$ cells and FLCs. FC represents log2 fold change.

We have established changes in transcripts as a consequence of DNAJ-PKAc expression in AML12$^{DNAJ-PKAc}$ cells. Next, we used kinase inhibitor regularization (KiR), in collaboration with the Gujral lab, to identify key upstream kinases that are important for a given cell phenotype. KiR integrates a small kinase inhibitor screen with elastic net regression to identify kinases that are most significantly contributing to a specific phenotype, such as viability[115]. KiR exploits polypharmacology, the fact that pharmaceutical agents are non-specific and have multiple targets[116], and uses the known activity profiles of 300 kinases in response to over 150 kinase inhibitors to assess kinase dependency[115]. Here, we used KiR to identify kinases responsible for AML12$^{DNAJ-PKAc}$ cell growth. After eliminating the kinases that are not expressed in AML12 cells, a total of 15 kinases were predicted to be important for the growth of AML12 and AML12$^{DNAJ-PKAc}$ cells (**Fig. 2.4**).

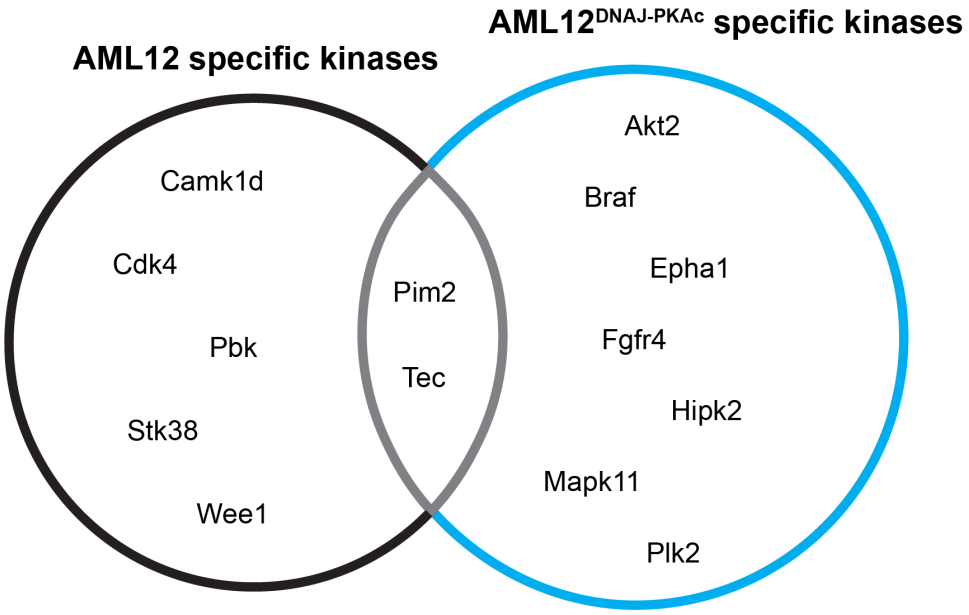

Figure 2.4. Potential key kinases in AML12 and AML12$^{DNAJ-PKAc}$ cells. Kinase Inhibitor Regularization identified 7 kinases important for clone 14 AML12$^{DNAJ-PKAc}$ cell phenotype (**blue**); 5 kinases important for AML12 phenotype (**black**); and 2 kinases that are potentially important for both cell lines (**gray**).

Five of these, Calcium/Calmodulin Dependent Protein Kinase ID (Camk1d), Cyclin-dependent kinase 4 (Cdk4), PDZ-binding kinase (Pbk), Serine/Threonine Kinase 38 (Stk38), and Wee1-like

protein kinase (Wee1) are predicted to be important for wild type AML12 growth maintenance. There were two kinases predicted to be common for the growth of both AML12 and AML12$^{DNAJ\text{-}PKAc}$ cells: Serine/threonine-protein kinase pim-2 (Pim2) and Tyrosine-protein kinase Tec (Tec). Of greatest translational interest are the 8 kinases identified to preferentially support growth of AML12$^{DNAJ\text{-}PKAc}$ cells: RAC-beta serine/threonine-protein kinase (Akt2), Serine/threonine-protein kinase B-raf (Braf), Ephrin type-A receptor 1 (Epha1), Fibroblast growth factor receptor 4 (Fgfr4), Homeodomain-interacting protein kinase 2 (Hipk2), Mitogen-activated protein kinase 11 (Mapk11), Casein kinase 1 gamma 2 (Ck1g2) and Polo-like kinase 2 (Plk2). It will be important to validate the dependency of AML12$^{DNAJ\text{-}PKAc}$ cells to each of these kinases, either using RNAi, CRISPR gene editing, or direct drug treatments in our cell line. Inhibitors of these kinases may be valuable as a new therapeutic strategy for FLC, and are worthy of further investigation.

2 Discussion

Our *in vitro* model of FLC, which we developed using CRISPR gene editing of murine hepatocytes, has allowed us to further explore the mechanism of action of the oncogenic fusion PKA. These novel cell lines can be easily manipulated, and affords a unique opportunity to study disease initiation in FLC. While there is one other FLC PDX model[23], that model is limited as it was developed from a patient with malignant ascites, a very rare event even in advanced FLC cases. Thus, it may not be accurate or reflect early carcinogenic events. The two *in vivo* mouse models of FLC recapitulate some aspects of FLC[104,105], however a major disadvantage of these models is that tumors take over 12 months to develop, limiting the utility in therapeutic testing. Our gene-edited AML12$^{DNAJ\text{-}PKAc}$ cells provide new reagents for studying the mechanism of oncogenesis in FLC.

We show that the kinase activity of the new oncogenic PKAc fusion is under control of the PKA regulatory subunits. Perhaps due to the overexpression of DNAJ-PKAc compared to wild type

PKAc, there is a compensatory increase in RIα as we might expect[111], which is consistent with the increase in RIα protein seen in FLC[107]. Constitutively active fusion kinases are not uncommon in cancers; BCR-ABL causes increased tyrosine kinase activity giving rise to CML[117] and ALK fusions give rise to lung carcinoma[118]. However, basal kinase activity in AML12$^{DNAJ\text{-}PKAc}$ cells is similar to kinase activity in wild type AML12 cells, consistent with the observation that kinase activity measured in FLCs, similar to that of normal liver[107]. There is a cAMP-dependent increase in PKA activity in both AML12$^{DNAJ\text{-}PKAc}$ cells and FLCs[107] compared to their controls; this is thought to be due to the overall increase in mutant PKA expression over wild type PKAc. One potential explanation for this increase in expression is that is the oncogenic DNAJ-PKAc protein is now transcribed off the *DNAJB1* promoter. This hypothesis conflicts with our mRNA data measuring both mutant and wild type transcripts of PKAc (**Fig. 2.1h**) and the protein expression of DNAJ-PKAc (**Fig. 2.1j**). We estimate that DNAJ-PKAc is expressed 3-fold higher in clone 14 AML12$^{DNAJ\text{-}PKAc}$ cells compared to wild type PKAc in AML12 cells (**Fig. 2.1g**) while the mRNA transcript of total PKAc in clone 14 is 1.5-fold increased over wild type AML12. One over-arching hypothesis is that the fusion of the heat shock protein DNAJ to PKA stabilizes the entire protein. This theory would explain the differences in mRNA and protein expression seen in our cell lines. In FLCs however, total PKAc mRNA is estimated to be expressed at about 10-fold higher levels in FLCs than normal adjacent liver, while PKAc protein expression in FLCs is about 2.5-fold overexpressed compared to wild type PKAc in normal liver[107]. This is perhaps suggestive of the difference between a simple model (AML12$^{DNAJ\text{-}PKAc}$ cell line) and a complex human tumor (FLC).

AML12$^{DNAJ\text{-}PKAc}$ cells have a striking increase in cell proliferation compared to parental AML12 cells, consistent with its oncogenic properties[109]. Human FLC has been considered a slow growing cancer, however[119]. While there is still some debate about its slow growth in patients,

we still expect cancer cells to proliferate faster than those of surrounding normal tissue. Interestingly, most of the pathways that were up-regulated in RNA sequencing analysis of AML12$^{DNAJ\text{-}PKAc}$ cells were cell cycle control pathways: E2F targets, chromosome segregation, and G2M checkpoint pathways. The E2F target pathway in the MSigDB contain genes that are known to be regulated by E2F transcription factors which are important for S-phase entry into the cell cycle and thus regulate cell cycle progression[120]. The G2M checkpoint pathway contain genes that are involved in ensuring that damaged DNA does not enter mitosis, and thus provides an opportunity to repair damaged cells[121]. This pathway is of particular interest to the cancer field, as damaged cells that enter mitosis by bypassing the G2M checkpoint are known to contribute to oncogenesis[122]. Our finding of increased proliferation in AML12$^{DNAJ\text{-}PKAc}$ cells is further supported by GO analysis, wherein 8 out of the 14 pathways significantly increased in clone 14 AML12$^{DNAJ\text{-}PKAc}$ cells were involved in cell cycle regulation. Another interesting finding was that 4 GO pathways that were involved in mitochondrial function were induced: inner mitochondrial membrane protein complex, mitochondrial respiratory chain complex, oxidative phosphorylation, and mitochondrial protein complex. This finding relates back to one of the early papers describing FLC in which researchers found increased number and volume of mitochondria that filled the cytoplasm by electron microscopy, along with intramitochondrial inclusions and fragmented cristae[3,123]. These data suggest that there is a component of this disease that disrupts normal mitochondrial processes. This phenomenon will be discussed more in **chapter 4**.

For obvious reasons, drug discovery for patients with FLC is of great interest[124]. Armed with a cell model that mimics certain aspects of human FLC, we can begin to predict targets that might be valuable for early drug discovery. Using a novel kinome regularization analysis, we highlighted potential kinase dependency for AML12$^{DNAJ\text{-}PKAc}$ cell proliferation, including Braf and Fgfr4, which independently share signaling through MEK/ERK. ERK involvement in FLC

pathogenesis will be discussed in **chapter 3**. Of additional recent interest are Hipk2, which was also identified by KiR and is known to regulate cell cycle[125], and Plk2, which is important in mitosis[126]. Taken together with data presented earlier highlighting the prominent role cell cycle progression plays in AML12$^{DNAJ\text{-}PKAc}$ cells, these two kinases might hold promise as therapeutic targets, if their importance in cell proliferation in AML12$^{DNAJ\text{-}PKAc}$ cells can be validated by RNAi or other pharmacologic methods.

Chapter 3: An acquired scaffolding function of the DNAJ-PKAc fusion enhances oncogenesis in fibrolamellar carcinoma

Fibrolamellar carcinoma (FLC) is a variant of liver cancer that has distinctive histologic features. This rare cancer afflicts healthy adolescents and young adults between the ages of 15-25 with no history of liver disease[3]. This latter feature can compromise early diagnosis of FLC as patients frequently present with vague symptoms that include abdominal pain, loss of appetite, or a palpable mass. The diagnosis is often made after disease has spread outside the liver, leading to an overall survival of 35%[7]. Unfortunately, FLC frequently recurs, as it is intractable to standard chemotherapies and radiation. Surgical resection is currently the only opportunity for a cure[8].

Recent transformative advances in our understanding of the molecular basis of FLC offer renewed hope for the development of drug therapies to treat this disease[12]. Sequencing tumor genomes of FLCs identified the underlying genetic defect as a heterozygous in-frame deletion of ~400 kb in chromosome 19[12-19]. This genetic lesion leads to translation of a *de novo* chimeric gene product where the chaperonin-binding domain of heat shock protein 40 (DNAJ) is fused to the Ca subunit of PKA. We have recently shown that DNAJ-PKAc is solely expressed in FLCs, is cAMP-responsive, and importantly is incorporated into A-Kinase Anchoring protein (AKAP) signaling complexes[107]. This latter property provides a mechanism by which this pathological kinase is sequestered within defined subcellular locations and in immediate proximity to a subset of target substrates[64,127,128]. Here we report that the DNAJ-PKAc fusion kinase is recruited into AKAP signaling complexes where it selectively interacts with the chaperonin heat shock protein 70 (Hsp70). This cellular chaperonin is frequently up-regulated in cancers and facilitates protein folding thereby providing an explanation as to why levels of DNAJ-PKAc

protein are elevated over wild type PKA in FLCs, and creating a unique therapeutic target for combinations of Hsp70 and kinase inhibitors.

3 Results

3.1 Differential substrate binding in AML12$^{DNAJ\text{-}PKAc}$ cells

The active site of DNAJ-PKAc is identical to that of the native kinase; both PKA forms are inhibited by PKI and are sensitive to ATP analog inhibitors[107,112]. Yet, it remained important to ascertain whether the substrate specificity of this pathological fusion enzyme is altered in FLC. To determine the differential protein-protein interactions, doxycycline-inducible flag-PKAc and flag-DNAJ-PKAc AML12 cells were subjected to affinity-purified mass spectrometry in collaboration with the Gordan lab. While RIα and RIIα were found to interact with wild type PKAc, only RIIα and RIIβ came down with DNAJ-PKAc (**Table 3.1**). Interestingly, the other hit found in DNAJ-PKAc that was not identified in PKAc pulldown is BCL2 associated athanogene 2 (Bag2). Through its BAG domain, Bag2 can interact with Hsp70 and promote the release of client proteins through Hsp70's ATPase domain[129].

Bait	Prey Gene	Prey Protein	Avg. Intensity	Fold Change	FDR
PKAc	*Gsto1*	Glutathione S-Transferase Omega 1	2.458	6.364	0
PKAc	*Prkaca*	Protein kinase A, catalytic subunit alpha	4.95	13.171	0
PKAc	*Prkar2a*	Protein kinase A, regulatory subunit 2 alpha	8.786	36.885	0
PKAc	*Akt2*	AKT2	0.901	3.556	0
PKAc	*Akap9*	Akap9; Yotiao	2.183	5.809	0
PKAc	*Prkar1a*	Protein kinase A, regulatory subunit 1 alpha	2.466	6.562	0
PKAc	*Nt5c2*	Cytosolic purine 5-nucleotidase	1.911	3.327	0.001
PKAc	*Prkacb*	Protein kinase A, catalytic subunit beta	1.147	3.053	0.002
PKAc	*Uso1*	Transcytosis Associated Protein	0.856	2.654	0.01
PKAc	*Zrab2*	Zinc finger Ran-binding domain-containing protein 2	1.606	2.442	0.037
DNAJ-PKAc	*Dnajb1*	Heat shock protein 40	3.863	9.052	0
DNAJ-PKAc	*Prkaca*	Protein kinase A, catalytic subunit alpha	3.699	8.921	0.001
DNAJ-PKAc	*Prkar2a*	Protein kinase A, regulatory subunit 2 alpha	6.061	8.767	0.001
DNAJ-PKAc	*Prkar2b*	Protein kinase A, regulatory subunit 2 beta	2.237	5.241	0.001
DNAJ-PKAc	*Bag2*	BCL2 associated athanogene 2	3.568	6.787	0.021

Table 3.1. Affinity-purified mass spectrometry identifies differential binding partners with DNAJ-PKAc. Virally infected AML12 cells expressing either wild type PKAc or DNAJ-PKAc were bait proteins for affinity-purified mass spectrometry. Proteins identified as interacting partners are identified as prey proteins; average intensity, fold change, and false discovery rate (FDR) are presented.

Given the presence of an intact J-domain, we next evaluated the formation of DNAJ-PKAc/Hsp70 complexes in our cell lines. Immunoblot analysis detected DNAJ-PKAc within Hsp70 immune complexes isolated from our AML12$^{DNAJ-PKAc}$ cell line, while PKAc was not detected in Hsp70 immune complexes isolated from control AML12 cells (**Fig. 3.1a**). Further immunoprecipitation experiments in our clinical samples revealed that DNAJ-PKAc interacts with heat shock protein 70 (Hsp70; **Fig. 3.1b**), a cellular chaperonin that facilitates protein folding and is frequently up-regulated in cancers[130,131]. *In situ* analysis by proximity ligation (PLA), a technique that amplifies detection of native protein-protein interactions that occur within in a range of 40-60nm[132], was used to measure DNAJ-PKAc/Hsp70 sub-complexes (**Fig. 3.1 c & d**). In control cells, few puncta were evident when PLA was performed with antibodies against PKAc and Hsp70 (**Fig. 3.1c**). Counterstaining with antibodies against actin (green) and DAPI

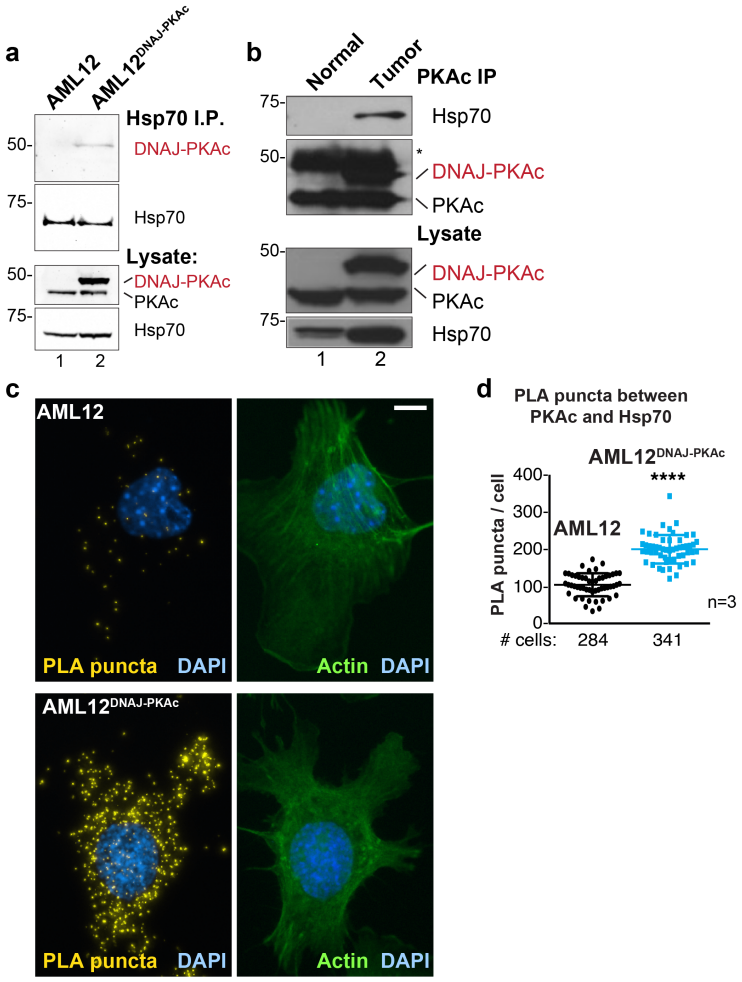

Fig. 3.1. Identification of Hsp70 interaction with DNAJ-PKAc. a) Immunoblot detection of PKA in Hsp70 immune complexes isolated from clone 14 AML12$^{DNAJ-PKAc}$ cells but not detected in wild type AML12 cells. Lysate loading controls indicate both forms of PKA and levels of Hsp70**. b)** Immunoblot detection of Hsp70 in PKAc immune complexes isolated from FLC but not detected in normal adjacent liver. Lysate loading controls indicate both forms of PKA and levels of Hsp70**. c-d).** Proximity Ligation (PLA) detection of proteins within 40-60 nm of each other in AML12 and clone 14 AML12$^{DNAJ-PKAc}$ cells. **Yellow puncta** identify Hsp70-kinase sub-complexes. Actin stain (**green**) marks cytoskeleton and DAPI staining **(blue)** marks nuclei. **d)** Box-whisker plots of Hsp70-kinase sub-complexes**.** Amalgamated data **(PLA puncta/cell)** from AML12 **(black)** and AML12$^{DNAJ-PKAc}$ **(blue)** cells. Number of cells analyzed over 3 independent experiments is indicated below each plot; data are shown as mean ± s.d., $p<0.0001$ by Student's t-test.

(blue) defined whole-cell and nuclear boundaries respectively. In contrast, quantitation of PLA puncta (yellow) from >200 AML12$^{DNAJ\text{-}PKAc}$ cells revealed increased amounts of the DNAJ-PKAc/Hsp70 sub-complex in our gene-edited cell lines (**Fig. 3.1 c & d**). Thus, our AML12$^{DNAJ\text{-}PKAc}$ cell line affords a disease relevant model with sufficient material to explore the mechanism of action of DNAJ-PKAc/Hsp70 assemblies.

3.2 Combination drug screening of the DNAJ-PKAc complex

We showed AML12$^{DNAJ\text{-}PKAc}$ cells have similar levels of PKA activity and comparable migratory properties to the wild type cell line (**Fig. 2.2 & supplemental Fig. S1**). Therefore, we surmised that the oncogenic nature of DNAJ-PKAc may not be simply due to changes in intrinsic kinase activity, but rather results from the recruitment of Hsp70. A logical extension of this premise is to determine whether pharmacologically blocking Hsp70 influences proliferation of AML12$^{DNAJ\text{-}PKAc}$ cells. Ver-155008 is an ATP-analog inhibitor of Hsp70 (IC50 = 0.5μM) that halts cell proliferation in several cancer models[133,134]. However, sole application of this drug over a range of concentrations did not have a differential effect on the viability of AML12$^{DNAJ\text{-}PKAc}$ cells compared to wild type AML12 cells as assessed by MTS assay at 72 hours (**Fig. 3.2a**). Consequently, we screened drug combinations that target additional elements within DNAJ-PKAc/Hsp70 signaling complexes, in collaboration with SEngine Precision Medicine. Cells were seeded and screened against a panel of 125 FDA-approved anti-cancer compounds[135] in the presence or absence of Ver-155008 (**Fig. 3.2b-f**). Cell viability was assessed by CellTiter-Glo assay and plotted against a standard deviation (Z-score) derived from collated mean responses (**Fig. 3.2b & c**). Drug combinations in the lower right quadrant (*Sensitivity*) are more effective at reducing proliferation than drug combinations plotted in the upper right quadrant (*Resistance*). In wild type AML12 cells, which lack the fusion enzyme, there was little change in the response to any of the FDA-approved drugs irrespective of whether the Hsp70 inhibitor was present (**Fig. 3.2b**). However, AML12$^{DNAJ\text{-}PKAc}$ cells were refractory to most FDA approved anti-cancer drugs in the absence of

Ver-155008, suggesting that the expression of DNAJ-PKAc is sufficient to induce chemoresistance. Moreover, when we repeated the drug screen was repeated in the presence of 10μM Ver-155008, AML12$^{DNAJ-PKAc}$ cells became responsive to many drugs (**Fig. 3.2c & d**). Of particular interest is a cluster of three drugs (**Fig. 3.2b-d**, pink dots) that preferentially suppressed the growth of AML12$^{DNAJ-PKAc}$ cells compared to parental cells.

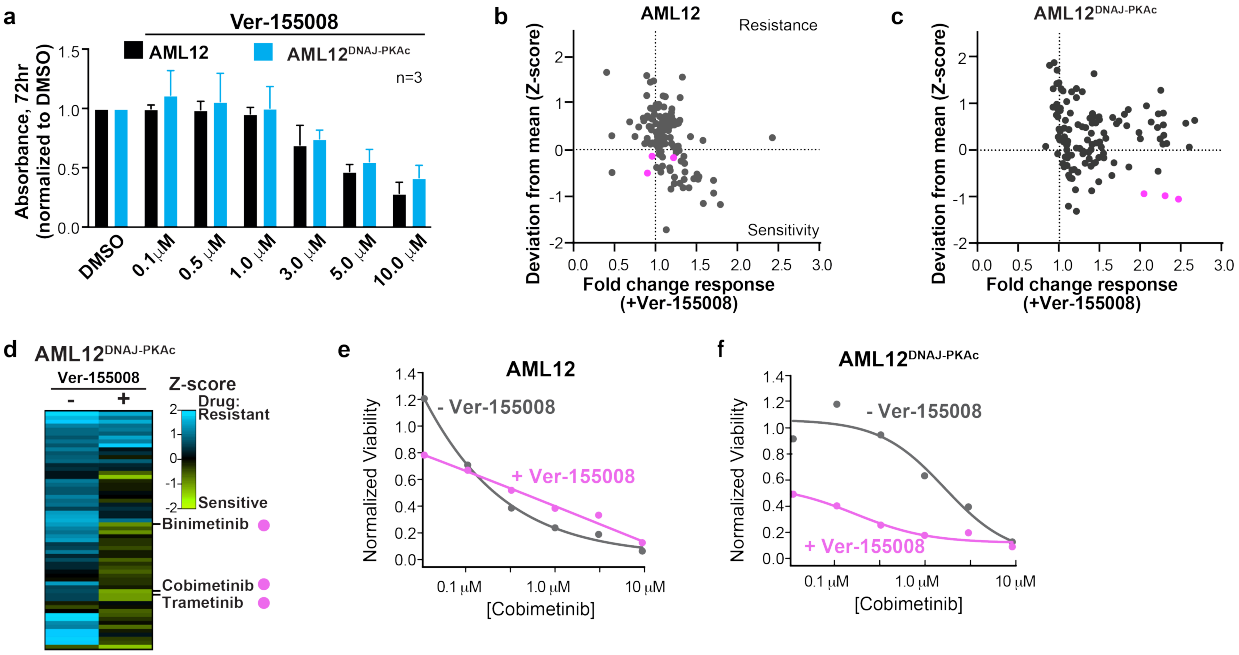

Fig. 3.2. Combination drug sensitivity screening of AML12$^{DNAJ-PKAc}$ cells. a) Cell growth with the Hsp70 inhibitor Ver-155008 in wild type AML12 **(black)** and clone 14 AML12$^{DNAJ-PKAc}$ **(blue)** cells measured by MTS assay. Concentrations of drug used in each condition are indicated below each column. **b & c)** Scatterplots show relative resistance or sensitivity of **b)** AML12 and **c)** AML12$^{DNAJ-PKAc}$ cells to the combination of 125 different chemotherapeutic drugs with Ver-155008. Drug combinations in the lower right quadrant are more sensitive to drug treatment than those in the upper right quadrant. Three drug combinations (**pink circles**) were identified for further validation, as they were more toxic to cells expressing DNAJ-PKAc than cells only expressing wild type kinase. **d)** Heat map of a subset of these data compares AML12$^{DNAJ-PKAc}$ cell survival with and without Ver-155008. AML12$^{DNAJ-PKAc}$ cells show drug resistance when treated with binimetinib, cobimetinib, or trametinib alone (**left, blue**) but they are more sensitive when these drugs are combined with Ver-155008 (**right, green**). **e & f)** Analysis of **e)** wild type AML12 and **f)** AML12$^{DNAJ-PKAc}$ cell survival. Dose-response of cobimetinib alone, (**grey**) or in combination with Ver-155008 (**pink**). Drug concentrations (μM) are indicated.

Deconvolution of our screening data revealed that the compounds indicated by the pink dots were all MEK kinase inhibitors cobimetinib, binimetinib and trametinib. Further validation that these Hsp70/MEK inhibitor cocktails selectively target AML12$^{DNAJ-PKAc}$ cells was obtained when

the combination drug screen was repeated using lower doses of Ver-155008 (3μM; **supplemental Fig. S2**). Dose response curves revealed that wild type AML12 cells are sensitive to cobimetinib alone (**Fig. 3.2e**) whereas AML12$^{DNAJ\text{-}PKAc}$ cells were more resistant to this drug over the same concentration range (**Fig. 3.2f**). Importantly, in the presence of Ver-155008 the cytotoxic effect of cobimetinib in AML12$^{DNAJ\text{-}PKAc}$ cells was enhanced (**Fig. 3.2f**). Taken together, results of our drug screen provided two exciting new pieces of information: 1) inhibition of Hsp70 in conjunction with blocking the RAF-MEK-ERK kinase cascade selectively affects the growth of cells expressing a single allele of DNAJ-PKAc, and 2) drug combinations that target DNAJ-PKAc/Hsp70 assemblies offer a therapeutic strategy for FLC that warrants further investigation.

3.3 Localizing the DNAJ-PKAc complex to AKAPs

On the basis of our understanding of how local signaling events are organized, we reasoned that AKAPs may be integral components of DNAJ-PKAc complexes[128]. A logical candidate was AKAP-Lbc, a multifunctional anchoring protein and enhancer of ERK signaling that interacts with another scaffolding protein, kinase suppressor of Ras (KSR-1), to form the core of a signaling network that integrates cAMP regulation of RAF-MEK-ERK signaling[128] (**Fig. 3.3a**). We found that AKAP-Lbc protein is up-regulated in human FLCs as compared to normal adjacent liver (**Fig. 3.3b**) and immunoblot analysis detected DNAJ-PKAc in AKAP-Lbc immune complexes isolated from FLCs (**Fig. 3.3c**). Parallel experiments show that DNAJ-PKAc/Hsp70 sub-complexes co-fractionate with this anchoring protein in AML12$^{DNAJ\text{-}PKAc}$ cells (**Fig. 3.3d**). Thus AKAP-Lbc can sequester Hsp70 and DNAJ-PKAc with an ERK signaling cascade in AML12$^{DNAJ\text{-}PKAc}$ cells and human FLCs.

Detection of phospho-ERK1/2 is frequently used as a biochemical readout for activation of the RAF-MEK-ERK kinase cascade[136]. Notably, basal levels of phospho-ERK 1/2 were elevated 2.8

± 1.5 fold (n=4) in AML12$^{DNAJ\text{-}PKAc}$ cells as compared to wild type controls (**Fig. 3.3e**). Immunofluorescent detection of phospho-ERK provided *in situ* confirmed this finding as phospho-ERK signal was barely detectable in control AML12 cells (**Fig. 3.3f & g**), but clearly evident in the cytoplasm of AML12$^{DNAJ\text{-}PKAc}$ cells (**Fig. 3.3h & i**). Actin (red) and DAPI (blue) were used as cytoskeletal and nuclear markers respectively. We next monitored the efficacy of Hsp70/MEK inhibitor cocktails on basal ERK activity in AML12$^{DNAJ\text{-}PKAc}$ cells. In wild type cells, treatment with Ver-155008 (3μM) alone had no effect on ERK activation (**Fig. 3.3j**). However, administration of cobimetinib (100nM) or a combination of both drugs abolished detection of the phospho-ERK signal (**Fig. 3.3j**). In contrast, basal phospho-ERK levels were high in AML12$^{DNAJ\text{-}PKAc}$ cells, treatment with Ver-155008 (3μM) alone had a modest effect on phospho-ERK signal and application of cobimetinib (100nM) or in combination with Ver-155008 abolished detection of phospho-ERK signals (**Fig. 3.3j**). Thus, dual inhibition of Hsp70 and the RAF-MEK-ERK cascade impedes mitogenic signals to preferentially block proliferation of AML12$^{DNAJ\text{-}PKAc}$ cells.

One intriguing query resulting from our findings is whether or not interrupting the association between DNAJ-PKAc and Hsp70 impacts activation of the RAF-MEK-ERK cascade. Mutation of a conserved HPD motif that demarks a critical loop in DNAJ domain abolishes interaction with Hsp70[33] (**Fig 3.3k**), thus substitution of H33 to Q DNAJ-PKAc would be expected to prevent association with endogenous Hsp70 in AML12 cells (**Fig. 3.3l**). Wild type AML12 cells were transfected with vectors encoding DNAJ-PKAc or DNAJ-PKAc H33Q. Immunoblot detection confirmed that basal levels of phospho-ERK were elevated upon introduction of DNAJ-PKAc in wild type AML12 cells but transfection with the DNAJ-PKAc H33Q mutant prevented ERK activation (**Fig. 3.3m**). Densitometry analysis of four independent experiments confirmed this result (**Fig 3.3m**, graph). Control immunoblotting monitored total ERK levels as a loading control and confirmed equivalent expression of each DNAJ-PKAc form in transfected cells.

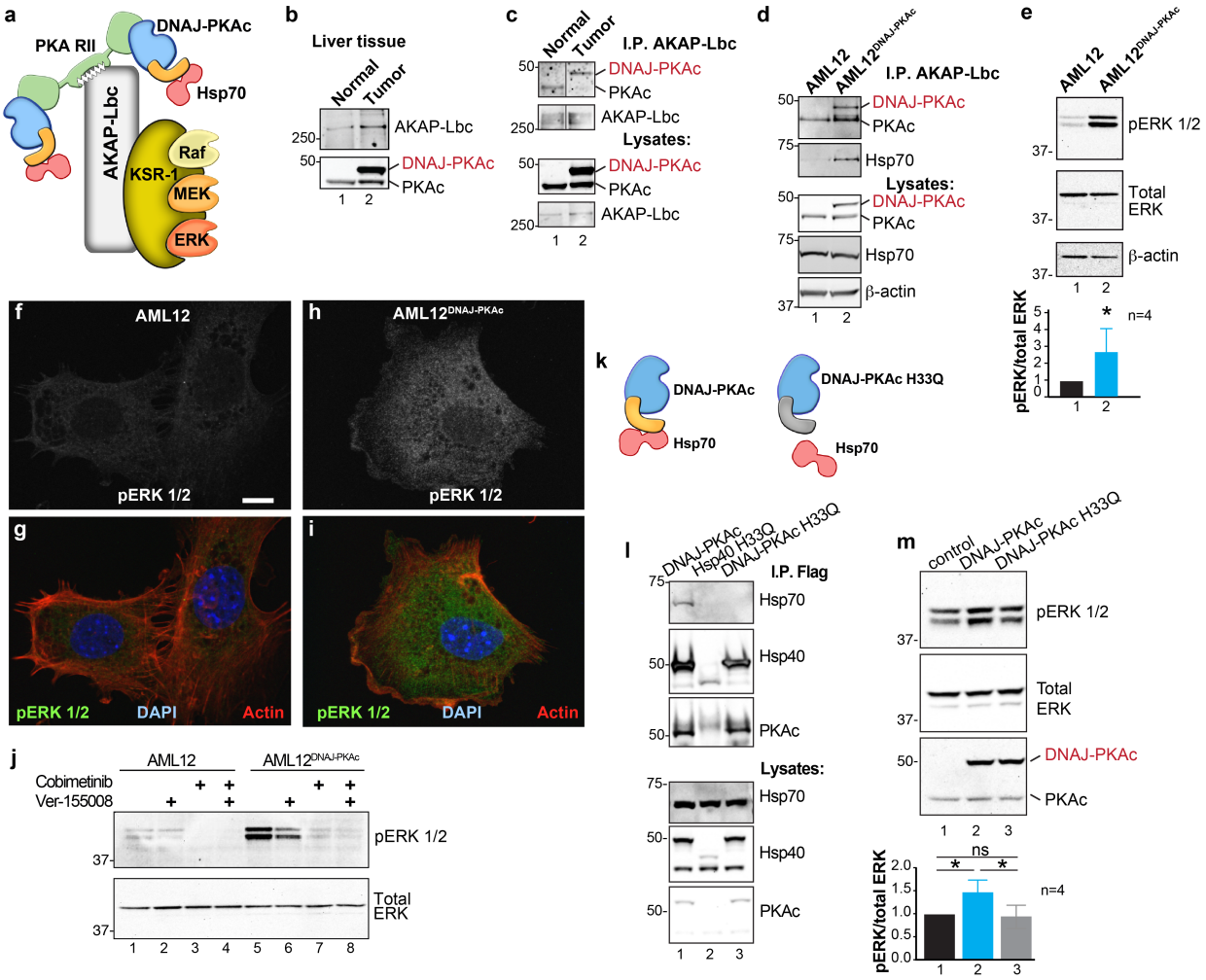

Fig. 3.3. Pharmacologically targeting DNAJ-PKAc assemblies. a) Schematic of an AKAP-Lbc-KSR-1 macromolecular assembly that sequesters Hsp70 and DNAJ-PKAc with elements of the ERK kinase cascade. **b)** Immunoblots of paired FLC and normal adjacent liver probed with antibodies to AKAP-Lbc and PKAc. **c)** Immunoblot detection of PKAc in AKAP-Lbc immune complexes from normal adjacent tissue and FLC. PKAc and AKAP-Lbc in tissue lysates are indicated. DNAJ-PKAc **(red)** is indicated. **d)** Co-immunoprecipitation of signaling elements with AKAP-Lbc. Immunoblot detection of PKAc and Hsp70 in immune complexes isolated from clone 14 AML12$^{DNAJ\text{-}PKAc}$ cells. PKAc and Hsp70 detected in lysates from wild type and AML12$^{DNAJ\text{-}PKAc}$ cells. Actin served as loading control. **e)** Immunoblot detection of phospho-ERK1/2 **(top)** as an index of ERK kinase activity in cell lysates from AML12 and clone 14 AML12$^{DNAJ\text{-}PKAc}$ cells. **Bottom)** Immunoblot detection of total ERK served as a loading control. Quantification of immunoblots (n=4); mean ± s.d. and p=0.04. **f-l**) *In situ* immunofluorescence of basal ERK activity. Grayscale images depicting immunofluorescent detection of phospho-ERK in **(f)** wild type and **(h)** clone 14 AML12$^{DNAJ\text{-}PKAc}$ cells. Composite images of phospho-ERK **(green),** actin **(red)** and nuclei **(blue)** in **(g)** wild type and **(i)** AML12$^{DNAJ\text{-}PKAc}$ cells. Scale bar (10 μm). **j)** Immunoblot detection of phospho-ERK 1/2 in wild type AML12 **(lanes 1-4)** and AML12$^{DNAJ\text{-}PKAc}$ cells **(lanes 5-8)**. Cells were treated with 100nM cobimetinib, 3μM Ver-155008 or combination of both drugs. Detection of total ERK served as loading control. **k)** Schematics of native DNAJ-PKAc (**left**) and DNAJ-PKAc H33Q mutant that cannot bind Hsp70 (**right**, **gray**). **l)** Flag immunoprecipitation of Hsp70 in AML12 cells expressing DNAJ-PKAc (**lane 1**) but not in DNAJ-PKAc H33Q cells (**lane 3**). Controls for IP are listed. **m)** Immunoblot detection of phospho-ERK1/2 in AML12 cells transiently transfected with DNAJ-PKAc (**lane 2**) or DNAJ-PKAc H33Q (**lane 3**). Total ERK served as a loading control. Detection of PKAc monitored transfection efficiency. Quantitation of blots from 4 experiments, p=0.01.

3.4 Downstream substrate bias towards ERK in FLC and AML12$^{DNAJ\text{-}PKAc}$ cells

Independent support for our hypothesis was provided through a collaboration with the Ong lab with a label-free phosphoproteomic screen[137] that identified 2,912 unique phosphopeptides in wild type and AML12$^{DNAJ\text{-}PKAc}$ cells lines (**Fig. 3.4a**). Of these, 96 phosphopeptides were increased (orange) and 76 were reduced in AML12$^{DNAJ\text{-}PKAc}$ cells (black). A list of the top 50 dysregulated phosphopeptides is found in **Appendix I, supplementary table S3**. Substrate profiling using the NetworKIN platform[138] revealed that 23% of ERK phosphosites were up-regulated in AML12$^{DNAJ\text{-}PKAc}$ cells whereas only 3% of PKA consensus sites were enriched (**Fig. 3.4b**). Significant enrichment of PKC (7%), DAP kinase (5%) and CDK (3%) phosphosites was also evident. Parallel experiments in human FLC supported our hypothesis. Phosphoproteomic profiling of human FLC and adjacent normal liver samples by label-free LC-MS/MS analysis identified 7,697 phosphopeptides[137] (**Fig. 3.4c**). Of these, 628 phosphopeptides were significantly enriched in FLCs as compared to adjacent normal liver (**Fig. 3.4c**; **orange**; statistical significance calculated by ANOVA t test, $\log_2$ ratio >1). Substrate profiling with the NetworKIN platform predicted consensus kinase phosphorylation motifs[138]. Of the phospho-sites increased in FLC, 20% were putative PKC targets and 8% were ERK-MAPK sites (**Fig. 3.4d**). Interestingly, PKA phosphosites were only enriched by 7% (**Fig. 3.4d**). These systemwide analyses suggest that DNAJ-PKAc/Hsp70 macromolecular assemblies bias the signaling landscape toward ERK activation and mobilize other downstream kinase networks.

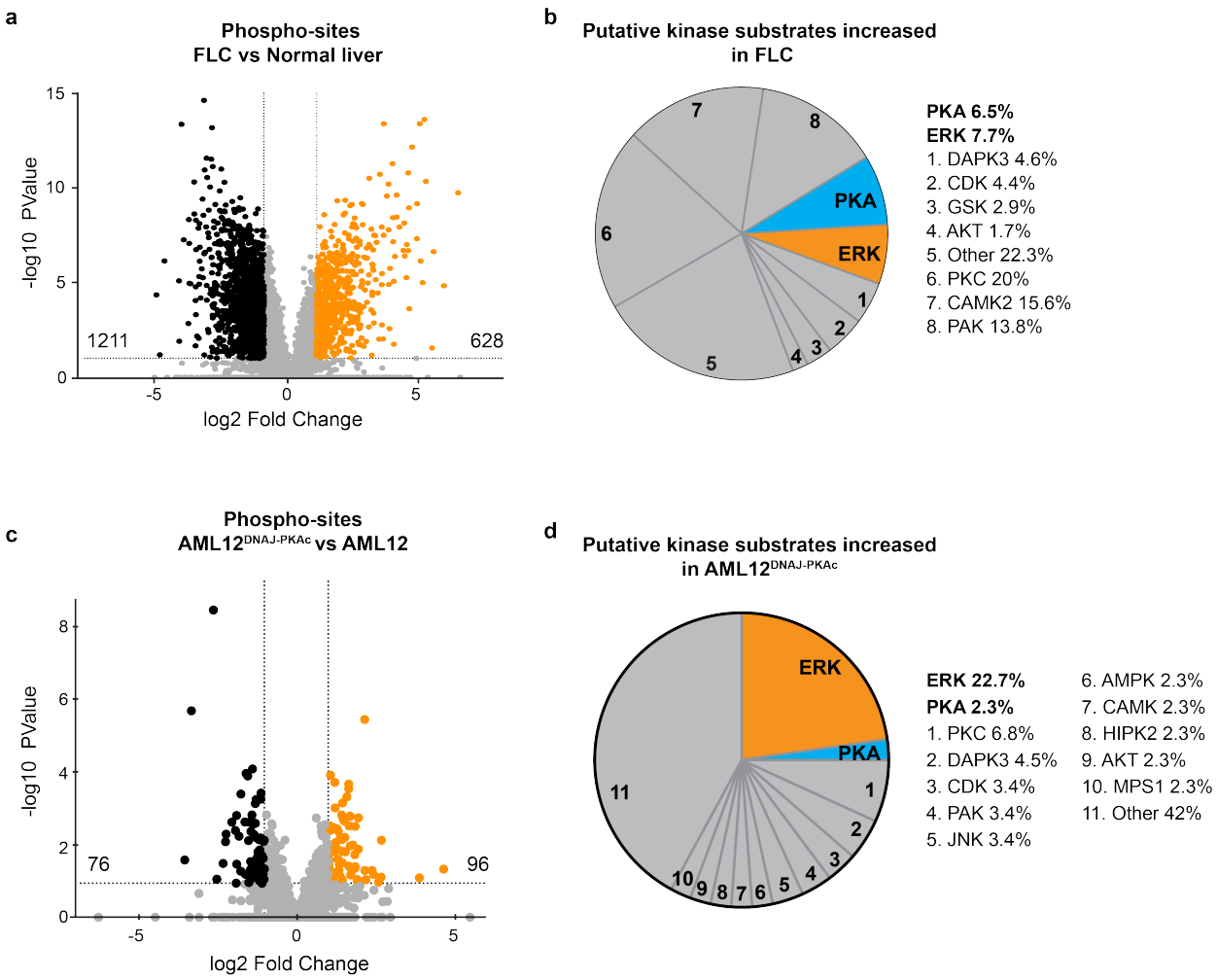

Fig. 3.4. Phosphoproteomic profiling of FLC and AML12$^{DNAJ-PKAc}$ cells. a & b) Phosphoproteomic profiling of FLC. Statistical significance was calculated by students t test with Log_{10}-transformed p-values of individual phosphopeptides plotted against log_2-transformed fold change in abundance in FLC. **a)** Volcano plot showing phosphosites upregulated (**orange**) and downregulated (**black**) in FLC as compared to normal adjacent liver (<0.05 false discovery rate). **b)** Pie chart of putative kinase substrates (predicted by NetworKIN) increased in FLC. 82.8% of sites identified were in the NetworKIN platform. Percentages of sites ascribed to particular kinase are listed. "Other" kinases include: CK1, TTK, GRK, RSK, MAK, JNK, ROCK, P70S6K, AMPK, CLK, HIPK2, PDHK, ACTR2, ATM, DMPK, IKK, MOK, NEK4, PKD1, PKG, TGFBR2, and p38-MAPK. **c & d)** Differential phosphoproteomic profiling of AML12$^{DNAJ-PKAc}$ cells. **c)** Volcano plot showing abundance (**orange**) and reduction (**black**) of phosphopeptides in clone 14 AML12$^{DNAJ-PKAc}$ cells. Statistical significance was calculated by Student's t test with Log_{10}-transformed p-values of individual phosphopeptides plotted against log_2-transformed fold change. **d)** Pie chart of putative kinase substrates increased in AML12$^{DNAJ-PKAc}$ cells. Sites identified by NetworKIN platform. Individual kinases are listed. "Other" kinases include: CK, ABL2, GRK, GSK3, JAK2, NLK, and SRC.

3 Discussion

We have discovered that DNAJ-PKAc, a unique fusion protein that is emblematic of FLC, functions as a scaffolding protein that assembles additional signaling elements that contribute to the pathogenesis of this cancer. More specifically, we show that the chaperonin-binding domain of this FLC-specific fusion enzyme supports recruitment of the co-chaperonin Hsp70, creating a unique molecular context in which the DNAJ-PKAc chimera acts in FLCs. Chaperones such as Hsp70 have been shown to contribute to carcinogenesis in multiple ways[130,131,139]. They can repair misfolded proteins to reduce cellular stress or, as we believe is the case of FLC, recruitment of Hsp70 through the DNAJ domain preferentially stabilizes the chimeric PKAc fusion protein. This hypothesis is borne out by data in **figure 2.1** wherein we demonstrate that protein levels of the DNAJ-PKAc variant are elevated in tumor samples and cell lines as compared to native PKA. Two cellular consequences could result from the preferential stabilization of DNAJ-PKAc. Since aberrant kinase activity drives many cancers, we initially reasoned that augmented PKA activity could boost cAMP responses in a manner that contributes to the pathobiology of FLC[117,118]. However, enzymological data in **figure 2.2** shows that basal and cAMP responsive kinase activity in AML12$^{DNAJ\text{-}PKAc}$ cells is similar to wild type hepatocytes. Additionally, DNAJ-PKAc and the native kinase share similar sensitivities to the inhibitor PKI, efficiently bind R subunits to form PKA holoenzymes, and associate with AKAPs[107,112]. Our second postulate is that re-localization of Hsp70 to AKAP complexes by DNAJ-PKAc may be a critical event in transformation in FLC patients. Thus, the chaperonin binding properties of DNAJ-PKAc may be more relevant to oncogenesis than its intrinsic kinase activity. On the basis of these findings, we propose that the genetic lesion in chromosome 19 that is a hallmark of FLC incorporates a new binding interface that transforms PKA from a single-function enzyme into a scaffolding protein with pathological implications.

Chaperonopathies are a group of diseases caused by genetic lesions or aberrant post-translational modifications of molecular chaperones[140]. "Chaperonopathies by mistake" are a group of related disorders, including certain cancers, in which chaperonin activity is normal, but becomes inappropriately assimilated into molecular pathways that enhance disease progression[140]. We believe that formation of DNAJ-PKAc/Hsp70 sub-complexes in FLC is emblematic of this latter category. Moreover, the abnormal pairing of these enzymes creates new and unique drug targets, which provided rationale to screen a panel of recognized chemotherapeutics in combination with an Hsp70 inhibitor to ascertain if certain whether drug pairings act synergistically to inhibit proliferation of AML12$^{DNAJ\text{-}PKAc}$ cells (**Fig. 3.2b-f**)

Our findings have opened up a surprising new line of inquiry by implicating ERK signaling in FLC. Although molecular links between ERK and DNAJ-PKAc were not immediately evident, we reasoned that one commonality was the proto-oncogene AKAP-Lbc. PKA activity has been implicated in the phosphorylation of RAF kinase and KSR-1 in the context of AKAP-Lbc signaling complexes[141]. As shown in **figure 3.3b-d**, AKAP-Lbc is upregulated in human FLCs, and interacts directly with RAF-MEK-ERK kinase signaling scaffolds. Our drug screening data provided the first evidence that this mitogenic signaling pathway is up-regulated in our FLC model.

The relationship between cAMP and ERK signaling is complex and context dependent[142], and PKA has pleotropic effects on tumor-initiation[104,143]. Paradoxically, a recent report postulates that PKA activity leads to mesenchymal-to-epithelial transitions that impede oncogenesis, yet DNAJ-PKAc kinase activity is thought to be necessary for tumor initiation[104,143]. Therefore, one pertinent and unanswered question is whether or not the kinase activity residing within DNAJ-PKAc is necessary for FLC progression. We therefore generated an analog-sensitive form of the fusion kinase (DNAJ-PKAc M176A) that is targeted by the kinase inhibitor analog 1NM-PP1[144].

Application of 1NM-PP1 did not exert an additional inhibitory effect on basal ERK activation in cells expressing this form of DNAJ-PKAc (**supplemental Fig. S3**). Together our results imply that recruitment of Hsp70 enhances basal ERK signaling in AML12$^{DNAJ\text{-}PKAc}$ cells and infers that the intrinsic PKA activity is less essential for this process. This view is corroborated by our drug-screening data in **figure 3.2**, demonstrating that combinations of Hsp70 and clinically available MEK inhibitors halt the growth of AML12$^{DNAJ\text{-}PKAc}$ cells.

One advantage of screening FDA-approved compounds is that the pharmacotoxicity, therapeutic indices, and off-target effects of most components are well documented. Accordingly, each MEK inhibitor identified in our screen has been approved for the treatment of melanoma and other cancers[145]. Another benefit of the combination screening approach is the potential to identify drug combinations that can be used at lower effective doses; however there is also the possibility that new drug combinations may prove more toxic. This could be an important consideration for Ver-155008 as clinical trials with other Hsp70 inhibitors hold promise for the treatment of cancers[146]. Although the utility of Hsp70 and MEK inhibition as combination therapy for FLC is far from clear, our discovery of drug pairs that halt the growth of AML12$^{DNAJ\text{-}PKAc}$ cells but not wild type hepatocytes provides a valuable tool to further the investigation for new treatments of this debilitating disease that afflicts children and young adults.

Chapter 4: Changes in mitochondrial dynamics in AML12$^{DNAJ\text{-}PKAc}$ cells

The neoplastic hepatocytes in fibrolamellar carcinoma (FLC) have been classically characterized as eosinophilic, and since FLC was first described in 1980, an increased number and size of mitochondria have been reported in these cells[3,123]. Indeed, one group performed electron microscopy on three FLCs in 1982, and reported many swollen mitochondria with intramitochondrial inclusions and sparse, fragmented cristae, all packed tightly in the cytoplasm of tumor cells[123]. Mitochondria are known to be the "powerhouses of the cell", are key generators of ATP[147], and are involved in other processes in the cell, including apoptosis[148], calcium signaling[149], and cellular metabolism[150]. Interestingly, mitochondrial mutations and changes in mitochondrial DNA have previously been reported in classic HCCs[151-153]. When mitochondrial DNA content was measured in FLCs, researchers found that despite the apparent increases in number of mitochondria, total mitochondrial DNA was decreased compared to surrounding normal liver; however, metastatic FLCs had very high levels of mitochondrial DNA[154]. These data suggest that total mitochondrial DNA content does not necessarily correlate with mitochondria number in FLC, and that additional studies are necessary. As a corollary, FLC patients can develop hyperammonemia, *i.e.* toxic levels of ammonia in the blood that can cause acute encephalopathy[155-163]. Serum ammonium is normally broken down by the urea cycle, some of which happens in the mitochondria of hepatocytes. While hyperammonemia has been described in other cancers, such as HCC[164], acute myeloblastic leukemia[165], and multiple myeloma[166], the cause in FLC remains uncertain. Here, we explore mitochondrial dynamic changes resulting from DNAJ-PKAc overexpression specifically by investigating apoptosis, mitochondrial respiration, and mitochondrial membrane potential in our AML12$^{DNAJ\text{-}PKAc}$ cell line.

4 Results

4.1 Pro-survival phenotype of AML12$^{DNAJ\text{-}PKAc}$ cells

Investigation into the differences between DNAJ-PKAc and wild type PKAc led us to examine protein stability and degradation. Cyclohexamide is an inhibitor of protein synthesis in eukaryotic cells, and is used to assess protein stability. Cyclohexamide can also induce apoptosis in hepatocytes, potentially via the extrinsic pathway[167]. Wild type AML12 and AML12$^{DNAJ\text{-}PKAc}$ cells in standard cultures were subjected to cyclohexamide treatment for up to 48 hours, and lysates were collected at various timepoints and probed for PKAc, with Gapdh as a loading control (**Fig. 4.1a**). Cyclohexamide treatment for 32 hours decreased the overall viability of wild type AML12 cells, and by 48 hours, there were no viable cells left. In AML12$^{DNAJ\text{-}PKAc}$ cells, DNAJ-PKAc protein was stable out to 48 hours, and these cells were still viable after treatment with cyclohexamide for that length of time. These data showed that DNAJ-PKAc protein is more stable than wild type PKAc, and AML12$^{DNAJ\text{-}PKAc}$ cells are more resistant to cyclohexamide-induced apoptosis than parent cells.

To investigate the potential anti-apoptotic phenotype of AML12$^{DNAJ\text{-}PKAc}$ cells, we explored different mechanisms of inducing apoptosis in these cells. Staurosporine (STS) is a general kinase inhibitor and a well-known potent inducer of apoptosis by activation of capase-3[168]. Parental AML12 and AML12$^{DNAJ\text{-}PKAc}$ cells were cultured and different concentrations of STS were added, with cell viability assayed by cell confluence (**Fig. 4.1b**). AML12$^{DNAJ\text{-}PKAc}$ cells showed resistance to STS treatment, while AML12 cells were sensitive to even small amounts of STS.

Etoposide is another way to induce apoptosis, by inhibiting DNA synthesis. Etoposide forms a complex with DNA and topoisomerase II, induces breaks in DNA, and prevents DNA repair, thus leading to cell death[169]. Etoposide was included in SEngine's library of 125 compounds[135], thus

was administered to parental AML12 and AML12$^{DNAJ\text{-}PKAc}$ cells at 6 dilutions, with cell growth assayed by luminescence (**Fig 3.2**). AML12$^{DNAJ\text{-}PKAc}$ cells were more resistant to etoposide treatment than parental AML12 cells (**Fig. 4.1c**). Importantly, combination treatment with the Hsp70 inhibitor Ver-155008 and etoposide caused AML12$^{DNAJ\text{-}PKAc}$ cells to revert back to the phenotype of the wild type cells, which also showed increased sensitivity to dual treatment (**Fig. 4.1d**). Taken together, our data demonstrate that AML12$^{DNAJ\text{-}PKAc}$ cells are more resistant to multiple different mechanisms of inducing apoptosis: extrinsic death receptor pathway, caspase-3-induced apoptosis, and DNA damage-induced apoptosis.

Evidence for a potential mechanism behind the anti-apoptotic phenotype observed in AML12$^{DNAJ\text{-}PKAc}$ cells came from a reverse-phase protein array (RPPA). RPPA is a targeted proteomics method that can quantify the expression of a specific set of proteins across a collection of tissues or cell lines, and can also measure post-translational modifications such as phosphorylation or acetylation[170]. Compared to mass spectrometry, RPPA has a higher sensitivity for low abundance proteins, although it is restricted to proteins to which there are good phospho-specific antibodies. Whole cell lysates from wild type AML12, clone 10, and clone 14 AML12$^{DNAJ\text{-}PKAc}$ cells were extracted and subjected to RPPA, in collaboration with the Gujral lab. Forty of the antibodies showed differential signal between these cell lines (heatmap, **Fig. 4.1e**). Five phospho-sites were significantly increased in both clone 10 and clone 14 AML12$^{DNAJ\text{-}PKAc}$ cells. Four of these phospho-sites are activated by the Akt-mTOR-S6 pathway: p-Akt (S473), p-mTOR (S2448), and p-S6 (S240/244 and S235/236). The fifth phospho-site that was enriched in AML12$^{DNAJ\text{-}PKAc}$ cells was on Bcl1 antagonist of cell death (Bad; S112) (**Fig. 4.1e**). Increased p-S6 (S240/244) along with p-Akt (S473) and p-Bad (S112) in AML12$^{DNAJ\text{-}PKAc}$ cells was confirmed by western blotting, as was p-Bad (S155), a known PKA target (**Fig. 4.1f & g**). This finding of increased mTOR signaling in AML12$^{DNAJ\text{-}PKAc}$ cells mirrors the increased mTOR signaling found in human FLCs[16,28,171]. Specifically, an increase in p-S6(Thr389) and p-

S6(Ser235/236) was identified by Riehle *et.al* by immunohistochemistry in FLC sections[28]; increased p-S6(Ser240/244) was identified by Cornella *et.al*[16]; and p-mTOR(Ser2448) was identified by Sahin *et.al*[171] While the connection between increased mTOR activity and expression of DNAJ-PKAc is unknown, these data strengthens the rationale for use of AML12$^{DNAJ\text{-}PKAc}$ cells as a *bona fide* model of FLC.

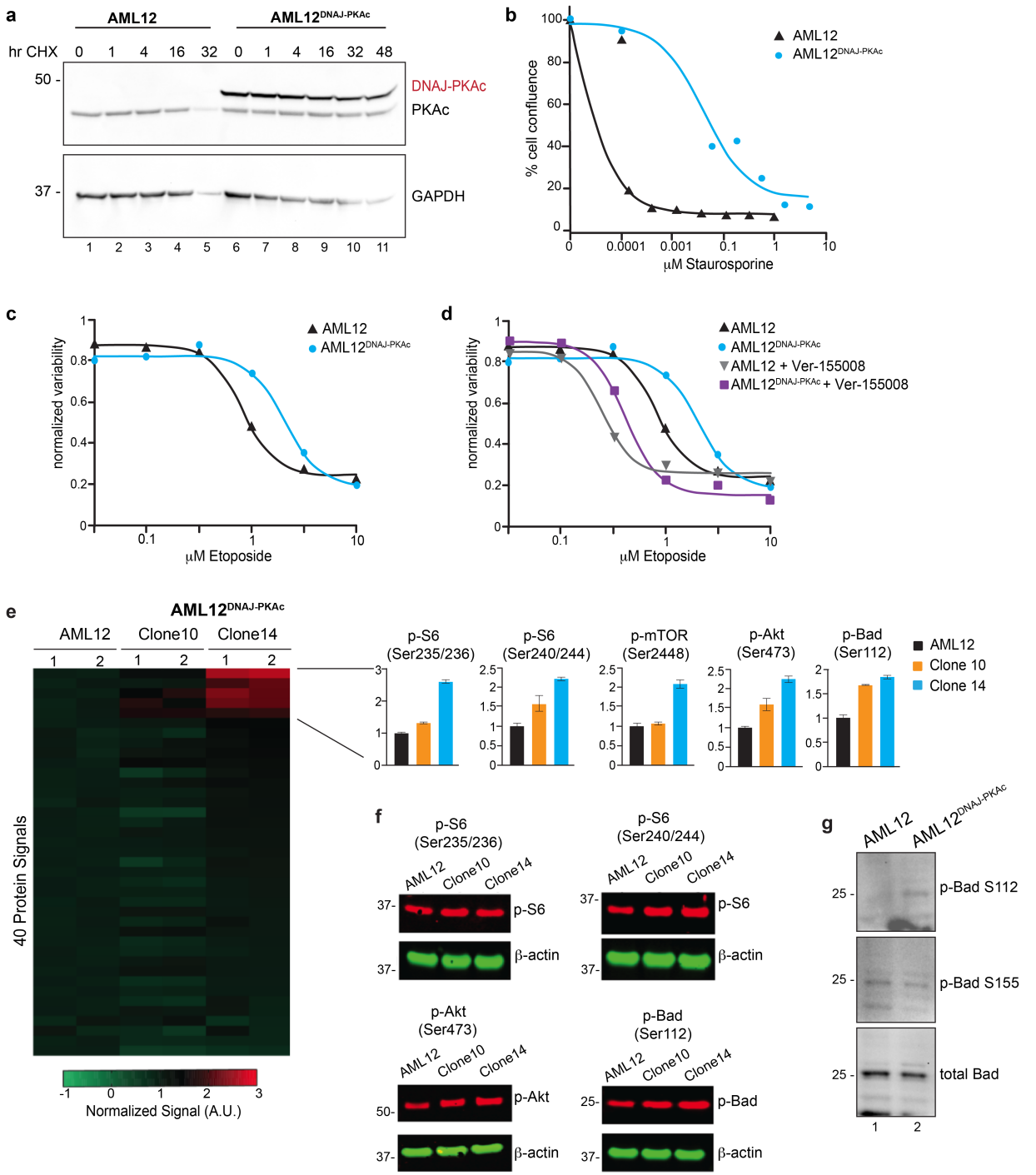

Fig. 4.1. Identification of a pro-survival phenotype and increased p-Bad Ser112 in AML12$^{DNAJ\text{-}PKAc}$ cells. a) Immunoblot detection of PKA following cyclohexamide treatment. Parental AML12 and clone 14 AML12$^{DNAJ\text{-}PKAc}$ cell lysates were collected at 0, 1, 4, 16, 32, and 48 hours; parental AML12 cells did not survive past 32 hours with cyclohexamide treatment. Gapdh (bottom panel) served as loading control. **b)** Analysis of cell survival after etoposide treatment in AML12 (**black**) and AML12$^{DNAJ\text{-}PKAc}$ cells (**blue**) from SEngine drug screen. Dose response of etoposide alone is presented. Drug concentrations (μM) are indicated. **c)** Analysis of cell survival with etoposide treatment with Ver-155008 in AML12 (**gray**) and clone 14 AML12$^{DNAJ\text{-}PKAc}$ cells (**purple**) from SEngine drug screen. Dose responses to etoposide with and

without Ver-155008 are presented. Drug concentrations (μM) are indicated. **e)** RPPA analysis of wild type AML12 (**black**), clone 10 (**orange**) and clone 14 (**blue**) AML12$^{DNAJ\text{-}PKAc}$ cells. Heatmap (left) of 40 protein signals with normalized signal; red indicates increased signal. Bar graphs of 5 signals that are in clone 10 and clone 14 versus wild type AML12 cells; p-Akt (S473), p-mTOR (S2448), p-S6 (S240/244 and S235/236) and p-Bad (S112). Signals are normalized to those of wild type AML12=1. **f)** Immunoblot validation of p-Akt (S473), p-S6 (S240/244 and S235/236) and p-Bad (S112) in wild type AML12, clone 10, and clone 14 lysates in Gujral laboratory. β-actin served as loading control. **g)** Immunoblot validation of p-Bad S112 and p-Bad S155 in wild type AML12 and clone 14 AML12$^{DNAJ\text{-}PKAc}$ cells. Total Bad served as internal control.

4.2 Increased oxidative phosphorylation and mitochondrial membrane potential in AML12$^{DNAJ\text{-}PKAc}$ cells

Mitochondria are involved in apoptosis[148], calcium signaling[149], and the citric acid cycle[147], and are considered the powerhouses of the cell by producing ATP via oxidative phosphorylation[150]. In the matrix of the mitochondria, the citric acid cycle consumes and regenerates citrate. Two reducing agents, NADH and FADH2, are produced through the citric acid cycle and are key for initiating oxidative phosphorylation. Production of ATP occurs in the inner mitochondrial membrane, and is highly dependent on the electrochemical transmembrane potential ($\Delta\psi_m$). Back in the 1920's, Warburg and Cori observed increased glucose consumption in cancer cells and assumed that the mitochondria were generating energy directly from glucose rather than via oxidative phosphorylation. This is famously called the Warburg effect (reviewed most recently in [172]). However, many studies have shown that the mitochondria are functional in many cancer types, and are able to produce ATP via oxidative phosphorylation[173].

While these two hypotheses are at odds in terms of whether or not cancer cells decrease oxidative phosphorylation, it is agreed that cell metabolism changes in cancer[174]. We thus wanted to characterize the cellular metabolism of AML12$^{DNAJ\text{-}PKAc}$ cells, specifically to determine oxygen consumption rates (OCR) and extracellular acidification rate (ECAR) as readouts of mitochondrial oxidative phosphorylation and glycolysis, respectively. Using a Seahorse XF96 Extracellular Flux Analyzer in collaboration with the Hockenbery lab, we examined mitochondrial

bioenergetics by taking baseline OCR measurements, then measuring real-time changes in OCR following sequential addition of oligomycin, carbonyl cyanide-4-(trifluoromethoxy)phenylhydrazone (FCCP), and a mix of antimycin A and rotenone, which measure ATP-linked respiration, maximal respiration, and non-mitochondrial respiration, respectively. Raw OCR and ECAR results are presented in **figure 4.2a.** Averaging data from **figure 4.2a** with the addition of FCCP, AML12$^{DNAJ\text{-}PKAc}$ cells had increased maximal respiration rate compared to parental AML12 cells (**Fig. 4.2b**). Spare respiratory capacity (measured by subtracting basal respiration from maximum respiration) is also increased in AML12$^{DNAJ\text{-}PKAc}$ cells (**Fig. 4.2c**), as is ATP-linked respiration (after normalization to basal respiration) (**Fig. 4.2d**). Proton leak can be measured by non-mitochondrial respiration subtracted from ATP-linked respiration and is increased in AML12$^{DNAJ\text{-}PKAc}$ cells (**Fig. 4.2e**). While these preliminary data require increased vigor before making definitive conclusions, they suggest that AML12$^{DNAJ\text{-}PKAc}$ cells have higher oxidative phosphorylation than wild type AML12 cells; opposite to that of the Warburg effect

As mentioned above, ATP synthesis requires an electrochemical transmembrane potential ($\Delta\psi_m$), and since AML12$^{DNAJ\text{-}PKAc}$ cells have increased ATP synthesis, we surmised that AML12$^{DNAJ\text{-}PKAc}$ cells have increased mitochondrial membrane potential as well. We explored this hypothesis with tetramethylrhodamine (TMRM). TMRM is a cationic fluorophore that accumulates in hyperpolarized mitochondria and correlates with $\Delta\psi_m$[175]. Parental AML12 and AML12$^{DNAJ\text{-}PKAc}$ cells were treated with TMRM and Mitotracker Green (a mitochondrial dye that is non-membrane-potential dependent) and images were collected (**Fig. 4.1f & g**). Quantification of the ratio of TMRM:Mitotracker Green from one experiment (>90 cells each) showed that AML12$^{DNAJ\text{-}PKAc}$ cells had a higher membrane potential than parental AML12 cells (**Fig. 4.2h**), which correlates with the observed increase in oxidative phosphorylation.

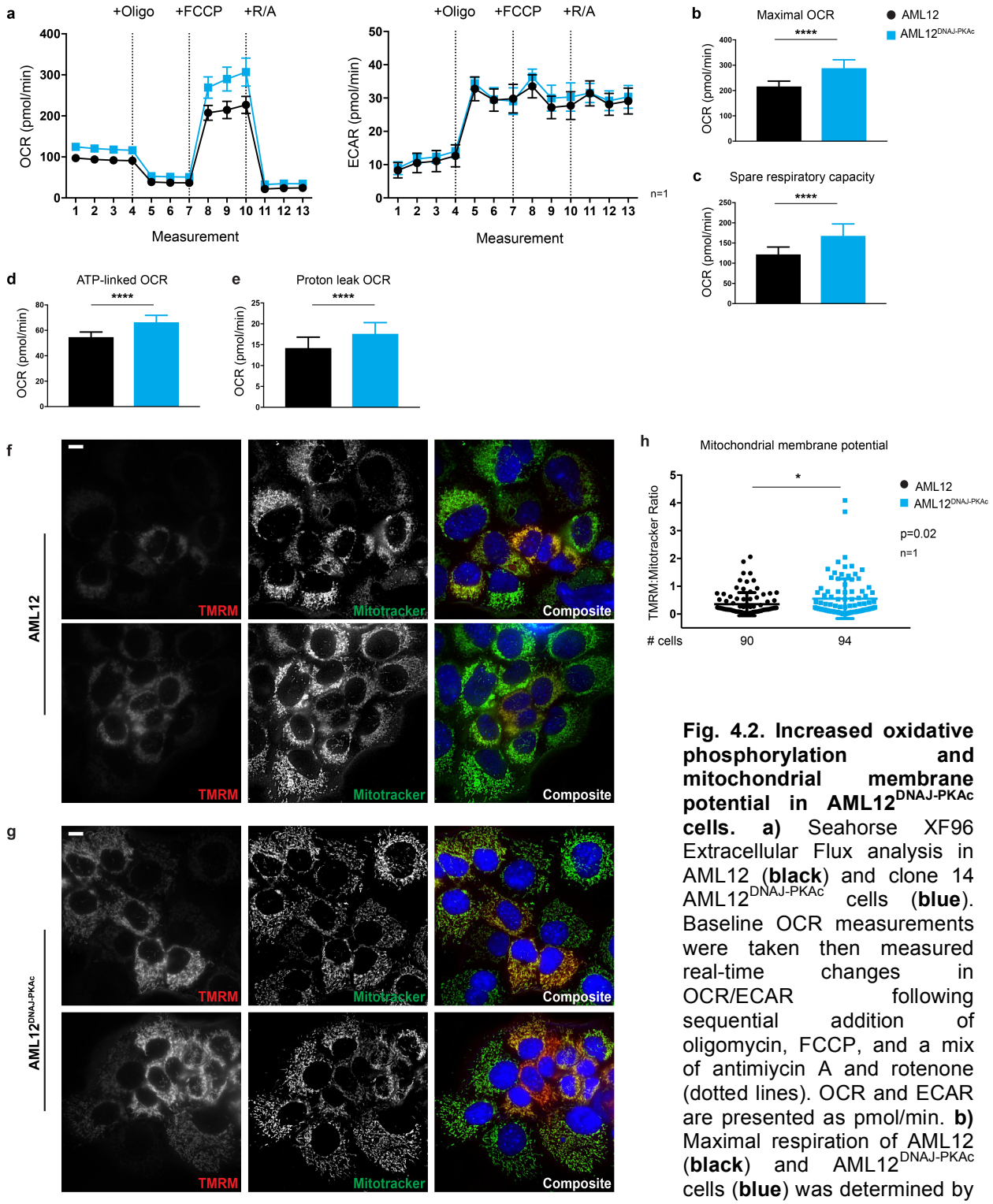

Fig. 4.2. Increased oxidative phosphorylation and mitochondrial membrane potential in AML12$^{DNAJ-PKAc}$ cells. a) Seahorse XF96 Extracellular Flux analysis in AML12 (**black**) and clone 14 AML12$^{DNAJ-PKAc}$ cells (**blue**). Baseline OCR measurements were taken then measured real-time changes in OCR/ECAR following sequential addition of oligomycin, FCCP, and a mix of antimiycin A and rotenone (dotted lines). OCR and ECAR are presented as pmol/min. **b)** Maximal respiration of AML12 (**black**) and AML12$^{DNAJ-PKAc}$ cells (**blue**) was determined by averaging measurements 8-10. Data presented as mean ± s.d. **f-h)** Mitochondrial membrane potentials were quantified as the ratio of TMRM (red, left panels) to Mitotracker Green (green, middle panels) in **f)** AML12 cells and **g)** AML12$^{DNAJ-PKAc}$ cells. Composite shows overlaid images, scale bars represent 10μm. **h)** Quantification of ≥90 cells from one experiment show increased mitochondrial membrane potential in AML12$^{DNAJ-PKAc}$ cells.

MKT-077, a cationic rhodacyanine dye and relative of TMRM, is an allosteric Hsp70 inhibitor that has been shown to bind Hsp70's nucleotide binding domain and inhibits DNAJ-stimulated ATP hydrolysis[176,177]. Specifically, MKT-077 inhibits a mitochondrial-localized Hsp70 known as Grp75 (*Hspa9*; also known as mortalin-2)[176], and has been shown to selectively inhibit growth in a variety of cancer cells[176,178,179]. The current theory to explain these findings is that MKT-077 is positively charged, so it can pass through hydrophobic barriers of the cell membrane and accumulates in the negatively charged mitochondria. Cancer cells are generally thought to have a higher mitochondrial membrane potential[180], thus MKT-077 is preferentially retained in oncogenic cells compared to healthy ones[176,178]. One emerging hypothesis is that Grp75 sequesters p53 in the cytoplasm of transformed cells; however upon treatment with MKT-077, it binds Grp75 and induces release of p53 which translocates back to the nucleus to restore function and arrest growth[176,179]. This sequence of molecular events was confirmed in NIH3T3 cells[176]; however, in human thyroid carcinoma cells (TT and MZ-CRC-1), the toxicity of MKT-077 was independent of p53[181]. To determine the effect of MKT-077 in cells expressing DNAJ-PKAc, parental AML12 and AML12$^{DNAJ\text{-}PKAc}$ cells were cultured with and without MKT-077 at the indicated concentrations for 72 hours, and cell viability was measured by MTS. Treatment with increasing concentrations of MKT-077 (**Fig. 4.3a**) led to a striking decrease in growth in AML12$^{DNAJ\text{-}PKAc}$ cells when compared to parental AML12 cells.

To determine whether this profound effect on AML12$^{DNAJ\text{-}PKAc}$ cell proliferation is dependent on p53, parental AML12 and AML12$^{DNAJ\text{-}PKAc}$ cells were treated with MKT-077 or DMSO for 48 hours, fixed in paraformaldehyde, and stained with antibodies against p53, actin and nuclei (**Fig. 4.3b and c**). Quantification of mean intensity of p53 expression in the nucleus with or without MKT-077 treatment in parental AML12 and AML12$^{DNAJ\text{-}PKAc}$ cells revealed that there was a slight decrease in p53 localization to the nucleus in MKT-077-treated parental AML12 cells, but p53 localization was not altered in AML12$^{DNAJ\text{-}PKAc}$ cells after MKT-077 treatment (**Fig. 4.3d**). This

result might be counterintuitive, as one group showed p53 translocation into the nucleus in HCC cell lines (Huh7 and Hep3B), but only with combination of Hsp70 and Hsp90 inhibition (MKT-077 and 17-AAG, respectively)[182]. The addition of an Hsp90 inhibitor might be necessary for p53 re-localization to the nucleus upon treatment, and might explain the mechanism of MKT-077 sensitivity in AML12$^{DNAJ\text{-}PKAc}$ cells.

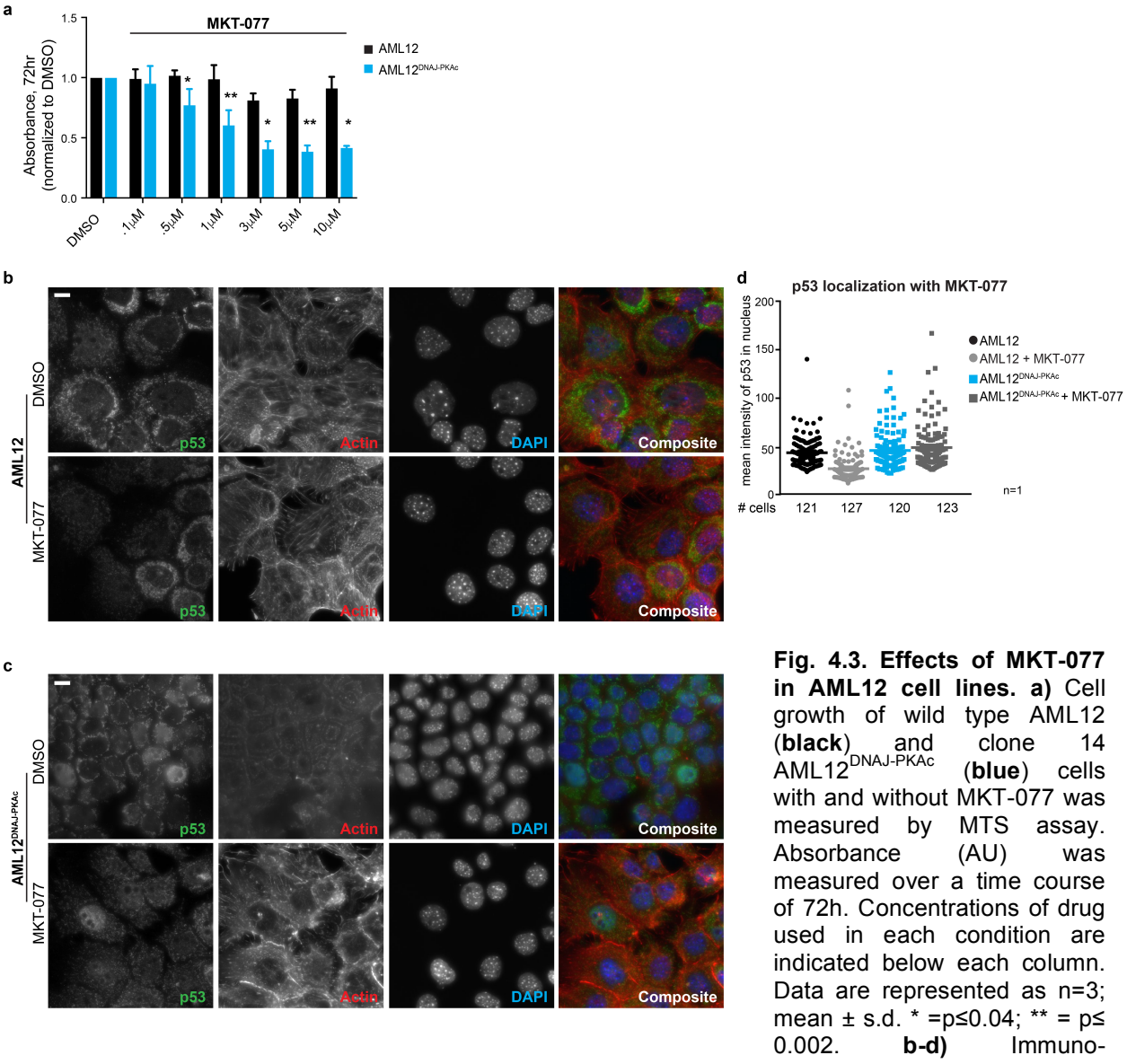

Fig. 4.3. Effects of MKT-077 in AML12 cell lines. a) Cell growth of wild type AML12 (**black**) and clone 14 AML12$^{DNAJ\text{-}PKAc}$ (**blue**) cells with and without MKT-077 was measured by MTS assay. Absorbance (AU) was measured over a time course of 72h. Concentrations of drug used in each condition are indicated below each column. Data are represented as n=3; mean ± s.d. * =p≤0.04; ** = p≤ 0.002. **b-d)** Immuno-fluorescent images from **b)** AML12 and **c)** clone 14 AML12$^{DNAJ\text{-}PKAc}$ cells treated with or without MKT-077 for 48 hours. Endogenous p53 is stained in green; actin and DAPI are in red and blue, respectively. Composite shows overlaid images, scale bars represent 10μm. **d)** Quantification of the mean gray value of p53 staining in the nucleus in AML12 (**black**), AML12 + MKT-077 (**gray**), AML12$^{DNAJ\text{-}PKAc}$ (**blue**), and AML12$^{DNAJ\text{-}PKAc}$ + MKT-077 (**dark gray**). Over 100 cells were analyzed in one experiment.

4 Discussion

Serendipitously, in the course of other experiments, we found that AML12$^{DNAJ\text{-}PKAc}$ cells are more resistant to several apoptosis-inducing agents, including cyclohexamide, staurosporine, and etoposide. This suggests a pro-survival phenotype in cells expressing DNAJ-PKAc. Evidence for one potential mechanism behind these findings came from RPPA data showing increased phospho-Bad at Ser112 in AML12$^{DNAJ\text{-}PKAc}$ cells. Interestingly, this RPPA also highlighted increased mTOR signaling in AML12$^{DNAJ\text{-}PKAc}$ cells, specifically p-Akt (S473), p-mTOR (S2448), and p-S6 (S240/244 and S235/236). These data correlate with those from human FLCs, wherein mTORC signaling is also increased, as observed by increased p-mTOR (S2448), and p-S6 (S240/244 and S235/236)[16,28,171]. These data further support our use of AML12$^{DNAJ\text{-}PKAc}$ cells as an *in vitro* model of FLC.

Bad is a protein involved in regulating the intrinsic pathway of apoptosis. When Bad is dephosphorylated in the absence of growth signals or glucose, Bad binds to Bcl-xL and Bcl-2; this binding leaves Bax to dimerize with Bak and initiate mitochondrial outer membrane permeabilization (MOMP) and release of cytochrome c[183,184]. MOMP is thought of as the point of no return for apoptotic cell death. When Bad is phosphorylated, it is unable to bind Bcl-xL or Bcl-2, and is instead sequestered to the cytoplasm by 14-3-3 proteins and has pro-survival functions[185]. So, the phosphorylation event seen in cells expressing DNAJ-PKAc inhibits the pro-apoptotic function of Bad. There are 3 phosphorylation sites that influence the activity of Bad: Ser112 (human Ser75), phosphorylated by both ribosomal protein S6 kinase alpha-1 (Rps6ka1)[186] and by PKAc[187]; Ser136 (human Ser99), phosphorylated by Akt[188]; and Ser155 (human Ser118), a PKAc phosphorylation site[189]. One proposed theory is that phosphorylation of at least two serines is required before Bad's pro-apoptotic function is fully inhibited[190,191]. It was further determined that mitochondrial-anchored PKAc was responsible for Bad-phosphorylation at Ser112[192]. There are three AKAPs that are known to localize to the

mitochondria, and could thus regulate this phosphorylation event; sphingosine kinase interacting protein (SKIP, inner mitochondrial membrane)[72]; AKAP1 (dAKAP1 or AKAP149)[193] and Wave-1[194] (outer mitochondrial membrane). As described in chapter 3, we have discovered that DNAJ-PKAc is able to form a complex with AKAPs[107] (**Fig. 3.3**). Other investigators showed that AKAP1-anchored PKA increased the survival of PC12 cells by phosphorylating Bad at Ser155, while an AKAP1 mutant that couldn't bind PKA promoted apoptosis[195].

Mitochondrial-anchored PKA is also a key regulator of mitochondrial fragmentation and elongation. Dynamin-related protein 1 (Drp1), along with other outer mitochondrial membrane proteins, is thought to constrict the mitochondria in a GTP-dependent process, resulting in mitochondrial fragmentation[196]. While Drp1 has several phosphorylation sites, PKA is the only known kinase that phosphorylates Ser647, which inhibits Drp1 and prevents mitochondrial fission[197,198]. Mitochondrial fission is an early event in apoptosis, and elongated mitochondria can protect against degradation and thus maintain ATP production[199,200]. One group in particular showed that upon starvation of HCC cell lines, PKA-dependent Drp1 phosphorylation is protective against mitophagy, and an increase in phos-Drp1 predicted poor prognosis in HCC patients[199]. AKAP1 has been established as an important regulator of Drp1 activity, as it promotes Drp1 phosphorylation by sequestering local PKA to the outer mitochondrial membrane[197,198,201]. Drp1 inhibition is also predicted to coincide with the activation of Bax to initiate MOMP and apoptosis[202]. Interestingly, other investigators demonstrated that a Drp1 phospho-mimetic (Ser647Asp) showed resistance to staurosporine- and etoposide-induced apoptosis, while a mutant of Drp1 that could not be phosphorylated by PKA (Ser647Ala) sensitizes cells to the same apoptosis inducers when compared to wild type Drp1[197].

Based on our data, deonstrating increased Bad phosphorylation and a pro-survival phenotype in cells expressing DNAJ-PKAc, we hypothesize that DNAJ-PKAc is incorporated into

mitochondria-anchored AKAPs such as AKAP1 or WAVE-1. We further hypothesize that due to the increased abundance of DNAJ-PKAc compared to wild type PKAc, both in AML12$^{DNAJ-PKAc}$ cells and FLCs, more DNAJ-PKAc proteins are incorporated into mitochondrial AKAPs, potentially increasing the cAMP-responsive PKA activity of DNAJ-PKAc. This increased PKA activity at the mitochondria would be expected to drive enhanced Bad and Drp1 phosphorylation, thus contributing to the pro-survival phenotype observed in AML12$^{DNAJ-PKAc}$ cells. This potential increase in occupation of AKAPs by DNAJ-PKAc may be independent of increased AKAP levels, and could represent a shift in affinity towards DNAJ-PKAc anchoring. Specifically, expression levels of the transcripts that result in *AKAP1* and *WAVE-1* mRNA are not changed in RNAseq analysis between parental AML12 and AML12$^{DNAJ-PKAc}$ cells, and there is a trend towards a decrease in clone 14 AML12$^{DNAJ-PKAc}$ cells (logFoldChange= -0.61 and -0.96 for AKAP1 and WAVE-1, respectively). In human FLCs, *AKAP1* mRNA levels are also slightly decreased (logFoldChange= -0.9), and interestingly, phosDrp1 (S647) is increased in FLCs as compared to normal liver (data not shown). Nevertheless, it will be important to establish the expression of mitochondrial-anchored AKAPs in AML12 cell lines and human FLCs, and investigate the Drp1 phosphorylation state in AML12$^{DNAJ-PKAc}$ cells.

Cellular metabolism is a highly regulated process and is often altered in cancer[174]. The Warburg effect is the phenomenon by which cancer cells switch from oxidative phosphorylation to anaerobic glycolysis[172]. This effect is present in many cancer models, but other studies have shown that certain cancer cells are still able to use oxidative phosphorylation[173]. Another model, coined the Reverse-Warburg effect, hypothesizes that cancer cells induce neighboring fibroblasts to switch to anaerobic glycolysis[203]. These fibroblasts then secrete glycolytic metabolites, and the surrounding cancer cells take up these metabolites for use in the oxidative phosphorylation pathway. Researchers describe this process of cancer-associated fibroblasts feeding surrounding cancer cells as a host-parasite relationship[203]. Regardless, it is clear that

cancer cells can alter cellular metabolism to favor growth. In our experiments, we demonstrate that AML12$^{DNAJ\text{-}PKAc}$ cells have increased mitochondrial membrane potential and increased oxidative phosphorylation and compared to parental AML12 cells. These two observations are linked, as ATP synthesis is dependent on $\Delta\psi_m$. In **chapter 2**, we highlighted increased expression of oxidative phosphorylation and respiratory chain complex genes in AML12$^{DNAJ\text{-}PKAc}$ cells via GO analysis (**Fig. 2.3**). One obvious hypothesis generated by our data is that increased expression of genes involved in cellular metabolism leads to the increase in oxidative phosphorylation as measured by Seahorse assay. Knocking down key genes involved in ATP synthesis by RNAi in AML12$^{DNAJ\text{-}PKAc}$ cells and measuring oxidative phosphorylation will be key experiments to validate this hypothesis. While the link between DNAJ-PKAc and increased cellular respiration remains unclear, this phenotype could prove important to the pathogenesis of human FLC.

One question that remains to be investigated is whether or not AML12$^{DNAJ\text{-}PKAc}$ cells have hyper-fused mitochondria. It is wuidely accepted that cells with hyper-fused mitochondria generate more ATP, maintain a high $\Delta\psi_m$, undergo less mitophagy, and are more likely to be resistant to cellular stresses[204]. We have identified three out of these five characteristics in AML12$^{DNAJ\text{-}PKAc}$ cells. One way of confirming that DNAJ-PKAc expression leads to hyper-fused mitochondria would be to quantify the dispersal of mitochondrial-targeted photoactivatable GFP in AML12$^{DNAJ\text{-}PKAc}$ cells. This method of viewing the mitochondria generates an index of the mitochondrial fusion and morphology in cells; we hypothesize that AML12$^{DNAJ\text{-}PKAc}$ cells have more fused mitochondria than parental AML12 cells based on data in **figure 4**.

AML12$^{DNAJ\text{-}PKAc}$ cells are significantly and specifically susceptible to treatment with MKT-077, even at a low dose (0.5μM). This result remains very exciting as although MKT-077 was suspended in clinical trials due to renal toxicity[52], other derivatives of this compound warrant

further investigation. The mechanism behind this exquisite susceptibility in our cell model remains unclear. Treatment with MKT-077 alone is insufficient to re-localize p53 back to the nucleus, although this lack of effect could be due to the timepoint at which this experiment was conducted; and a shorter treatment time could be warranted. Alternatively, due to the high variation observed in our quantification data, increasing the number of replicates could begin to reveal an effect. Addition of an Hsp90 inhibitor to MKT-077 treatment would be another key experiment to determine if whether co-inhibition of Hsp70 and Hsp90 is sufficient to bring p53 back to the nucleus to induce apoptosis, as it has been previously shown in a hepatocyte cell line[182]. However, those data do not fully explain the profound effect of MKT-077 alone on AML12$^{DNAJ\text{-}PKAc}$ cell viability shown in **figure 4.3a**. Another possibility is that DNAJ-PKAc can anchor Grp75 (as it can anchor Hsp70, shown in **Fig. 3.1**), and that inhibiting this Hsp70 causes a decrease in cell proliferation specifically in AML12$^{DNAJ\text{-}PKAc}$ cells. Grp75 is primarily expressed in mitochondria, but has also been detected in the cytosol, the endoplasmic reticulum[205], and in cytoplasmic vesicles[206]. Expanding on the hypothesis presented earlier in this chapter, DNAJ-PKAc can bind AKAPs at the mitochondria and sequester Grp75 to this location via interaction with the DNAJ domain. Inhibition of Grp75 by MKT-077 could limit client proteins of Grp75, while also de-stabilizing the complex, potentially decreasing PKA activity and decreasing the pro-survival phenotype of AML12$^{DNAJ\text{-}PKAc}$ cells. At this time, these claims are unsubstantiated, and further studies are necessary to delineate the mechanism behind the substantial decrease in proliferation of AML12$^{DNAJ\text{-}PKAc}$ cells after MKT-077 treatment.

One last query worth mentioning is the non-hepatic hyperammonemia seen in FLC patients[162]. The urea cycle (also known as the Krebs cycle) is the pathway that expels excess ammonia that is produced during the metabolism of amino acids, and occurs both in the mitochondria and in the cytoplasm[207]. Ammonium reacts with carbon dioxide (a product of mitochondrial respiration) to form carbamoyl phosphate, a process catalyzed by the enzyme carbamoyl phosphate

synthetase I (Cps1). This reaction is the rate-limiting step of the urea cycle, and occurs in the mitochondria of hepatocytes. Next, carbamoyl phosphate reacts with ornithine via ornithine transcarbamylase (OTC) to produce citrulline. Citrulline is then transferred to the cytosol of hepatocytes, where arginosuccinate synthetase produces arginosuccinate, which is subsequently broken down to arginine and fumarate by the enzyme arginosuccinase. Arginine is then further broken down by arginase to produce urea and ornithine. Urea travels through the bloodstream to the kidney and is excreted in the urine, while ornithine is recycled back to the hepatocyte mitochondria to await the next cycle. In FLC patients, hyperammonemia has been reported in the absence of hepatocyte failure or chemotherapy exposure, suggesting that the urea cycle is directly disrupted by tumors[155]. This toxic accumulation of ammonia in the blood can cause acute encephalopathy and subsequent neurologic defects. In addition to general hepatocyte failure, hyperammonemia may result from mutations in *OTC*. However, several studies have identified hyperammonemia in FLC patients without liver failure *OTC* mutations[156,163,164]. One hypothesis for this increased ammonia load is that overexpression of *AURKA* in FLC[14] leads to up-regulation of c-Myc[208], which is known to increase OTC and thus drive ornithine to produce polyamines[156,209]. This process then decreases the availability of ornithine for the urea cycle, and could lead to ammonia accumulation in FLC patients. Another hypothesis for their increased serum ammonia levels is that FLCs utilize arginine to drive hepatocyte proliferation, thus leading to a relative deficiency in ornithine for the urea cycle, and again, backup of ammonia. This hypothesis is consistent from data reported by Malouf *et.al,* who found up-regulation of pyruvate dehydrogenase kinase 1 (PDK1) and lactate dehydrogenases (LDHA and LDHB)[21]. In FLCs, increased PDK1 activity would be expected to inactivate pyruvate dehydrogenase, which suppresses the Krebs cycle[210]. Simultaneously, increase of LDHA and LDHB could promote the conversion of pyruvate into lactate, and decreasing delivery of acetyl-coenzyme A to the Krebs cycle[21]. Interestingly, in our RNAseq analyses of AML12$^{DNAJ\text{-}PKAc}$ cells, we found that expression of the gene for PDK1 is increased

2.2-fold as compared to parental AML12 cells. However, genes encoding the lactate dehydrogenase A and D are expressed at similar levels in both cell lines. Further exploration into our RNAseq data highlighted similar expression levels of most genes responsible in the urea cycle, except one: *Cps1*. As stated above, this enzyme is not only the rate-limiting step of the urea cycle, but is also responsible for transforming ammonium and carbon dioxide into carbamoyl phosphate. Expression of the gene for this enzyme is decreased -6.5-fold in AML12$^{DNAJ\text{-}PKAc}$ cells as compared to parental AML12 cells, and is also decreased by -1.22-fold in an FLC mouse model (tumor versus normal liver)[104]. *CPS1* has also been shown to be mutated in 2 FLC patients[13]. Decreased expression of this enzyme would be expected to prevent clearance of ammonium through the urea cycle, and instead cause a buildup of ammonium. While we have only been able to investigate if this gene is dysregulated in one human FLC RNAseq dataset so far, the data presented above suggest a potentially new mechanism explaining increased ammonia in FLC, and a possible target to alleviate hyperammonemia in FLC patients. While the link between DNAJ-PKAc and *CPS1* is far from clear, our findings warrant further investigation.

Chapter 5: Discussion and future directions

5.1 Development of an *in vitro* model of FLC

Dissecting the molecular pathogenesis of FLC has been difficult to date due to lack of *in vitro* or *in vivo* models. Human hepatocytes are difficult to propagate, and while many labs have tried to culture primary FLCs, all have failed. There is currently one reported PDX model, derived from a FLC patient who had malignant ascites (a very rare event even in advanced FLC); this model recapitulates some but not all aspects of FLC[23]. Two independent groups introduced the DNAJ-PKAc fusion into mouse livers, and FLC-like tumors have been propagated in those animals[104,105]. These tumors take over 1 year to develop, however, limiting the utility of this mouse model for therapeutic testing. Actually, all three of the above models require a mouse as the host to propagate tumors. While these may be the best currently available for preclinical testing of novel therapeutics, we sought to develop a simpler model that we could easily manipulate, in order to precisely study the oncogenesis driven by DNAJ-PKAc. Fortunately, the region between *DNAJB1* and *PRKACA* is conserved from mice to humans, indicating the importance of that region from an evolutionary perspective. We used CRISPR/Cas9 gene editing to delete a 400kb region in non-transformed mouse hepatocytes, as human FLCs arise healthy young livers. We developed five clones containing this heterozygous 400kb deletion and in-frame fusion transcript. Clone 14 was chosen for the majority of our subsequent analyses, as it expresses the DNAJ-PKAc fusion protein and wild type PKAc at a similar ratio as human FLC, while still expressing the genes in-between *DNAJB1* and *PRKACA*. Of additional potential mechanistic interest is clone 10, which seems to be a homozygous knockout of wild type PKAc and overexpresses DNAJ-PKAc to an even greater extent than does clone 14, but still expresses genes in between *Dnajb1* and *Prkaca* (**Fig. 2.1**). Although clone 14 may be more relevant to FLC pathogenesis, clone 10 provides a model that eliminates wild type PKA signaling, allowing exclusive focus on the functions of the DNAJ-PKAc fusion protein.

Our novel cell line, termed AML12$^{DNAJ\text{-}PKAc}$ cells, proliferate faster than parental AML12 cells, as evidenced by MTS and BrdU incorporation assays. This pro-proliferative phenotype is also supported by our gene ontology analysis of RNA sequencing data, as many genes involved in cell cycle control pathways are up-regulated in AML12$^{DNAJ\text{-}PKAc}$ cells. We confirmed similar basal PKA kinase activity in AML12$^{DNAJ\text{-}PKAc}$ cells compared to AML12 similar to our reported findings in human FLC[107]. AML12$^{DNAJ\text{-}PKAc}$ cells do have slightly increased cAMP-stimulated PKA activity, also mirroring human FLCs[107]. This increase in stimulated kinase activity is thought to be due to the overexpression of both forms of PKA in human FLCs and AML12$^{DNAJ\text{-}PKAc}$ cells, though we propose an alternative hypothesis in **chapter 3**: binding of HSPs to DNAJ-PKAc stabilizes the protein complex. Evidence to support the latter hypothesis includes the cyclohexamide chase data reported in **chapter 4**, shich suggest that DNAJ-PKAc protein has a longer half-life than wild type PKAc. This result was confounded by the fact that cyclohexamide can also induce apoptosis, thus, addition of a protease inhibitor will be necessary to determine the half-life of DNAJ-PKAc.

5.2 Key findings and implications

Equipped with new reagents geared for studying initiating events in FLC, we were interested in identifying drugs that selectively decrease proliferation in AML12$^{DNAJ\text{-}PKAc}$ cells. SEngine, a precision medicine company in Seattle, has a screening library that includes FDA-approved chemotherapies as well as drugs in clinical development[135]. This feature is important, as we wanted to identify existing drugs that could be repurposed to treat FLC, as current FLC patients do not have the time for us to design a drug *de novo*. The SEngine drug screen was applied to our cells alone or in combination with Ver-155008, an Hsp70 inhibitor, since in **chapter 3** we describe that Hsp70 binds to DNAJ-PKAc. Our hypothesis regarding the importance of Hsp70 in the pathogenesis of FLC resulted from our understanding that the kinase domain of the fusion protein DNAJ-PKAc is extremely similar to that of native PKAc[112], thus a PKA kinase inhibitor

would not be able to distinguish between the two. Since Hsp70 is also a potential drug target, we surmised that drug combinations that target additional elements within DNAJ-PKAc could be successful. In concert with this notion, we found that dual inhibition of MEK and Hsp70 decreases cell viability in our cell model. Further, we identified increased ERK signaling in AML12$^{DNAJ\text{-}PKAc}$ cells (**Fig. 3.3)**, though FLC lysates did not show a similar increase in ERK signaling (data not shown). This discrepancy in our data could be because: 1) AML12$^{DNAJ\text{-}PKAc}$ cells are a model of disease initiation, and the human FLC lysates in our repository come from large tumors *i.e.* later in the disease process, so it may be that increased ERK signaling is only necessary in early tumor initiation; 2) this increase in ERK signaling is specifically localized to hepatocytes, and when FLC lysates are collected, we get many other cell types included in lysates, thus diluting the MEK/ERK signaling in tumors; and 3) when screening human tumors, we do not have the luxury of inhibiting phosphatases before collection or controlling the time from tumor excision to homogenous lysates, so we could be diluting ERK signaling due to the practicality of the operating room. Further investigation into ERK signaling in our AML12$^{DNAJ\text{-}PKAc}$ cells led to the identification of DNAJ-PKAc/Hsp70 complexes incorporated into AKAPs, specifically AKAP-Lbc (*AKAP13*). AKAP-Lbc is known to enhance ERK signaling by interacting with kinase suppressor of Ras (KSR-1), to integrate cAMP regulation of RAF-MEK-ERK signaling[141]. This led to our current model, wherein under normal conditions in cells expressing DNAJ-PKAc, Hsp70 bound to the fusion protein is chemo-protective and augments ERK signaling. In the presence of the Hsp70 inhibitor Ver-155008, the DNAJ-PKAc complex is no longer protected, and only then is susceptible to other means of inhibition. When Hsp70 activity is concurrently inhibited, MEK inhibitors may be effective in decreasing proliferation in AML12$^{DNAJ\text{-}PKAc}$ cells. While the utility of dual Hsp70 and MEK inhibition for the treatment of FLC patients is far from clear, drug screening in AML12$^{DNAJ\text{-}PKAc}$ cells provides initial insight into potential treatments for these patients.

Preliminary investigations into mitochondrial processes in AML12$^{DNAJ\text{-}PKAc}$ cells were inspired in part by the SEngine drug screen performed in these cells. Etoposide, an apoptosis inducer and current chemotherapeutic agent used for the treatment of lung cancer[211], testicular cancer[212], neuroblastoma[213], and ovarian cancers, among others[214], was not able to inhibit proliferation in AML12$^{DNAJ\text{-}PKAc}$ cells, while it inhibited parental AML12 cells. Evidence for a potential mechanism behind etoposide resistance in cells expressing DNAJ-PKAc came from the identification of increased pBad (Ser112) in these cells. While this finding is yet unconfirmed in human FLC, pro-survival signals could be considered as future drug targets for FLC. Cancer cells undergo changes in their cellular metabolism, either by switching cellular machinery to favor glycolysis (the Warburg effect[172]), inducing neighboring fibroblasts to switch to glycolysis and subsequently taking up metabolites produced to utilize in oxidative phosphorylation (the Reverse-Warburg effect[203]), or by maintaining oxidative phosphorylation[173]. Investigations into oxygen consumption rates in our cell lines revelaed that AML12$^{DNAJ\text{-}PKAc}$ cells undergo increased oxidative phosphorylation compared to parental AML12 cells, and maintain an increased mitochondrial membrane potential. Whether these cells exhibit this phenotype due to alterations in downstream signaling pathways by DNAJ-PKAc or simply because their increased proliferation rate requires more ATP production (*i.e.* independent of DNAJ-PKAc itself) remains to be seen. Validation of these findings in human samples will also be essential, as establishment of the metabolic changes in FLCs will further our understanding of this disease.

5.3 Future directions

Given the implications of the kinase dependency of AML12$^{DNAJ\text{-}PKAc}$ cells reported in **figure 2.4**, it will be crucial to follow up these studies in order to develop new therapies for FLC patients. Kinome regularization identified key upstream kinases important for AML12$^{DNAJ\text{-}PKAc}$ cell maintenance. To determine the addiction of AML12$^{DNAJ\text{-}PKAc}$ cells to each of these kinases, systematic knock-down experiments using RNAi or knock-out experiments using CRISPR of

each predicted kinase are crucial. We could then identify the most important kinases responsible for AML12$^{DNAJ\text{-}PKAc}$ cell proliferation, and identify whether depletion of that kinase brings the proliferative rate back to that of parental AML12 cells. Inhibitors of these kinases may be valuable as potential therapeutic strategies, and though kinase inhibitors are known to have off-target effects[215], data from this experiment could ultimately generate new treatments for human FLC.

Another aspect of our work that merits for further exploration is the remarkable effect of MKT-077 in AML12$^{DNAJ\text{-}PKAc}$ cells compared to their parental line. MKT-077 is a cationic dye that allosterically inhibits mitochondrial Hsp70 (Grp75)[177]; we have shown that Hsp70 can bind DNAJ-PKAc and protect cells expressing DNAJ-PKAc from other cellular insults. We have also shown that AML12$^{DNAJ\text{-}PKAc}$ cells have a higher mitochondrial potential; MKT-077 has been previously shown to accumulate in the mitochondria of cancer cells specifically, and can re-localize p53 to the nucleus to induce apoptosis[176]. Therefore, it will be necessary to parse out the effect of MKT-077 inhibition on other cellular processes. For example, addition of a mitochondrial uncoupler such as carbonyl cyanide m-chlorophenylhydrazone[216] (CCCP) can prevent the development of a electrochemical transmembrane potential ($\Delta\psi_m$). Thus, dual addition of CCCP and MKT-077 and subsequent measures of proliferation could help to determine whether the mitochondrial membrane potential is necessary for the AML12$^{DNAJ\text{-}PKAc}$ cell-specific effect of MKT-077. It will also be important to determine whether Grp75 can anchor DNAJ-PKAc, thus providing another potential mechanism of action for MKT-077. While validation of cellular metabolism and the effect of MKT-077 in human FLC may be difficult, investigation into cellular energetics and metabolomics in FLC will provide hints to the metabolism of this detrimental tumor and additional therapeutic targets.

Chapter 6: Materials and Methods

Cell lines and culture

AML12 cells, a gift from the laboratory of Dr. Kim Riehle, were cultured in DMEM/F12 supplemented with 10% FBS, 0.04μg/mL dexamethasone, 0.1% gentamicin, 1μg/mL recombinant human insulin, 0.55μg/mL human transferrin, and 0.5ng/mL sodium selenite. All cell lines were maintained in a 5% CO2 incubator at 37°C. For lysates probed with phospho-ERK and phospho-Bad antibodies, cells were serum-starved for 16-24 hours and lysed. Serum-starved media was prepared as above with the exception of addition of FBS. Cells for cobimetinib (Sigma-Aldrich, ADV465749767) and Ver-155008 (Sigma-Aldrich, 1134156-31-2) treatment were serum-starved for 16-24 hours and then incubated with 3μM Ver-155008 for 30 minutes, and either DMSO or 100nM cobmetinib was incubated for 10 minutes. AML12 cells for transient transfection were transfected with constructs as indicated with TransIT-LT1 (Mirus Bio). After 24 hours, cells were either switched to serum-free media for 16-24 hours and 2μM 1NM-PP1 or DMSO was added for 1 hour, or collected for immunoprecipitation after 24 hours. Cells for cyclohexamide-chase were incubated with 100μg/μL cyclohexamide and collected at indicated timepoints.

Generation of CRISPR-edited AML12$^{DNAJ\text{-}PKAc}$ cells

Guide (g) RNAs were designed to target intron 1 of either mouse *Dnajb1* or *Prkaca* in order to introduce DNA double-stranded breaks in the regions similar to the deletion seen in FLC. We engineered constructs expressing Cas9 and both guide (g)RNAs into pX459-hSpCas9-2A-Puro V2.0 (Addgene plasmid number 62988[217]; guide RNA sequences in **supplementary table S4**), and transfected the vector into AML12 cells using lipofectamine LTX with plus (Thermo Fisher) according to manufacturer's instructions. Cells were subjected to 2μg/mL puromycin selection

48 hours post-transfection. After 3 days in puromycin-containing media, cells were clonally isolated. After selection, cells were dissociated using 0.25% trypsin-EDTA (Gibco) and 200 cells were plated into 15cm^2 dish and incubated for 48-96 hours or until single-cell derived colonies were visible. Single-cell derived colonies were hand-picked with cloning disks (3.2mm diameter, Sigma-Aldrich) soaked with 0.25% trypsin-EDTA and plated into single wells of a 96-well plate. Genomic DNA was extracted (GeneJET Genomic DNA purification kit, Thermo Fisher) to screen clonally-isolated cells.

Genomic DNA PCR

Genomic DNA was amplified by PCR with Kapa HiFi PCR Kit (Kapa Biosystems) with primers found in **supplementary Table S5**. The resulting amplification of genomic *Dnajb1-Prkaca* PCR products were Sanger sequenced to determine the CRISPR/Cas9-induced breakpoint.

Stable cell line generation

Doxycycline-inducible cells were generated using lentiviral transduction to stably incorporate DNAJ, PKAc and DNAJ-PKAc in a pLVX backbone. Lentiviral particles were incubated with AML12 cells for 48 hours. Cells were recovered in normal media for 24 hours before undergoing 2μg/mL puromycin selection for 48 hours. After selection, cells were expanded and tested for induction with 1μg/mL doxycycline for 48 hours. Cell lines with comparable induced expression of Flag-tagged constructs were selected for use in this study.

Human liver samples

Human FLCs with paired normal liver were consented for tissue donation under IRB-approved protocols (#31281 and #51710).

RNA and qPCR

Total RNA was extracted from wild type AML12 and *Dnajb1-Prkaca* clones using Trizol and RNeasy Mini Kits (Qiagen) either reverse transcribed using iScript Reverse Transcription Supermix for RT-qPCR (Bio-Rad) according to manufacturer's instructions, or subjected to Bioanalyzer and eventually RNAseq (FHCRC Genomics Core). The cDNA was subjected to PCR (Kapa HiFi PCR Kit, Kapa Biosystems) with primers against *Dnajb1-Prkaca* fusion, and the resulting amplification was subjected to Sanger sequencing. Quantitative PCR was performed on ABI Fast 7500 using PowerUp SYBR Green Master Mix (Thermo Fisher) according to manufacturer's instructions with primers against *Dnajb1-Prkaca* fusion, wild type *Dnajb1*, wild type *Prkaca,* and both forms of *Prkaca*. Data are reported as delta delta Ct after normalizing to *Gapdh*.

Immunoblotting

Cells and human FLCs were lysed in ice-cold RIPA buffer (10mM Tris-HCl, 150mM NaCl, 1% sodium deoxycholate, 1% Nonidet P-40, 0.1% SDS, 2mM EDTA, 50mM sodium fluoride) with protease inhibitors. Cleared lysate was measured using BCA Protein Assay (Pierce). Lysate was boiled in 1X LDS buffer (Thermo Fisher), separated on 4-12% NuPAGE gradient gels (Thermo Fisher) and transferred onto nitrocellulose using standard techniques. Membranes were incubated overnight at 4°C in 5%w/v milk with TBST and the following antibodies: PKAc (BD Transduction, 610981), RIIα (BD Transduction, 612243), RIIβ (BD Transduction, 610626), RIα (BD Transduction, 610610), Hsp70 (Proteintech, 10995-1), Hsp40 (Proteintech 13174-1) AKAP-Lbc (V096, 1μgml^{-1}), phospho p44/42 MAPK (CST, 9101), p44/42 (CST, 9102), p-Bad S112 (CST, clone 409A, 5284), p-Bad S155 (CST, 9297), Bad (CST 9292), β-actin (Sigma-Aldrich, A1978), Gapdh-HRP (Novus NB110-40405). Membranes were washed in TBST, incubated with HRP-labeled secondary antibodies (Jackson Immunoresearch), washed as

before and developed using ECL (Thermo Fisher) on an iBright FL1000. For re-probing, membranes were striped with 1X Re-Blot Plus Strong (Millipore) for 15 minutes and then re-blocked in Blotto before incubation with primary antibodies again. Densitometry for blot quantification was done using ImageJ software (NIH; http://rsb.info.nih.gov/ij).

Immunoprecipitation

Human tissue and cell lysates were lysed in a 1% Triton-X buffer (50mM Tris-HCl, 130mM NaCl, 20mM NaF, 2mM EDTA, 1% Triton-X with protease inhibitors). Lysates were measured by BCA and pre-cleared with IgG and protein A/G agarose beads (Millipore) then incubated with anti-PKAc (BD Transduction, 610981), anti-HSP70 (Proteintech, 10995-1), or anti-AKAP-Lbc (V096, 1$\mu g ml^{-1}$) antibodies overnight at 4°C. Immunocomplexes were separated by incubation with protein A/G agarose beads for 2 hours at 4°C and washed 4 x 1mL in lysis buffer. For FLAG immunoprecipitation, lysates were incubated with anti-FLAG M2 magnetic beads (Sigma M8823) overnight. Immunocomplexes were washed 4 x 1mL in lysis buffer.

Protein Kinase A activity assay

SignaTECT cAMP-dependent Protein Kinase (PKA) Assay System (Promega, V7480) was used to measure kinase activity in AML12 cell lines. Cells were lysed and PKA activity was measured according to protocol (ATP, [γ-32P]- 3000Ci/mmol 10mCi/ml EasyTide; Perkin Elmer, BLU502A001MC). Experiments were carried out ± 25μM cAMP to stimulate PKA, ± Kemptide (Leu-Arg-Arg-Ala-Ser-Leu-Gly) substrate for normalization, and ± 50μM PKI to inhibit PKA. Purified DNAJ-PKAc and PKAc were normalized to .5μg of protein and kinase assays were performed using PKA substrate peptide Kemptide. Non-specific PKA activity was measured in the presence of 4μg/ml protein kinase inhibitor (PKI).

DNAJ-PKAc protein purification

Expression vectors were transformed into competent *E. coli* BL21 cells (NEB) and proteins were expressed using media supplemented with 100 μg/mL ampicillin. Initial noninducing starter cultures were grown at 37°C in shaking flasks containing LB media overnight, then diluted 6-fold into glass bottles containing .5L of LB. Cultures were incubated at 37°C until Optical Density reaches 0.4-0.6 and induce with 0.5μM IPTG and place in shaker for 16hr overnight. Cells were pelleted by centrifugation and frozen -20 ^{o}C. Pellets were resuspended in lysis buffer (50mM NaH2PO4 pH 7.8, 100mM NaCl, 5mM imidazole, 2mM TCEP, 4mg/mL lysozyme and protease inhibitors) and nutated for 10min. Triton-x was added to 0.5% and nutated for 10min. 1μL benzonase and 1mM MgCl2 was added and rotated for 20min. Constructs were expressed in the soluble fraction. Supernatant was cleared by centrifugation and proteins were purified by two-step nickel-affinity/gel filtration/desthiobiotin purification (1mL HiTrap chelating, HP/HiLoad 16/60 Superdex columns) chromatography using the AKTAxpress system (GE Healthcare). The nickel-affinity elution buffer was identical to the binding buffer except the concentration of salt was increased to 500mM, with increasing concentration of imidazole. Optimal elution fractions were concentrated and loaded onto AKTAxpress gel filtration column. 4mLs desthiobiotin bead slurry was added to fractions of interest, eluting with 100mM Tris-HCl pH 8, 150mM NaCl, 1mM EDTA, and 5mM desthiobiotin.

Reverse-phase protein array (RPPA), Gujral Lab

Whole cell lysates from wild type AML12, clone 10, and clone 14 AML12$^{DNAJ\text{-}PKAc}$ cells were extracted. Seven nitrocellulose slides were printed with the three cell lysates, and 5 of the slides were probed with a library of 80 antibodies.

Kinase Inhibitor Regularization (KiR), Gujral Lab

KiR screen was performed according to the Gujral Lab[115]. Briefly, AML12 and clone 14 AML12$^{DNAJ\text{-}PKAc}$ cells were cultured on a 96-well plate and inhibitors were added. Cell confluence was measured using Incucyte Live-Cell Imaging System (Essen Instruments). Regularized regression was performed by T. Bello.

Affinity-purified mass spectrometry (AP-MS), Gordan Lab

Virally-infected AML12 cells with either flag-PKAc or flag-DNAJ-PKAc were induced with either 1μg/mL doxycycline or PBS for 48 hours. Whole cells were collected by centrifugation, washed 1X, and flash-frozen. Cells were sent to the Gordan lab where lysates were made and flag-immunoprecipitation and affinity-purified LC-MS/MS was performed[218]. G. Chan performed AP-MS and statistics.

Immunofluorescence and proximity ligation assay (PLA)

Cells were grown on coverslips and fixed with 4% paraformaldehyde/PBS for 20 minutes. After several washes in PBS, cells were permeabilized in 0.5% Triton X-100/PBS for 10 minutes and washed extensively in PBS. Cells were then subjected to PLA or immunofluorescence. For PLA, cells were processed according to[219] and manufacturers instructions using Duolink® *In Situ* Orange Starter Kit Mouse/Rabbit, Sigma-Aldrich, DUO92102) using PKAc (BD Transduction, 610981) and Hsp70 (Proteintech, 10995-1). Z-stacks of fluorescent images were collected using a Keyence BZ-X710 using relevant filter cubes. Maximum intensity images were quantified for puncta number using Fiji/ImageJ. Images were smoothened and a duplicate image was created for use as a mask. The duplicate file was thresholded to capture as many puncta as possible without significant blending of densely packed signal. The binary mask was then used to measure selected regions from the original image. Total cell number per field of view was counted as DAPI-stained nuclei (Dapi, Thermo Fisher, 62248) and actin marked cell boundaries

(ActinGreen-488, Molecular Probes, R37110). Images for immunofluorescence were immunostained with primary antibodies (PKAc (CST, 5842), PKA RIIa (BD Transduction, 610626) or phospho p44/42 MAPK (CST, 9101) overnight at 4C. Cells were washed three times in PBS and incubated with Alexa Fluor conjugated secondary antibodies (Thermo Fisher) for 2 hours at room temperature. Cells were washed again nuclei were stained with DAPI (Thermo Fisher, 62248) and actin (ActinGreen-555, Molecular Probes, R37112) and mounted on glass slides using ProLong anti-fade media (Invitrogen). Images of human tissues were taken on Leica DMI6000B inverted microscope with a spinning disk confocal head (Yokagawa) and a CoolSnap HQ camera (Photometrics) controlled by MetaMorph 7.6.4 (Molecular Devices), and immunofluorescent images of AML12 and AML12$^{DNAJ\text{-}PKAc}$ cells were collected on BZ-X710 (Keyence).

Cell viability by MTS assay

Cells were seeded at 3,000 cells per well or at the indicated density into 96-well plates, allowed to recover for 16-24 hours and either treated with Ver-155008 (Sigma-Aldrich, 1134156-31-2), MKT-077 (Cayman Chemical, 14395), or DMSO at designated concentrations, or left untreated. MTS reagent was added per the manufacturer's instructions, and absorbance was read at 490nm 3 hours later (CellTiter 96 Aqueous One Solution, Promega, G3582).

Staurosporine treatment, Gujral Lab

Wild type AML12 and AML12$^{DNAJ\text{-}PKAc}$ cells were plated in a 96-well plate and incubated with indicated concentrations of staurosporine (STS). Cell confluence was measured using Incucyte Live-Cell Imaging System (Essen Instruments).

BrdU labeling

Wild type AML12 and AML12$^{DNAJ\text{-}PKAc}$ cells were seeded at 20,000 cells per well on a 2-well chamber slide (Lab-Tek). Fourty-eight hours after plating, cells were treated with 25ug/mL BrdU (Roche Diagnostics) for 4 hours. Cells were washed twice in ice-cold PBS and fixed with 100% ice-cold methanol. BrdU labeling was then determined by immunohistochemistry by using anti-BrdU antibody (DAKO).

Drug screen

Drug screening of AML12 and AML12$^{DNAJ\text{-}PKAc}$ cells was performed using a drug library assembled by SEngine Precision Medicine that includes FDA-approved chemotherapies as well as drugs in clinical development. Cells were tested in 2D and data evaluated as described[135].

Phosphoproteomics

Human FLC and normal adjacent liver were harvested according to above IRB and flash frozen. AML12 and AML12$^{DNAJ\text{-}PKAc}$ cells were grown on a 15cm dish and after rinsing twice with ice cold PBS, cells were harvested in 750µLof 6M aq. Guanidine hydrochloride (Gdn*HCl) containing 100mM Tris, 5mM TCEP*HCl, and 10mM chloroacetamide (CAM), pH 8.5, using a cell scraper. Frozen human FLC specimens of ca. 100mg wet weight were ground into a fine powder using the CryoGrinder Kit from OPS Diagnostics (Lebanon, NJ) and added to the Gdn*HCl buffer described above. Cell lysates were pipetted into 1.5µLmicrotubes, voretexed briefly and heated to 95°C for 5 minutes. Samples were then sonicated in a Qsonica cup sonicator (Newton, CT) at 100 W for 10 min (30 seconds on, 30 seconds off) on ice. Protein content was measured using the Pierce 660 nm assay reagent (Thermo Fisher Scientific, Waltham, MA). Aliquots of 300 µg of protein were pipetted into a new tube and diluted 2-fold with 100mM triethylammonium bicarbonate (TEAB) pH = 8.5. 3µg of sequencing-grade endoproteinase Lys-C (Wako, Richmond, VA) were added (1:100 ratio) and the mixture agitated on a thermomixer at 1400

rpm at 37°C for 2 h. The mixture was diluted another 2-fold with 100mM TEAB pH = 8.5 and 3µg of trypsin were added. The mixture was agitated on a thermomixer at 1400 rpm at 37°C for overnight, acidified with formic acid (1% final), and cleared by centrifugation for 10 min at RT and 14,000 rcf. Peptides were extracted from the supernatant using Oasis HLB 1cc (10µg) extraction cartridges (Waters, Milford, MA). Cartridges were activated by passing through 200µL of methanol followed by 200µL 80% aq. ACN containing 0.1% TFA, equilibrated with 400µL 1% aq. formic acid. Peptides were loaded and then washed with 400µL 1% aq. formic acid. Peptides were eluted with 300µL 80% aq. ACN containing 0.1% TFA and directly subjected to the published batch IMAC phosphopeptide enrichment protocol with the following minor modifications[220,221] 20µL of a 50% IMAC bead slurry composed of 1/3 commercial PHOS-select iron affinity gel (Sigma Aldrich), 1/3 in-house made Fe3+-NTA superflow agarose and 1/3 in-house made Ga3+-NTA superflow agarose were used for phosphopeptide enrichment[222]. The IMAC slurry was washed three times with 10 bed volumes of 80% aq. ACN containing 0.1% TFA and phosphopeptide enrichment was performed in the same buffer. Phosphopeptides were desalted using C18 StageTips according to the published protocol with the following minor modifications[223]. After activation with 50µL methanol and 50µL 80% aq. ACN containing 0.1% TFA the StageTips were equilibrated with 50µL 1% aq. formic acid. Then the peptides that were reconstituted in 50µL 1% aq. formic acid were loaded and washed with 50µL 1% aq. formic acid. The use of 1% formic acid instead of 5% aq. ACN containing 0.1% TFA prevents the loss of highly hydrophilic phosphopeptides.

nanoLC-MS/MS phosphoproteomics analysis

The LC-MS/MS analyses were performed on a Thermo Fisher Scientific Orbitrap Elite instrument (AML12 cell lines) or a Thermo Fisher Scientific Orbitrap Fusion (human FLC specimens) as described previously with the following minor modifications[224]. Peptide samples were separated on a Thermo-Dionex RSLCNano UHPLC instrument (Sunnyvale, CA) using 20

cm long fused silica capillary columns (100µm ID) packed with 3µm 120Å reversed phase C18 beads (Dr. Maisch, Ammerbuch, DE). For phosphopeptide samples the LC gradient was 120 min long with 3−30% B at 300nL/min. LC solvent A was 0.1% aq.acetic acid and LC solvent B was 0.1% acetic acid, 99.9% acetonitrile. Data-dependent analysis was applied using Top15 selection with CID fragmentation.

Computation of MS raw files

Raw files were analyzed by MaxQuant/Andromeda[225] version 1.5.2.8 using protein, peptide and site FDRs of 0.01 and a score minimum of 40 for modified peptides, 0 for unmodified peptides; delta score minimum of 17 for modified peptides, 0 for unmodified peptides. MS/MS spectra were searched against the UniProt human database (updated July 22nd, 2015). MaxQuant search parameters: Variable modifications included Oxidation (M) and Phospho (S/T/Y). Carbamidomethyl (C) was a fixed modification. Max. missed cleavages was 2, enzyme was Trypsin/P and max. charge was 7. The MaxQuant "match between runs" feature was enabled. The initial search tolerance for FTMS scans was 20ppm and 0.5 Da for ITMS MS/MS scans.

Data processing and statistical analysis

MaxQuant raw data was processed, statistically analyzed and clustered using the Perseus software package v1.5.6.095[226]. Human gene ontology (GO) terms (GOBP, GOCC and GOMF) were loaded from the Perseus Annotations file downloaded on the 01.08.2017. Expression columns (phosphopeptide MS intensities) were log2 transformed and normalized by subtracting the median log2 expression value of each column from each expression value of the corresponding column. Potential contaminant, reverse hits and proteins only identified by site were removed. Reproducibility was analyzed by column correlation (Pearson's r) and replicates that showed a variation of >0.25 in the r-value compared to the mean r-values of all replicates of the same experiment were removed as outliers. Significant differences in phosphopeptide

expression between experiments were quantified with a two-tailed two sample t-test with unequal variances and Benjamini-Hochberg correction for multiple comparisons was applied (FDR = 0.05).

NetworKIN analyses

For human FLC and normal adjacent liver, significantly enriched phosphosites in FLC were input into the NetworKIN platform[60]. For sites significantly enriched in AML12$^{DNAJ-PKAc}$ cells, the conserved phosphosite in human was identified in PhosphoSitePlus and then input into NetworKIN. Minimum score cutoff was 1.

Seahorse

AML12 and AML12$^{DNAJ-PKAc}$ cells were plated 20,000 cells per well and recovered for 24h. The next day, culture medium was removed from each well and replaced by 175µl of unbuffered Seahorse XF Base Medium base (Agilent Technologies, 102353-100) pre-warmed at 37°C, supplemented with 10mM glucose, 1mM Pyruvate and 2mM glutamine. Cells were incubated in a CO_2 free incubator at 37°C for 1h. Prior to the rate measurements, the XF96 Analyzer (Seahorse biosciences, North Billerica, MA) automatically mixed the assay media in each well for 10 min to allow the oxygen partial pressure to reach equilibrium. Each measurement cycle consisted of a mixing time of 2 minutes and a data acquisition period of 4 minutes (12 data points). ECAR (extracellular acidification rate) and OCR (oxygen consumption rate) data points refer to the average rates during the measurement cycles and were reported as absolute rates (mpH/min for ECAR, pmoles/min for OCR). The following compounds were prepared at appropriate concentrations as reported below, and adjusted to pH 7.4. OCR measurements: 2µm Oligomycin, 1µm FCCP, 1µm Rot/AntA. A volume of 25µL of compound was added to each injection port, and 3 baseline measurements were taken prior to the addition of any compound. Then, after a 3 min wait, 3 response measurements were taken after each addition.

Mitochondrial membrane potential of cell lines

AML12 and AML12$^{DNAJ\text{-}PKAc}$ cells were plated on glass-bottom plates (Thermo Fisher) and recovered for 24 hours. On the day of imaging, media was replaced with 40nM TMRM (ThermoFisher, T668) and 50nM Mitotracker Green FM (Invitrogen, M7514) in media without phenol red, and incubated for 45 minutes at 37°C. Cells were rinsed twice in PBS and further incubated in media containing NucBlue Hoescht 33342 stain (Invitrogen, R37605, 1 drop/mL) for 15 minutes at 37°C. Media was aspirated and replaced with Fluorobrite DMEM +10% FBS. Cells were imaged on a Keyence BZ-X710 microscope with a humidified chamber with 5% CO2 at 37°C and imaged using a 60X objective. Images were acquired using the relevant filter cubes for nuclei, TMRM, and Mitotracker Green. Images were quantified by averaging two representative equivalent rectangles in each cell with each treatment condition. Images were processed using ImageJ software (NIH; http://rsb.info.nih.gov/ij).

MKT-077 treatment and p53 localization

AML12 and AML12$^{DNAJ\text{-}PKAc}$ cells were plated on glass coverslips (Thermo Fisher) and recovered for 24h. Cells were then treated with either 3μM MKT-077 (Cayman Chemical, 14395) or DMSO for 48 hours. Cells were then fixed and stained for p53 (Proteintech, 10442-1-AP), actin (ActinRed-555, Molecular Probes, R37112) and DAPI (Thermo Fisher, 62248) as mentioned above and imaged on a Keyence BZ-X710 using a 60X objective. Images were acquired using the relevant filter cubes. Images were quantified by circling the nuclei and processed using ImageJ software.

Statistical analyses

Statistically significant differences between samples are calculated by using Student's two-tailed t-test and all results are presented as the mean ± s.d unless otherwise indicated. Sample size (n) indicated the number of independent experiments represented in amalgamated data; total

cell numbers used in experiments are indicated. P values of <0.05 were considered statistically significant.

Appendix I

Fig S1

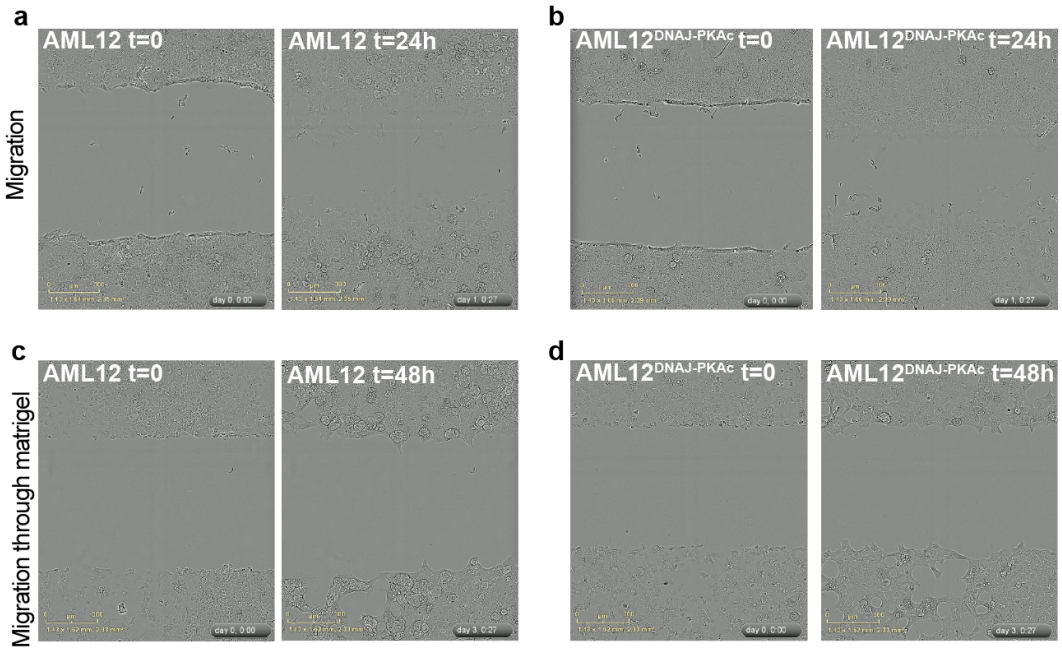

Figure S1. Migratory and transmigratory properties of AML12$^{DNAJ-PKAc}$ cells as measured by scratch wound. Migration of **a)** AML12 and **b)** clone 14 AML12$^{DNAJ-PKAc}$ cells after a scratch. Images were collected every 45 minutes over 24 hours of n>3 replicates. Time 0 (t=0) is immediately after scratch-wounding. Migration through matrigel of **c)** AML12 and **d)** AML12$^{DNAJ-PKAc}$ cells. Images were taken every 45 minutes for 48 hours of n>3 replicates; representative data shown. Time 0 (t=0) is immediately after scratch-wounding. Scale bar is 300μm.

Fig S2

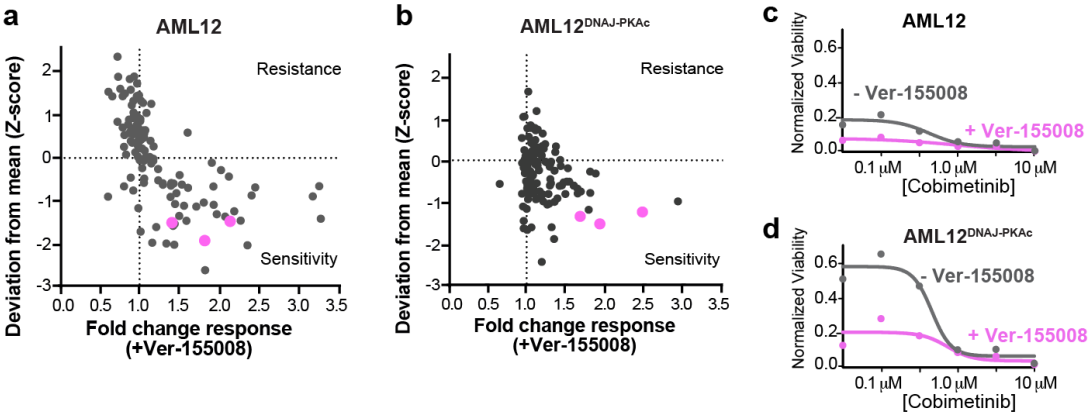

Figure S2. Repeat combination drug screens with 3μM Ver-155008. a & b) Scatterplots show relative resistance or sensitivity of **a)** AML12 and **b)** AML12$^{DNAJ-PKAc}$ cells to the combination of 125 different chemotherapeutic drugs with Ver-155008. Drug combinations in the lower right quadrant are more sensitive to drug treatment than those in the upper right quadrant. Binimetinib, cobimetinib and trametinib are highlighted **(pink circles)**. **c & d)** Analysis of **c)** wild type AML12 and **d)** AML12$^{DNAJ-PKAc}$ cell survival: Dose-response of the drug cobimetinib alone (**grey**) or in combination with Ver-155008 (**pink**). Drug concentrations (μM) are indicated.

Fig S3

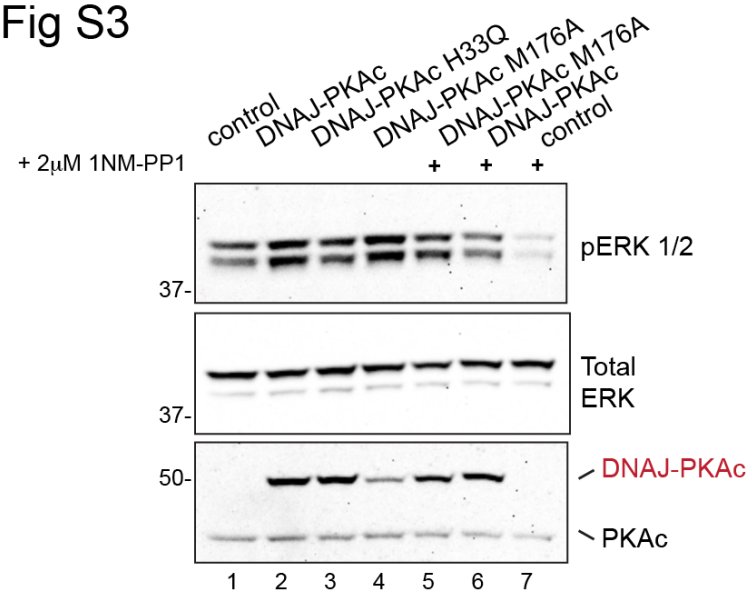

Figure S3. Selective inhibition of PKA activity does not alter ERK signaling. Immunoblot detection of phospho-ERK1/2 in AML12 cells transiently transfected with DNAJ-PKAc (**lanes 2 & 6**), DNAJ-PKAc H33Q (**lane 3**), or DNAJ-PKAc M176A (**lane 4 & 5**) and treated with 2μM 1NM-PP1 (**lanes 5-7**). Detection of PKAc (**middle**) monitored transfection efficiency. Total ERK (**bottom**) served as a loading control. Lanes 1-3 shown in Fig. 4m.

Supplementary Table S1. Top 50 dysregulated genes in AML12$^{DNAJ\text{-}PKAc}$ cells compared to wild type AML12 cells identified by RNA sequencing.

Gene Symbol	description	logFC	logCPM	PValue	FDR
Kcnj16	potassium inwardly-rectifying channel, subfamily J, member 16	13.02785464	7.299871623	1.82142E-74	2.02432E-71
Sulf2	sulfatase 2	-11.81814265	3.418166173	2.08491E-56	8.91217E-54
Ptgfr	prostaglandin F receptor	-11.7513155	3.351773585	3.73248E-65	2.44017E-62
Cers4	ceramide synthase 4	-10.96479714	2.573259761	5.89987E-73	5.46426E-70
Cdh16	cadherin 16	10.79280439	5.069265523	1.42745E-14	5.56656E-13
Ckap4	cytoskeleton-associated protein 4	-10.65407501	2.267194305	7.49881E-56	3.08673E-53
Peg10	paternally expressed 10	-10.64908484	2.262315337	7.29692E-46	1.59016E-43
Cacna1h	calcium channel, voltage-dependent, T type, alpha 1H	-10.63459531	2.248035172	6.32293E-57	2.81092E-54
Bex4	brain expressed X-linked 4	-10.3084983	1.92805991	1.64829E-50	5.08864E-48
Bves	blood vessel epicardial substance	-10.30233041	1.922022041	1.30274E-49	3.81017E-47
Smoc1	SPARC related modular calcium binding 1	-10.29912419	3.758336152	6.20937E-86	7.66788E-83
Dio3os	deiodinase, iodothyronine type III, opposite strand	-10.22934729	1.850647277	1.46535E-48	3.97218E-46
Arrdc4	arrestin domain containing 4	-9.934753295	1.563334188	3.10407E-29	2.55545E-27
Tex15	testis expressed gene 15	-9.917928886	1.547176638	9.99761E-44	1.85189E-41
Hs6st2	heparan sulfate 6-O-sulfotransferase 2	-9.76820063	4.013028646	1.0827E-125	3.0083E-122
Tmem35	transmembrane protein 35	-9.557609917	1.198462929	2.0546E-44	4.07765E-42
Ppp1r26	protein phosphatase 1, regulatory subunit 26	-9.483258588	1.126884643	9.43755E-42	1.54248E-39
Rhoj	ras homolog family member J	-9.444376039	1.089557316	1.9456E-42	3.27627E-40
Sall2	sal-like 2 (Drosophila)	-9.393175799	2.857398837	1.76249E-72	1.5068E-69
St8sia3	ST8 alpha-N-acetyl-neuraminide alpha-2,8-sialyltransferase 3	-9.345838946	0.995056427	6.0997E-40	9.28658E-38
Dio3	deiodinase, iodothyronine type III	-9.321624207	0.971880374	8.68591E-37	1.1225E-34
Crtap	cartilage associated protein	-9.309133157	2.774268025	6.0432E-67	4.19776E-64
Eif4e3	eukaryotic translation initiation factor 4E member 3	-9.296896185	0.948258031	4.83983E-35	5.78386E-33
Sgce	sarcoglycan, epsilon	-9.277504507	4.939768308	9.7384E-150	5.4117E-146
Ptprz1	protein tyrosine phosphatase, receptor type Z, polypeptide 1	-9.271977396	0.924409457	1.72738E-30	1.58662E-28
Aldh1b1	aldehyde dehydrogenase 1 family, member B1	-9.207493637	0.862854342	5.00196E-36	6.24627E-34
Csmd1	CUB and Sushi multiple domains 1	-9.203414152	2.670147385	4.56021E-73	4.60748E-70
Pdzrn3	PDZ domain containing RING finger 3	-9.153445888	0.811437255	2.55696E-36	3.22933E-34
Atp9a	ATPase, class II, type 9A	-9.125395924	0.784879817	8.74875E-29	6.79955E-27
Gulp1	GULP, engulfment adaptor PTB domain containing 1	-9.097755425	0.758439587	6.16126E-30	5.30824E-28
Dmrt2	doublesex and mab-3 related transcription factor 2	-8.899299132	0.570778595	1.09307E-32	1.11453E-30
Ndn	necdin	-8.890898644	0.562917182	1.59163E-33	1.6847E-31
Dsc2	desmocollin 2	-8.874306351	0.547315006	1.05666E-30	9.78642E-29
Iqgap2	IQ motif containing GTPase activating protein 2	-8.805541328	2.281712376	6.65308E-52	2.3107E-49
Rcn1	reticulocalbin 1	-8.752982159	0.433426239	3.76774E-31	3.5487E-29
Pid1	phosphotyrosine interaction domain containing 1	-8.709121051	2.183751781	4.03363E-58	1.94912E-55
Fyn	Fyn proto-oncogene	-8.69744922	0.381573637	4.02889E-30	3.55374E-28
Aplp1	amyloid beta (A4) precursor-like protein 1	-8.639870484	0.327914448	2.53701E-29	2.10421E-27

Nes	nestin	-8.595710536	2.849316216	3.07746E-48	7.60064E-46
Gpc4	glypican 4	-8.551167942	3.310314149	5.14212E-63	3.17497E-60
Vtn	vitronectin	-8.444074178	4.935225238	5.19733E-95	7.2204E-92
Thsd4	thrombospondin, type I, domain containing 4	-8.442928386	1.924642231	1.14134E-53	4.3741E-51
Arhgap36	Rho GTPase activating protein 36	-8.321131575	6.088180241	4.2344E-154	4.7061E-150
Neto2	neuropilin (NRP) and tolloid (TLL)-like 2	-8.208235912	1.695958099	9.00151E-49	2.50107E-46
Soga1	suppressor of glucose, autophagy associated 1	-8.149789463	1.641922246	2.56433E-35	3.13186E-33
Mbnl3	muscleblind-like 3 (Drosophila)	-7.97391012	2.235643561	1.85319E-48	4.9039E-46
Adh7	alcohol dehydrogenase 7 (class IV), mu or sigma polypeptide	7.972789411	2.782895305	1.95178E-31	1.87E-29
Dlc1	deleted in liver cancer 1	-7.970915054	4.346944671	1.4453E-103	2.2947E-100
Aebp1	AE binding protein 1	-7.83358937	3.268032532	5.8786E-60	2.96976E-57

Supplementary Table S2. Gene set enrichment analysis from canonical pathways collection from the Molecular Signatures Database (MSigDB, Broad Institute, c2.cp). 37 pathways were differentially enriched in AML12$^{DNAJ\text{-}PKAc}$ cells.

Canonical pathways increased in AML12$^{DNAJ\text{-}PKAc}$	Size	ES	NES	NOM p-val	FDR q-val	FWER p-val	Rank at max
SOTIRIOU_BREAST_CANCER_GRADE_1_VS_3_UP	138	-0.6427	-2.5518	0	0.0000	0	2380
ZHANG_TLX_TARGETS_DN	84	-0.6516	-2.3653	0	0.0000	0	2091
REACTOME_MITOTIC_PROMETAPHASE	81	-0.6304	-2.3205	0	0.0000	0	2234
KAUFFMANN_MELANOMA_RELAPSE_UP	58	-0.6390	-2.2357	0	0.0001	0.001	2749
ZHAN_MULTIPLE_MYELOMA_PR_UP	40	-0.7088	-2.2425	0	0.0001	0.001	2106
WHITFIELD_CELL_CYCLE_LITERATURE	44	-0.6961	-2.2562	0	0.0001	0.001	2157
WHITEFORD_PEDIATRIC_CANCER_MARKERS	102	-0.5780	-2.2210	0	0.0002	0.003	2147
ISHIDA_E2F_TARGETS	51	-0.6824	-2.2239	0	0.0002	0.003	2147
KONG_E2F3_TARGETS	82	-0.6130	-2.2052	0	0.0002	0.004	2542
REN_BOUND_BY_E2F	56	-0.6504	-2.1879	0	0.0004	0.006	2243
HOFFMANN_LARGE_TO_SMALL_PRE_BII_LYMPHOCYTE_UP	144	-0.5538	-2.1679	0	0.0005	0.008	2517
KANG_DOXORUBICIN_RESISTANCE_UP	48	-0.6602	-2.1615	0	0.0007	0.012	2359
REACTOME_DEPOSITION_OF_NEW_CENPA_CONTAINING_NUCLEOSOMES_AT_THE_CENTROMERE	24	-0.7656	-2.1344	0	0.0012	0.022	1594
PUJANA_XPRSS_INT_NETWORK	156	-0.5165	-2.1200	0	0.0014	0.028	3047
FARMER_BREAST_CANCER_CLUSTER_2	30	-0.7138	-2.1168	0	0.0015	0.03	2723
ZHANG_TLX_TARGETS_36HR_DN	170	-0.5272	-2.0946	0	0.0024	0.049	2703
MORI_IMMATURE_B_LYMPHOCYTE_DN	85	-0.5782	-2.0932	0	0.0024	0.05	2147
EGUCHI_CELL_CYCLE_RB1_TARGETS	23	-0.7447	-2.0875	0.0048	0.0026	0.057	2157
REACTOME_ACTIVATION_OF_ATR_IN_RESPONSE_TO_REPLICATION_STRESS	35	-0.6628	-2.0713	0	0.0033	0.072	2795
AMUNDSON_GAMMA_RADIATION_RESPONSE	37	-0.6477	-2.0484	0	0.0046	0.106	1421
CROONQUIST_IL6_DEPRIVATION_DN	90	-0.5514	-2.0402	0	0.0053	0.124	2006
FINETTI_BREAST_CANCER_KINOME_RED	16	-0.7943	-2.0382	0	0.0052	0.127	1523
REACTOME_G2_M_CHECKPOINTS	41	-0.6421	-2.0258	0	0.0059	0.146	2795
MORI_LARGE_PRE_BII_LYMPHOCYTE_UP	78	-0.5444	-2.0201	0	0.0063	0.16	3286
GREENBAUM_E2A_TARGETS_UP	28	-0.6777	-2.0185	0	0.0061	0.161	1171
KEGG_DNA_REPLICATION	35	-0.6262	-1.9807	0	0.0108	0.27	1996
REACTOME_RESPIRATORY_ELECTRON_TRANSPORT	61	-0.5793	-1.9760	0	0.0111	0.281	3064
REACTOME_DNA_STRAND_ELONGATION	30	-0.6629	-1.9539	0	0.0141	0.356	1996
SCIAN_CELL_CYCLE_TARGETS_OF_TP53_AND_TP73_DN	22	-0.6837	-1.9530	0	0.0139	0.36	2528
SONG_TARGETS_OF_IE86_CMV_PROTEIN	56	-0.5890	-1.9527	0	0.0137	0.363	1869
PUJANA_BREAST_CANCER_WITH_BRCA1_MUTATED_UP	53	-0.5756	-1.9513	0	0.0135	0.366	1765

REACTOME_G0_AND_EARLY_G1	22	-0.6845	-1.9404	0.0039	0.0151	0.404	1947
WINNEPENNINCKX_MELANOMA_METASTASIS_UP	145	-0.4742	-1.9384	0	0.0151	0.41	2802
ROSTY_CERVICAL_CANCER_PROLIFERATION_CLUSTER	128	-0.4989	-1.9312	0	0.0163	0.438	2359
NADERI_BREAST_CANCER_PROGNOSIS_UP	35	-0.6256	-1.9280	0	0.0166	0.45	2301
PID_AURORA_B_PATHWAY	36	-0.6172	-1.9267	0	0.0164	0.454	2243
PUJANA_BRCA_CENTERED_NETWORK	114	-0.5059	-1.9262	0	0.0162	0.459	3226

Supplementary Table S3. Top 50 dysregulated phosphopeptides in AML12$^{DNAJ-PKAc}$ cells compared to wild type AML12 cells identified with phosphoproteomics.

Gene names	Protein names	Difference	Position	Amino acid	-Log PValue
Raver1	Ribonucleoprotein PTB-binding 1	4.6114	26	T	1.4201
2310022A 10Rik	Uncharacterized protein C19orf47 homolog	3.8496	38	S	1.1595
Dsp	Desmoplakin	-3.4859	1622	S	1.6876
Nrk	Nik-related protein kinase	-3.2781	850	S	6.0743
Hnrnpa3	Heterogeneous nuclear ribonucleoprotein A3	2.6652	300	Y	2.2685
Sorbs2	Sorbin and SH3 domain-containing protein 2	2.6487	496	S	1.1856
Sorbs2	Sorbin and SH3 domain-containing protein 2	2.6487	445	S	1.1856
Aldh1a7	Aldehyde dehydrogenase, cytosolic 1	-2.5938	3	S	9.0434
Smarca5	SWI/SNF-related matrix-associated actin-dependent regulator of chromatin subfamily A member 5	2.5752	55	T	1.0388
Zc3h3	Zinc finger CCCH domain-containing protein 3	-2.4836	345	T	1.1215
Zc3h3	Zinc finger CCCH domain-containing protein 3	-2.4836	341	T	1.1215
Zc3h3	Zinc finger CCCH domain-containing protein 3	-2.4836	338	T	1.1215
Zc3h3	Zinc finger CCCH domain-containing protein 3	-2.4836	333	S	1.1215
Zc3h3	Zinc finger CCCH domain-containing protein 3	-2.4836	330	T	1.1215
Zc3h3	Zinc finger CCCH domain-containing protein 3	-2.4836	329	T	1.1215
Atrx	Transcriptional regulator ATRX	2.4122	590	S	1.2619
Gigyf2	PERQ amino acid-rich with GYF domain-containing protein 2	2.3727	25	T	1.3804
Mtfr1l	Mitochondrial fission regulator 1-like	-2.2902	234	S	1.5834
Cdk17	Cyclin-dependent kinase 17	-2.2123	53	S	2.2245
Nup188	Nucleoporin NUP188 homolog	-2.1946	1719	S	2.4441
Ap2a1	AP-2 complex subunit alpha-1	2.1751	655	S	1.1050
Camk2d	Calcium/calmodulin-dependent protein kinase type II subunit delta	2.1483	337	T	1.3761
Bmp2k	BMP-2-inducible protein kinase	2.1388	715	S	5.8198
Knop1	Lysine-rich nucleolar protein 1	-2.0133	111	S	2.8002
Bmp2k	BMP-2-inducible protein kinase	1.9454	644	T	2.9301
Phldb2	Pleckstrin homology-like domain family B member 2	1.9434	392	S	2.0057
Prkab1	5'-AMP-activated protein kinase subunit beta-1	1.9154	108	S	1.0407
Stk10	Serine/threonine-protein kinase 10	-1.9023	416	S	2.5527
Ahnak	Neuroblast differentiation-associated protein/desmoyokin	1.9022	219	T	1.1153
Hnrnpu	Heterogeneous nuclear ribonucleoprotein U	-1.8797	3	S	1.0066
Reps1	RalBP1-associated Eps domain-containing protein 1	-1.8699	259	S	2.9928
Matr3	Matrin-3	-1.8587	598	S	1.5607
Rassf6	Ras association domain-containing protein 6	1.8442	159	S	2.6742
Rassf6	Ras association domain-containing protein 6	1.8442	126	S	1.4925
Camk2d	Calcium/calmodulin-dependent protein kinase type II subunit delta	1.8379	333	S	1.4465
Ybx1	Nuclease-sensitive element-binding protein 1	1.8306	172	S	1.8440
Ppfibp1	Liprin-beta-1	-1.7923	681	S	2.3855
Raly	RNA-binding protein Raly	1.7725	274	T	2.1290
Son	Protein SON	-1.7349	1723	S	1.3535
Ptk2	Focal adhesion kinase 1	1.7339	575	T	1.3631
Nqo2	Ribosyldihydronicotinamide dehydrogenase [quinone]	-1.7302	224	T	3.6248
Ptrf	Polymerase I and transcript release factor	1.7028	42	S	1.2466
Bmp2k	BMP-2-inducible protein kinase	1.6904	823	T	2.0997
Mapk8	Mitogen-activated protein kinase 8	1.6836	183	T	2.9710
Slk	STE20-like serine/threonine-protein kinase	1.6564	775	S	2.6876
Sik3	Serine/threonine-protein kinase SIK3	1.6438	456	S	1.5048
Bmp2k	BMP-2-inducible protein kinase	1.6437	993	Y	3.7863

Ahnak	Neuroblast differentiation-associated protein/desmoyokin	1.6411	136	S	3.9189
Znf609	Zinc finger protein 609	-1.6064	1057	S	2.8068
Egfr	Epidermal growth factor receptor	-1.5867	1034	T	1.2661
Ahnak	Neuroblast differentiation-associated protein/desmoyokin	1.5840	5512	S	3.5422
Filip1l	Filamin A-interacting protein 1-like	-1.5676	551	S	4.2286
Slk	STE20-like serine/threonine-protein kinase	1.5365	777	S	1.9268
Ahnak	Neuroblast differentiation-associated protein/desmoyokin	1.5232	213	S	2.3511

Supplementary Table S4. Sequences of guide RNAs.

Dnajb1	GCATTCCGGGGATCTAGCGG
Prkaca	GTAGTGCTGAGGAGAGTGGGG

Supplementary Table S5. Primers for identifying genomic DNA in AML12 cell lines.

Dnajb1ex1_F	TGAGGAGAAGTTCAAGGAGATCG
Dnajb1ex1_R	CAATGGCAATAGGAGCAAGAAAC
PKAcex2_F	CTACACTAGCTCTGCAGGCTTCC
PKAcex2_R	ATCAAACTGATCCAACTGGGCTG
Gipc1_F	GGGAAAGGACAAAAGGAACCC
Gipc1_R	CAGGGCATTTGCACCCCATGCC
Ddx39_F	CCGGGACTTTCTACTGAAGCC
Ddx39_R	GAATGGCCTGGGGAATACAC
Lphn1_F	ACCCCTTCCAGATGGAGAATGT
Lphn1_r	TGGGCAAGCATCTATGGCAC

Supplementary Table S6. Primers for amplifying cDNA.

Dnajb1_ex2_F	GGGACCAGACCTCGAACAAC
Dnajb1_ex2_R	GGCTAATCCTGGCTGGATAGAT
Prkaca_ex1_F	AAGAAGGGCAGCGAGCAGGA
Prkaca_ex_R	GCCGGTGCCAAGGGTCTTGAT
Prkaca_ex6_F	AGATCGTCCTGACCTTTGAGT
Prkaca_ex7_R	GGCAAAACCGAAGTCTGTCAC
Gapdh_F	ATTTGGCCGTATTGGGCGCCT
Gapdh_R	CCCGGCCTTCTCCATGGTGG
Dnaj-PKAc_F	ACGAGATCAAGCGAGCCTAC
Dnaj-PKAc_R	TTCCCACTCTCCTTGTGCTT

References

1 Torbenson, M. Fibrolamellar carcinoma: 2012 update. *Scientifica (Cairo)* **2012**, 743790, doi:10.6064/2012/743790 (2012).

2 Edmondson, H. A. Differential diagnosis of tumors and tumor-like lesions of liver in infancy and childhood. *AMA J Dis Child* **91**, 168-186 (1956).

3 Craig, J. R., Peters, R. L., Edmondson, H. A. & Omata, M. Fibrolamellar carcinoma of the liver: a tumor of adolescents and young adults with distinctive clinico-pathologic features. *Cancer* **46**, 372-379 (1980).

4 Ward, S. C. *et al.* Fibrolamellar carcinoma of the liver exhibits immunohistochemical evidence of both hepatocyte and bile duct differentiation. *Mod Pathol* **23**, 1180-1190, doi:10.1038/modpathol.2010.105 (2010).

5 Ross, H. M. *et al.* Fibrolamellar carcinomas are positive for CD68. *Mod Pathol* **24**, 390-395, doi:10.1038/modpathol.2010.207 (2011).

6 Mavros, M. N., Mayo, S. C., Hyder, O. & Pawlik, T. M. A systematic review: treatment and prognosis of patients with fibrolamellar hepatocellular carcinoma. *J Am Coll Surg* **215**, 820-830, doi:10.1016/j.jamcollsurg.2012.08.001 (2012).

7 Ang, C. S. *et al.* Clinicopathologic characteristics and survival outcomes of patients with fibrolamellar carcinoma: data from the fibrolamellar carcinoma consortium. *Gastrointest Cancer Res* **6**, 3-9 (2013).

8 Mayo, S. C. *et al.* Treatment and prognosis of patients with fibrolamellar hepatocellular carcinoma: a national perspective. *J Am Coll Surg* **218**, 196-205, doi:10.1016/j.jamcollsurg.2013.10.011 (2014).

9 Stipa, F. *et al.* Outcome of patients with fibrolamellar hepatocellular carcinoma. *Cancer* **106**, 1331-1338, doi:10.1002/cncr.21703 (2006).

10 Atienza, L. G. *et al.* Liver transplantation for fibrolamellar hepatocellular carcinoma: A national perspective. *J Surg Oncol* **115**, 319-323, doi:10.1002/jso.24515 (2017).

11 Couzin-Frankel, J. Breakthrough of the year 2013. Cancer immunotherapy. *Science* **342**, 1432-1433, doi:10.1126/science.342.6165.1432 (2013).

12 Honeyman, J. N. *et al.* Detection of a recurrent DNAJB1-PRKACA chimeric transcript in fibrolamellar hepatocellular carcinoma. *Science* **343**, 1010-1014, doi:10.1126/science.1249484 (2014).

13 Darcy, D. G. *et al.* The genomic landscape of fibrolamellar hepatocellular carcinoma: whole genome sequencing of ten patients. *Oncotarget* **6**, 755-770, doi:10.18632/oncotarget.2712 (2015).

14 Simon, E. P. *et al.* Transcriptomic characterization of fibrolamellar hepatocellular carcinoma. *Proc Natl Acad Sci U S A* **112**, E5916-5925, doi:10.1073/pnas.1424894112 (2015).

15 Sorenson, E. C. *et al.* Genome and transcriptome profiling of fibrolamellar hepatocellular carcinoma demonstrates p53 and IGF2BP1 dysregulation. *PLoS One* **12**, e0176562, doi:10.1371/journal.pone.0176562 (2017).

16 Cornella, H. *et al.* Unique genomic profile of fibrolamellar hepatocellular carcinoma. *Gastroenterology* **148**, 806-818 e810, doi:10.1053/j.gastro.2014.12.028 (2015).

17 Xu, L. *et al.* Genomic analysis of fibrolamellar hepatocellular carcinoma. *Hum Mol Genet* **24**, 50-63, doi:10.1093/hmg/ddu418 (2015).

18 Dinh, T. A. *et al.* Comprehensive analysis of The Cancer Genome Atlas reveals a unique gene and non-coding RNA signature of fibrolamellar carcinoma. *Sci Rep* **7**, 44653, doi:10.1038/srep44653 (2017).

19 Graham, R. P. *et al.* DNAJB1-PRKACA is specific for fibrolamellar carcinoma. *Mod Pathol* **28**, 822-829, doi:10.1038/modpathol.2015.4 (2015).

20 Griffith, O. L. *et al.* A genomic case study of mixed fibrolamellar hepatocellular carcinoma. *Ann Oncol* **27**, 1148-1154, doi:10.1093/annonc/mdw135 (2016).

21 Malouf, G. G. *et al.* Transcriptional profiling of pure fibrolamellar hepatocellular carcinoma reveals an endocrine signature. *Hepatology* **59**, 2228-2237, doi:10.1002/hep.27018 (2014).

22 Kannangai, R., Vivekanandan, P., Martinez-Murillo, F., Choti, M. & Torbenson, M. Fibrolamellar carcinomas show overexpression of genes in the RAS, MAPK, PIK3, and xenobiotic degradation pathways. *Hum Pathol* **38**, 639-644, doi:10.1016/j.humpath.2006.07.019 (2007).
23 Oikawa, T. *et al.* Model of fibrolamellar hepatocellular carcinomas reveals striking enrichment in cancer stem cells. *Nat Commun* **6**, 8070, doi:10.1038/ncomms9070 (2015).
24 Read, D., Shulkes, A., Fernley, R. & Simpson, R. Characterization of neurotensin(6-13) from an hepatic fibrolamellar carcinoma. *Peptides* **12**, 887-892 (1991).
25 Soreide, O., Czerniak, A., Bradpiece, H., Bloom, S. & Blumgart, L. Characteristics of fibrolamellar hepatocellular carcinoma. A study of nine cases and a review of the literature. *Am J Surg* **151**, 518-523 (1986).
26 Ehrenfried, J. A., Zhou, Z., Thompson, J. C. & Evers, B. M. Expression of the neurotensin gene in fetal human liver and fibrolamellar carcinoma. *Ann Surg* **220**, 484-489; discussion 489-491 (1994).
27 Collier, N. A. *et al.* Neurotensin secretion by fibrolamellar carcinoma of the liver. *Lancet* **1**, 538-540 (1984).
28 Riehle, K. J. *et al.* mTORC1 and FGFR1 signaling in fibrolamellar hepatocellular carcinoma. *Mod Pathol* **28**, 103-110, doi:10.1038/modpathol.2014.78 (2015).
29 Wu, J. *et al.* Heat Shock Proteins and Cancer. *Trends Pharmacol Sci* **38**, 226-256, doi:10.1016/j.tips.2016.11.009 (2017).
30 Russell, R., Wali Karzai, A., Mehl, A. F. & McMacken, R. DnaJ dramatically stimulates ATP hydrolysis by DnaK: insight into targeting of Hsp70 proteins to polypeptide substrates. *Biochemistry* **38**, 4165-4176, doi:10.1021/bi9824036 (1999).
31 Craig, E. A. & Marszalek, J. How Do J-Proteins Get Hsp70 to Do So Many Different Things? *Trends Biochem Sci* **42**, 355-368, doi:10.1016/j.tibs.2017.02.007 (2017).
32 Cheetham, M. E. & Caplan, A. J. Structure, function and evolution of DnaJ: conservation and adaptation of chaperone function. *Cell Stress Chaperones* **3**, 28-36 (1998).
33 Hennessy, F., Nicoll, W. S., Zimmermann, R., Cheetham, M. E. & Blatch, G. L. Not all J domains are created equal: implications for the specificity of Hsp40-Hsp70 interactions. *Protein Sci* **14**, 1697-1709, doi:10.1110/ps.051406805 (2005).
34 Pellecchia, M., Szyperski, T., Wall, D., Georgopoulos, C. & Wuthrich, K. NMR structure of the J-domain and the Gly/Phe-rich region of the Escherichia coli DnaJ chaperone. *J Mol Biol* **260**, 236-250, doi:10.1006/jmbi.1996.0395 (1996).
35 Kelley, W. L. & Georgopoulos, C. The T/t common exon of simian virus 40, JC, and BK polyomavirus T antigens can functionally replace the J-domain of the Escherichia coli DnaJ molecular chaperone. *Proc Natl Acad Sci U S A* **94**, 3679-3684 (1997).
36 Chatterjee, S. & Burns, T. F. Targeting Heat Shock Proteins in Cancer: A Promising Therapeutic Approach. *Int J Mol Sci* **18**, doi:10.3390/ijms18091978 (2017).
37 Kityk, R., Kopp, J. & Mayer, M. P. Molecular Mechanism of J-Domain-Triggered ATP Hydrolysis by Hsp70 Chaperones. *Mol Cell* **69**, 227-237 e224, doi:10.1016/j.molcel.2017.12.003 (2018).
38 Hasegawa, T., Yoshida, S., Sugeno, N., Kobayashi, J. & Aoki, M. DnaJ/Hsp40 Family and Parkinson's Disease. *Front Neurosci* **11**, 743, doi:10.3389/fnins.2017.00743 (2017).
39 Wilhelmus, M. M. *et al.* Specific association of small heat shock proteins with the pathological hallmarks of Alzheimer's disease brains. *Neuropathol Appl Neurobiol* **32**, 119-130, doi:10.1111/j.1365-2990.2006.00689.x (2006).
40 Takiyama, Y. Autosomal recessive spastic ataxia of Charlevoix-Saguenay. *Neuropathology* **26**, 368-375 (2006).
41 Millar, D. G. *et al.* Hsp70 promotes antigen-presenting cell function and converts T-cell tolerance to autoimmunity in vivo. *Nat Med* **9**, 1469-1476, doi:10.1038/nm962 (2003).
42 Oka, M. *et al.* Autoantibody to heat shock protein Hsp40 in sera of lung cancer patients. *Jpn J Cancer Res* **92**, 316-320 (2001).
43 Kanazawa, Y. *et al.* Expression of heat shock protein (Hsp) 70 and Hsp 40 in colorectal cancer. *Med Oncol* **20**, 157-164, doi:10.1385/MO:20:2:157 (2003).
44 Castle, P. E., Ashfaq, R., Ansari, F. & Muller, C. Y. Immunohistochemical evaluation of heat shock proteins in normal and preinvasive lesions of the cervix. *Cancer Lett* **229**, 245-252, doi:10.1016/j.canlet.2005.06.045 (2005).

45 Chen, J. S. *et al.* Identification of novel markers for monitoring minimal residual disease in acute lymphoblastic leukemia. *Blood* **97**, 2115-2120 (2001).
46 Trinh, D. L., Elwi, A. N. & Kim, S. W. Direct interaction between p53 and Tid1 proteins affects p53 mitochondrial localization and apoptosis. *Oncotarget* **1**, 396-404, doi:10.18632/oncotarget.100902 (2010).
47 Mitra, A. *et al.* Large isoform of MRJ (DNAJB6) reduces malignant activity of breast cancer. *Breast Cancer Res* **10**, R22, doi:10.1186/bcr1874 (2008).
48 Liu, T., Jiang, W., Han, D. & Yu, L. DNAJC25 is downregulated in hepatocellular carcinoma and is a novel tumor suppressor gene. *Oncol Lett* **4**, 1274-1280, doi:10.3892/ol.2012.903 (2012).
49 Murphy, M. E. The HSP70 family and cancer. *Carcinogenesis* **34**, 1181-1188, doi:10.1093/carcin/bgt111 (2013).
50 Yi, X. *et al.* Association of mortalin (HSPA9) with liver cancer metastasis and prediction for early tumor recurrence. *Mol Cell Proteomics* **7**, 315-325, doi:10.1074/mcp.M700116-MCP200 (2008).
51 Jin, H. *et al.* The clinicopathological significance of Mortalin overexpression in invasive ductal carcinoma of breast. *J Exp Clin Cancer Res* **35**, 42, doi:10.1186/s13046-016-0316-0 (2016).
52 Britten, C. D. *et al.* A phase I and pharmacokinetic study of the mitochondrial-specific rhodacyanine dye analog MKT 077. *Clin Cancer Res* **6**, 42-49 (2000).
53 Soberg, K., Jahnsen, T., Rognes, T., Skalhegg, B. S. & Laerdahl, J. K. Evolutionary paths of the cAMP-dependent protein kinase (PKA) catalytic subunits. *PLoS One* **8**, e60935, doi:10.1371/journal.pone.0060935 (2013).
54 Shoji, S. *et al.* Complete amino acid sequence of the catalytic subunit of bovine cardiac muscle cyclic AMP-dependent protein kinase. *Proc Natl Acad Sci U S A* **78**, 848-851 (1981).
55 Tasken, K. & Aandahl, E. M. Localized effects of cAMP mediated by distinct routes of protein kinase A. *Physiol Rev* **84**, 137-167, doi:10.1152/physrev.00021.2003 (2004).
56 Sim, A. T. & Scott, J. D. Targeting of PKA, PKC and protein phosphatases to cellular microdomains. *Cell Calcium* **26**, 209-217, doi:10.1054/ceca.1999.0072 (1999).
57 Carnegie, G. K., Means, C. K. & Scott, J. D. A-kinase anchoring proteins: from protein complexes to physiology and disease. *IUBMB Life* **61**, 394-406, doi:10.1002/iub.168 (2009).
58 Scott, J. D., Dessauer, C. W. & Tasken, K. Creating order from chaos: cellular regulation by kinase anchoring. *Annu Rev Pharmacol Toxicol* **53**, 187-210, doi:10.1146/annurev-pharmtox-011112-140204 (2013).
59 Krebs, E. G. & Beavo, J. A. Phosphorylation-dephosphorylation of enzymes. *Annu Rev Biochem* **48**, 923-959, doi:10.1146/annurev.bi.48.070179.004423 (1979).
60 Welch, E. J., Jones, B. W. & Scott, J. D. Networking with AKAPs: context-dependent regulation of anchored enzymes. *Mol Interv* **10**, 86-97, doi:10.1124/mi.10.2.6 (2010).
61 Cadd, G. & McKnight, G. S. Distinct patterns of cAMP-dependent protein kinase gene expression in mouse brain. *Neuron* **3**, 71-79 (1989).
62 Corbin, J. D. *et al.* Studies on the properties and mode of action of the purified regulatory subunit of bovine heart adenosine 3':5'-monophosphate-dependent protein kinase. *J Biol Chem* **253**, 3997-4003 (1978).
63 Corbin, J. D., Sugden, P. H., Lincoln, T. M. & Keely, S. L. Compartmentalization of adenosine 3':5'-monophosphate and adenosine 3':5'-monophosphate-dependent protein kinase in heart tissue. *J Biol Chem* **252**, 3854-3861 (1977).
64 Langeberg, L. K. & Scott, J. D. Signalling scaffolds and local organization of cellular behaviour. *Nat Rev Mol Cell Biol* **16**, 232-244, doi:10.1038/nrm3966 (2015).
65 Scott, J. D. *et al.* Type II regulatory subunit dimerization determines the subcellular localization of the cAMP-dependent protein kinase. *J Biol Chem* **265**, 21561-21566 (1990).
66 Dessauer, C. W. Adenylyl cyclase--A-kinase anchoring protein complexes: the next dimension in cAMP signaling. *Mol Pharmacol* **76**, 935-941, doi:10.1124/mol.109.059345 (2009).
67 Carr, D. W. *et al.* Interaction of the regulatory subunit (RII) of cAMP-dependent protein kinase with RII-anchoring proteins occurs through an amphipathic helix binding motif. *J Biol Chem* **266**, 14188-14192 (1991).
68 Bauman, A. L. *et al.* Dynamic regulation of cAMP synthesis through anchored PKA-adenylyl cyclase V/VI complexes. *Mol Cell* **23**, 925-931, doi:10.1016/j.molcel.2006.07.025 (2006).
69 Smith, F. D. *et al.* Intrinsic disorder within an AKAP-protein kinase A complex guides local substrate phosphorylation. *Elife* **2**, e01319, doi:10.7554/eLife.01319 (2013).

70 Huang, L. J., Durick, K., Weiner, J. A., Chun, J. & Taylor, S. S. Identification of a novel protein kinase A anchoring protein that binds both type I and type II regulatory subunits. *J Biol Chem* **272**, 8057-8064 (1997).
71 Huang, L. J., Durick, K., Weiner, J. A., Chun, J. & Taylor, S. S. D-AKAP2, a novel protein kinase A anchoring protein with a putative RGS domain. *Proc Natl Acad Sci U S A* **94**, 11184-11189 (1997).
72 Means, C. K. *et al.* An entirely specific type I A-kinase anchoring protein that can sequester two molecules of protein kinase A at mitochondria. *Proc Natl Acad Sci U S A* **108**, E1227-1235, doi:10.1073/pnas.1107182108 (2011).
73 Kovanich, D. *et al.* Sphingosine kinase interacting protein is an A-kinase anchoring protein specific for type I cAMP-dependent protein kinase. *Chembiochem* **11**, 963-971, doi:10.1002/cbic.201000058 (2010).
74 Bauman, A. L., Michel, J. J., Henson, E., Dodge-Kafka, K. L. & Kapiloff, M. S. The mAKAP signalosome and cardiac myocyte hypertrophy. *IUBMB Life* **59**, 163-169, doi:10.1080/15216540701358593 (2007).
75 Dodge, K. L. *et al.* mAKAP assembles a protein kinase A/PDE4 phosphodiesterase cAMP signaling module. *EMBO J* **20**, 1921-1930, doi:10.1093/emboj/20.8.1921 (2001).
76 Carlisle Michel, J. J. *et al.* PKA-phosphorylation of PDE4D3 facilitates recruitment of the mAKAP signalling complex. *Biochem J* **381**, 587-592, doi:10.1042/BJ20040846 (2004).
77 Klauck, T. M. *et al.* Coordination of three signaling enzymes by AKAP79, a mammalian scaffold protein. *Science* **271**, 1589-1592 (1996).
78 Coghlan, V. M. *et al.* Association of protein kinase A and protein phosphatase 2B with a common anchoring protein. *Science* **267**, 108-111 (1995).
79 Kritzer, M. D. *et al.* The scaffold protein muscle A-kinase anchoring protein beta orchestrates cardiac myocyte hypertrophic signaling required for the development of heart failure. *Circ Heart Fail* **7**, 663-672, doi:10.1161/CIRCHEARTFAILURE.114.001266 (2014).
80 McCartney, S., Little, B. M., Langeberg, L. K. & Scott, J. D. Cloning and characterization of A-kinase anchor protein 100 (AKAP100). A protein that targets A-kinase to the sarcoplasmic reticulum. *J Biol Chem* **270**, 9327-9333 (1995).
81 Wong, W., Goehring, A. S., Kapiloff, M. S., Langeberg, L. K. & Scott, J. D. mAKAP compartmentalizes oxygen-dependent control of HIF-1alpha. *Sci Signal* **1**, ra18, doi:10.1126/scisignal.2000026 (2008).
82 Nystoriak, M. A. *et al.* AKAP150 contributes to enhanced vascular tone by facilitating large-conductance Ca2+-activated K+ channel remodeling in hyperglycemia and diabetes mellitus. *Circ Res* **114**, 607-615, doi:10.1161/CIRCRESAHA.114.302168 (2014).
83 Hinke, S. A. *et al.* Anchored phosphatases modulate glucose homeostasis. *EMBO J* **31**, 3991-4004, doi:10.1038/emboj.2012.244 (2012).
84 Gold, M. G. *et al.* AKAP2 anchors PKA with aquaporin-0 to support ocular lens transparency. *EMBO Mol Med* **4**, 15-26, doi:10.1002/emmm.201100184 (2012).
85 Carnegie, G. K. *et al.* AKAP-Lbc mobilizes a cardiac hypertrophy signaling pathway. *Mol Cell* **32**, 169-179, doi:10.1016/j.molcel.2008.08.030 (2008).
86 Lacroix, A., Feelders, R. A., Stratakis, C. A. & Nieman, L. K. Cushing's syndrome. *Lancet* **386**, 913-927, doi:10.1016/S0140-6736(14)61375-1 (2015).
87 Cao, Y. *et al.* Activating hotspot L205R mutation in PRKACA and adrenal Cushing's syndrome. *Science* **344**, 913-917, doi:10.1126/science.1249480 (2014).
88 Sato, Y. *et al.* Recurrent somatic mutations underlie corticotropin-independent Cushing's syndrome. *Science* **344**, 917-920, doi:10.1126/science.1252328 (2014).
89 Goh, G. *et al.* Recurrent activating mutation in PRKACA in cortisol-producing adrenal tumors. *Nat Genet* **46**, 613-617, doi:10.1038/ng.2956 (2014).
90 Beuschlein, F. *et al.* Constitutive activation of PKA catalytic subunit in adrenal Cushing's syndrome. *N Engl J Med* **370**, 1019-1028, doi:10.1056/NEJMoa1310359 (2014).
91 Di Dalmazi, G. *et al.* Novel somatic mutations in the catalytic subunit of the protein kinase A as a cause of adrenal Cushing's syndrome: a European multicentric study. *J Clin Endocrinol Metab* **99**, E2093-2100, doi:10.1210/jc.2014-2152 (2014).
92 Espiard, S. & Bertherat, J. The genetics of adrenocortical tumors. *Endocrinol Metab Clin North Am* **44**, 311-334, doi:10.1016/j.ecl.2015.02.004 (2015).

93 Stratakis, C. A. E pluribus unum? The main protein kinase A catalytic subunit (PRKACA), a likely oncogene, and cortisol-producing tumors. *J Clin Endocrinol Metab* **99**, 3629-3633, doi:10.1210/jc.2014-3295 (2014).
94 Lodish, M. B. *et al.* Germline PRKACA amplification causes variable phenotypes that may depend on the extent of the genomic defect: molecular mechanisms and clinical presentations. *Eur J Endocrinol* **172**, 803-811, doi:10.1530/EJE-14-1154 (2015).
95 Carney, J. A., Lyssikatos, C., Lodish, M. B. & Stratakis, C. A. Germline PRKACA amplification leads to Cushing syndrome caused by 3 adrenocortical pathologic phenotypes. *Hum Pathol* **46**, 40-49, doi:10.1016/j.humpath.2014.09.005 (2015).
96 Berthon, A. S., Szarek, E. & Stratakis, C. A. PRKACA: the catalytic subunit of protein kinase A and adrenocortical tumors. *Front Cell Dev Biol* **3**, 26, doi:10.3389/fcell.2015.00026 (2015).
97 Kirschner, L. S. *et al.* Mutations of the gene encoding the protein kinase A type I-alpha regulatory subunit in patients with the Carney complex. *Nat Genet* **26**, 89-92, doi:10.1038/79238 (2000).
98 Horvath, A. *et al.* Mutations and polymorphisms in the gene encoding regulatory subunit type 1-alpha of protein kinase A (PRKAR1A): an update. *Hum Mutat* **31**, 369-379, doi:10.1002/humu.21178 (2010).
99 Graham, R. P. *et al.* Fibrolamellar carcinoma in the Carney complex: PRKAR1A loss instead of the classic DNAJB1-PRKACA fusion. *Hepatology* **68**, 1441-1447, doi:10.1002/hep.29719 (2018).
100 Porter, S. E., Dwyer-Nield, L. D. & Malkinson, A. M. Regulation of lung epithelial cell morphology by cAMP-dependent protein kinase type I isozyme. *Am J Physiol Lung Cell Mol Physiol* **280**, L1282-1289, doi:10.1152/ajplung.2001.280.6.L1282 (2001).
101 Cvijic, M. E., Kita, T., Shih, W., DiPaola, R. S. & Chin, K. V. Extracellular catalytic subunit activity of the cAMP-dependent protein kinase in prostate cancer. *Clin Cancer Res* **6**, 2309-2317 (2000).
102 Cho, Y. S. *et al.* Extracellular protein kinase A as a cancer biomarker: its expression by tumor cells and reversal by a myristate-lacking Calpha and RIIbeta subunit overexpression. *Proc Natl Acad Sci U S A* **97**, 835-840 (2000).
103 Moody, S. E. *et al.* PRKACA mediates resistance to HER2-targeted therapy in breast cancer cells and restores anti-apoptotic signaling. *Oncogene* **34**, 2061-2071, doi:10.1038/onc.2014.153 (2015).
104 Kastenhuber, E. R. *et al.* DNAJB1-PRKACA fusion kinase interacts with beta-catenin and the liver regenerative response to drive fibrolamellar hepatocellular carcinoma. *Proc Natl Acad Sci U S A* **114**, 13076-13084, doi:10.1073/pnas.1716483114 (2017).
105 Engelholm, L. H. *et al.* CRISPR/Cas9 Engineering of Adult Mouse Liver Demonstrates That the Dnajb1-Prkaca Gene Fusion Is Sufficient to Induce Tumors Resembling Fibrolamellar Hepatocellular Carcinoma. *Gastroenterology* **153**, 1662-1673 e1610, doi:10.1053/j.gastro.2017.09.008 (2017).
106 Iyer, G. H., Moore, M. J. & Taylor, S. S. Consequences of lysine 72 mutation on the phosphorylation and activation state of cAMP-dependent kinase. *J Biol Chem* **280**, 8800-8807, doi:10.1074/jbc.M407586200 (2005).
107 Riggle, K. M. *et al.* Enhanced cAMP-stimulated protein kinase A activity in human fibrolamellar hepatocellular carcinoma. *Pediatr Res* **80**, 110-118, doi:10.1038/pr.2016.36 (2016).
108 Wu, J. C., Merlino, G. & Fausto, N. Establishment and characterization of differentiated, nontransformed hepatocyte cell lines derived from mice transgenic for transforming growth factor alpha. *Proc Natl Acad Sci U S A* **91**, 674-678 (1994).
109 Hanahan, D. & Weinberg, R. A. Hallmarks of cancer: the next generation. *Cell* **144**, 646-674, doi:10.1016/j.cell.2011.02.013 (2011).
110 Amieux, P. S. *et al.* Compensatory regulation of RIalpha protein levels in protein kinase A mutant mice. *J Biol Chem* **272**, 3993-3998 (1997).
111 Uhler, M. D. & McKnight, G. S. Expression of cDNAs for two isoforms of the catalytic subunit of cAMP-dependent protein kinase. *J Biol Chem* **262**, 15202-15207 (1987).
112 Cheung, J. *et al.* Structural insights into mis-regulation of protein kinase A in human tumors. *Proc Natl Acad Sci U S A* **112**, 1374-1379, doi:10.1073/pnas.1424206112 (2015).
113 Anders, S. & Huber, W. Differential expression analysis for sequence count data. *Genome Biol* **11**, R106, doi:10.1186/gb-2010-11-10-r106 (2010).
114 Hanzelmann, S., Castelo, R. & Guinney, J. GSVA: gene set variation analysis for microarray and RNA-seq data. *BMC Bioinformatics* **14**, 7, doi:10.1186/1471-2105-14-7 (2013).

115 Gujral, T. S., Peshkin, L. & Kirschner, M. W. Exploiting polypharmacology for drug target deconvolution. *Proc Natl Acad Sci U S A* **111**, 5048-5053, doi:10.1073/pnas.1403080111 (2014).
116 Hopkins, A. L. Network pharmacology: the next paradigm in drug discovery. *Nat Chem Biol* **4**, 682-690, doi:10.1038/nchembio.118 (2008).
117 Sooknanan, R., Malek, L., Wang, X. H., Siebert, T. & Keating, A. Detection and direct sequence identification of BCR-ABL mRNA in Ph+ chronic myeloid leukemia. *Exp Hematol* **21**, 1719-1724 (1993).
118 Soda, M. *et al.* Identification of the transforming EML4-ALK fusion gene in non-small-cell lung cancer. *Nature* **448**, 561-566, doi:10.1038/nature05945 (2007).
119 Pinna, A. D. *et al.* Treatment of fibrolamellar hepatoma with subtotal hepatectomy or transplantation. *Hepatology* **26**, 877-883, doi:10.1002/hep.510260412 (1997).
120 Attwooll, C., Lazzerini Denchi, E. & Helin, K. The E2F family: specific functions and overlapping interests. *EMBO J* **23**, 4709-4716, doi:10.1038/sj.emboj.7600481 (2004).
121 Stark, G. R. & Taylor, W. R. Analyzing the G2/M checkpoint. *Methods Mol Biol* **280**, 51-82, doi:10.1385/1-59259-788-2:051 (2004).
122 Visconti, R., Della Monica, R. & Grieco, D. Cell cycle checkpoint in cancer: a therapeutically targetable double-edged sword. *J Exp Clin Cancer Res* **35**, 153, doi:10.1186/s13046-016-0433-9 (2016).
123 Farhi, D. C., Shikes, R. H. & Silverberg, S. G. Ultrastructure of fibrolamellar oncocytic hepatoma. *Cancer* **50**, 702-709 (1982).
124 Lalazar, G. & Simon, S. M. Fibrolamellar Carcinoma: Recent Advances and Unresolved Questions on the Molecular Mechanisms. *Semin Liver Dis* **38**, 51-59, doi:10.1055/s-0037-1621710 (2018).
125 Blaquiere, J. A. & Verheyen, E. M. Homeodomain-Interacting Protein Kinases: Diverse and Complex Roles in Development and Disease. *Curr Top Dev Biol* **123**, 73-103, doi:10.1016/bs.ctdb.2016.10.002 (2017).
126 van de Weerdt, B. C. & Medema, R. H. Polo-like kinases: a team in control of the division. *Cell Cycle* **5**, 853-864, doi:10.4161/cc.5.8.2692 (2006).
127 Scott, J. D. & Pawson, T. Cell signaling in space and time: where proteins come together and when they're apart. *Science* **326**, 1220-1224, doi:10.1126/science.1175668 (2009).
128 Smith, F. D. *et al.* Local protein kinase A action proceeds through intact holoenzymes. *Science* **356**, 1288-1293, doi:10.1126/science.aaj1669 (2017).
129 Qin, L., Guo, J., Zheng, Q. & Zhang, H. BAG2 structure, function and involvement in disease. *Cell Mol Biol Lett* **21**, 18, doi:10.1186/s11658-016-0020-2 (2016).
130 Calderwood, S. K., Khaleque, M. A., Sawyer, D. B. & Ciocca, D. R. Heat shock proteins in cancer: chaperones of tumorigenesis. *Trends Biochem Sci* **31**, 164-172, doi:10.1016/j.tibs.2006.01.006 (2006).
131 Mayer, M. P. & Bukau, B. Hsp70 chaperones: cellular functions and molecular mechanism. *Cell Mol Life Sci* **62**, 670-684, doi:10.1007/s00018-004-4464-6 (2005).
132 Soderberg, O. *et al.* Proximity ligation: a specific and versatile tool for the proteomic era. *Genet Eng (N Y)* **28**, 85-93 (2007).
133 Wen, W., Liu, W., Shao, Y. & Chen, L. VER-155008, a small molecule inhibitor of HSP70 with potent anti-cancer activity on lung cancer cell lines. *Exp Biol Med (Maywood)* **239**, 638-645, doi:10.1177/1535370214527899 (2014).
134 Eugenio, A. I. P. *et al.* Proteasome and heat shock protein 70 (HSP70) inhibitors as therapeutic alternative in multiple myeloma. *Oncotarget* **8**, 114698-114709, doi:10.18632/oncotarget.22815 (2017).
135 Pauli, C. *et al.* Personalized In Vitro and In Vivo Cancer Models to Guide Precision Medicine. *Cancer Discov* **7**, 462-477, doi:10.1158/2159-8290.CD-16-1154 (2017).
136 Rossomando, A. J. *et al.* Identification of Tyr-185 as the site of tyrosine autophosphorylation of recombinant mitogen-activated protein kinase p42mapk. *Proc Natl Acad Sci U S A* **89**, 5779-5783 (1992).
137 Hogrebe, A. *et al.* Benchmarking common quantification strategies for large-scale phosphoproteomics. *Nat Commun* **9**, 1045, doi:10.1038/s41467-018-03309-6 (2018).
138 Horn, H. *et al.* KinomeXplorer: an integrated platform for kinome biology studies. *Nat Methods* **11**, 603-604, doi:10.1038/nmeth.2968 (2014).

139 Whitesell, L. & Lindquist, S. L. HSP90 and the chaperoning of cancer. *Nat Rev Cancer* **5**, 761-772, doi:10.1038/nrc1716 (2005).
140 Macario, A. J. & Conway de Macario, E. Chaperonopathies by defect, excess, or mistake. *Ann N Y Acad Sci* **1113**, 178-191, doi:10.1196/annals.1391.009 (2007).
141 Smith, F. D. *et al.* AKAP-Lbc enhances cyclic AMP control of the ERK1/2 cascade. *Nat Cell Biol* **12**, 1242-1249, doi:10.1038/ncb2130 (2010).
142 Dumaz, N. & Marais, R. Integrating signals between cAMP and the RAS/RAF/MEK/ERK signalling pathways. Based on the anniversary prize of the Gesellschaft fur Biochemie und Molekularbiologie Lecture delivered on 5 July 2003 at the Special FEBS Meeting in Brussels. *FEBS J* **272**, 3491-3504, doi:10.1111/j.1742-4658.2005.04763.x (2005).
143 Pattabiraman, D. R. *et al.* Activation of PKA leads to mesenchymal-to-epithelial transition and loss of tumor-initiating ability. *Science* **351**, aad3680, doi:10.1126/science.aad3680 (2016).
144 Morgan, D. J. *et al.* Tissue-specific PKA inhibition using a chemical genetic approach and its application to studies on sperm capacitation. *Proc Natl Acad Sci U S A* **105**, 20740-20745, doi:10.1073/pnas.0810971105 (2008).
145 Caunt, C. J., Sale, M. J., Smith, P. D. & Cook, S. J. MEK1 and MEK2 inhibitors and cancer therapy: the long and winding road. *Nat Rev Cancer* **15**, 577-592, doi:10.1038/nrc4000 (2015).
146 Goloudina, A. R., Demidov, O. N. & Garrido, C. Inhibition of HSP70: a challenging anti-cancer strategy. *Cancer Lett* **325**, 117-124, doi:10.1016/j.canlet.2012.06.003 (2012).
147 van der Bliek, A. M., Sedensky, M. M. & Morgan, P. G. Cell Biology of the Mitochondrion. *Genetics* **207**, 843-871, doi:10.1534/genetics.117.300262 (2017).
148 Wang, C. & Youle, R. J. The role of mitochondria in apoptosis*. *Annu Rev Genet* **43**, 95-118, doi:10.1146/annurev-genet-102108-134850 (2009).
149 Nicholls, D. G. Mitochondria and calcium signaling. *Cell Calcium* **38**, 311-317, doi:10.1016/j.ceca.2005.06.011 (2005).
150 Huttemann, M., Lee, I., Samavati, L., Yu, H. & Doan, J. W. Regulation of mitochondrial oxidative phosphorylation through cell signaling. *Biochim Biophys Acta* **1773**, 1701-1720 (2007).
151 Lee, H. C. *et al.* Mitochondrial genome instability and mtDNA depletion in human cancers. *Ann N Y Acad Sci* **1042**, 109-122, doi:10.1196/annals.1338.011 (2005).
152 Yamada, S. *et al.* Correlation between copy number of mitochondrial DNA and clinico-pathologic parameters of hepatocellular carcinoma. *Eur J Surg Oncol* **32**, 303-307, doi:10.1016/j.ejso.2006.01.002 (2006).
153 Wong, L. J., Tan, D. J., Bai, R. K., Yeh, K. T. & Chang, J. Molecular alterations in mitochondrial DNA of hepatocellular carcinomas: is there a correlation with clinicopathological profile? *J Med Genet* **41**, e65 (2004).
154 Vivekanandan, P., Daniel, H., Yeh, M. M. & Torbenson, M. Mitochondrial mutations in hepatocellular carcinomas and fibrolamellar carcinomas. *Mod Pathol* **23**, 790-798, doi:10.1038/modpathol.2010.51 (2010).
155 Bartlett, A. L., Leslie, N. D., Gupta, A. & Geller, J. I. Acquired ornithine transcarbamylase deficiency in pediatric and adolescent patients with fibrolamellar hepatocellular carcinoma. *Pediatr Blood Cancer* **65**, e27392, doi:10.1002/pbc.27392 (2018).
156 Surjan, R. C., Dos Santos, E. S., Basseres, T., Makdissi, F. F. & Machado, M. A. A Proposed Physiopathological Pathway to Hyperammonemic Encephalopathy in a Non-Cirrhotic Patient with Fibrolamellar Hepatocellular Carcinoma without Ornithine Transcarbamylase (OTC) Mutation. *Am J Case Rep* **18**, 234-241 (2017).
157 Sulaiman, R. A. & Geberhiwot, T. Fibrolamellar hepatocellular carcinoma mimicking ornithine transcarbamylase deficiency. *JIMD Rep* **16**, 47-50, doi:10.1007/8904_2014_318 (2014).
158 Shinde, S. S., Sharma, P. & Davis, M. P. Acute hyperammonemic encephalopathy in a non-cirrhotic patient with hepatocellular carcinoma reversed by arginine therapy. *J Pain Symptom Manage* **47**, e5-7, doi:10.1016/j.jpainsymman.2014.01.002 (2014).
159 Sethi, S. *et al.* Hyperammonemic encephalopathy: a rare presentation of fibrolamellar hepatocellular carcinoma. *Am J Med Sci* **338**, 522-524, doi:10.1097/MAJ.0b013e3181bccfb4 (2009).
160 Jeffers, L. J. *et al.* Hepatic encephalopathy and orotic aciduria associated with hepatocellular carcinoma in a noncirrhotic liver. *Hepatology* **8**, 78-81 (1988).

161 Hashash, J. G., Thudi, K. & Malik, S. M. An 18-year-old woman with a 15-cm liver mass and an ammonia level of 342. *Gastroenterology* **143**, 1157-1402, doi:10.1053/j.gastro.2012.07.002 (2012).
162 Chapuy, C. I., Sahai, I., Sharma, R., Zhu, A. X. & Kozyreva, O. N. Hyperammonemic Encephalopathy Associated With Fibrolamellar Hepatocellular Carcinoma: Case Report, Literature Review, and Proposed Treatment Algorithm. *Oncologist* **21**, 514-520, doi:10.1634/theoncologist.2015-0267 (2016).
163 Bender, H. U., Staudigl, M., Schmid, I. & Fuhrer, M. Treatment of Paraneoplastic Hyperammonemia in Fibrolamellar Hepatocellular Carcinoma With Oral Sodium Phenylbutyrate. *J Pain Symptom Manage* **49**, e8-10, doi:10.1016/j.jpainsymman.2015.03.007 (2015).
164 Chan, J. S., Harding, C. O. & Blanke, C. D. Postchemotherapy hyperammonemic encephalopathy emulating ornithine transcarbamoylase (OTC) deficiency. *South Med J* **101**, 543-545, doi:10.1097/SMJ.0b013e31816bf5cc (2008).
165 Xu, S. R. *et al.* Plasma ammonia in patients with acute leukemia. *Chin Med J (Engl)* **105**, 713-716 (1992).
166 Kwan, L., Wang, C. & Levitt, L. Hyperammonemic encephalopathy in multiple myeloma. *N Engl J Med* **346**, 1674-1675, doi:10.1056/NEJM200205233462119 (2002).
167 Alessenko, A. V. *et al.* Mechanisms of cycloheximide-induced apoptosis in liver cells. *FEBS Lett* **416**, 113-116 (1997).
168 Feng, G. & Kaplowitz, N. Mechanism of staurosporine-induced apoptosis in murine hepatocytes. *Am J Physiol Gastrointest Liver Physiol* **282**, G825-834, doi:10.1152/ajpgi.00467.2001 (2002).
169 Mizumoto, K., Rothman, R. J. & Farber, J. L. Programmed cell death (apoptosis) of mouse fibroblasts is induced by the topoisomerase II inhibitor etoposide. *Mol Pharmacol* **46**, 890-895 (1994).
170 Gujral, T. S. *et al.* Profiling phospho-signaling networks in breast cancer using reverse-phase protein arrays. *Oncogene* **32**, 3470-3476, doi:10.1038/onc.2012.378 (2013).
171 Sahin, F. *et al.* mTOR and P70 S6 kinase expression in primary liver neoplasms. *Clin Cancer Res* **10**, 8421-8425, doi:10.1158/1078-0432.CCR-04-0941 (2004).
172 Potter, M., Newport, E. & Morten, K. J. The Warburg effect: 80 years on. *Biochem Soc Trans* **44**, 1499-1505, doi:10.1042/BST20160094 (2016).
173 DeBerardinis, R. J. & Chandel, N. S. Fundamentals of cancer metabolism. *Sci Adv* **2**, e1600200, doi:10.1126/sciadv.1600200 (2016).
174 Vander Heiden, M. G. & DeBerardinis, R. J. Understanding the Intersections between Metabolism and Cancer Biology. *Cell* **168**, 657-669, doi:10.1016/j.cell.2016.12.039 (2017).
175 Johnson, L. V., Walsh, M. L., Bockus, B. J. & Chen, L. B. Monitoring of relative mitochondrial membrane potential in living cells by fluorescence microscopy. *J Cell Biol* **88**, 526-535 (1981).
176 Wadhwa, R. *et al.* Selective toxicity of MKT-077 to cancer cells is mediated by its binding to the hsp70 family protein mot-2 and reactivation of p53 function. *Cancer Res* **60**, 6818-6821 (2000).
177 Rousaki, A. *et al.* Allosteric drugs: the interaction of antitumor compound MKT-077 with human Hsp70 chaperones. *J Mol Biol* **411**, 614-632, doi:10.1016/j.jmb.2011.06.003 (2011).
178 Koya, K. *et al.* MKT-077, a novel rhodacyanine dye in clinical trials, exhibits anticarcinoma activity in preclinical studies based on selective mitochondrial accumulation. *Cancer Res* **56**, 538-543 (1996).
179 Lu, W. J. *et al.* Mortalin-p53 interaction in cancer cells is stress dependent and constitutes a selective target for cancer therapy. *Cell Death Differ* **18**, 1046-1056, doi:10.1038/cdd.2010.177 (2011).
180 Yang, M. & Brackenbury, W. J. Membrane potential and cancer progression. *Front Physiol* **4**, 185, doi:10.3389/fphys.2013.00185 (2013).
181 Starenki, D. & Park, J. I. Selective Mitochondrial Uptake of MKT-077 Can Suppress Medullary Thyroid Carcinoma Cell Survival In Vitro and In Vivo. *Endocrinol Metab (Seoul)* **30**, 593-603, doi:10.3803/EnM.2015.30.4.593 (2015).
182 Guo, W. *et al.* Targeting GRP75 improves HSP90 inhibitor efficacy by enhancing p53-mediated apoptosis in hepatocellular carcinoma. *PLoS One* **9**, e85766, doi:10.1371/journal.pone.0085766 (2014).
183 Bui, N. L. *et al.* Bad phosphorylation as a target of inhibition in oncology. *Cancer Lett* **415**, 177-186, doi:10.1016/j.canlet.2017.11.017 (2018).

184 Dewson, G. & Kluck, R. M. Mechanisms by which Bak and Bax permeabilise mitochondria during apoptosis. *J Cell Sci* **122**, 2801-2808 (2009).
185 Masters, S. C. & Fu, H. 14-3-3 proteins mediate an essential anti-apoptotic signal. *J Biol Chem* **276**, 45193-45200, doi:10.1074/jbc.M105971200 (2001).
186 Bonni, A. *et al.* Cell survival promoted by the Ras-MAPK signaling pathway by transcription-dependent and -independent mechanisms. *Science* **286**, 1358-1362 (1999).
187 Virdee, K., Parone, P. A. & Tolkovsky, A. M. Phosphorylation of the pro-apoptotic protein BAD on serine 155, a novel site, contributes to cell survival. *Curr Biol* **10**, R883 (2000).
188 Datta, S. R. *et al.* Akt phosphorylation of BAD couples survival signals to the cell-intrinsic death machinery. *Cell* **91**, 231-241 (1997).
189 Lizcano, J. M., Morrice, N. & Cohen, P. Regulation of BAD by cAMP-dependent protein kinase is mediated via phosphorylation of a novel site, Ser155. *Biochem J* **349**, 547-557 (2000).
190 Datta, S. R. *et al.* 14-3-3 proteins and survival kinases cooperate to inactivate BAD by BH3 domain phosphorylation. *Mol Cell* **6**, 41-51 (2000).
191 Danial, N. N. BAD: undertaker by night, candyman by day. *Oncogene* **27 Suppl 1**, S53-70, doi:10.1038/onc.2009.44 (2008).
192 Harada, H. *et al.* Phosphorylation and inactivation of BAD by mitochondria-anchored protein kinase A. *Mol Cell* **3**, 413-422 (1999).
193 Chen, Q., Lin, R. Y. & Rubin, C. S. Organelle-specific targeting of protein kinase AII (PKAII). Molecular and in situ characterization of murine A kinase anchor proteins that recruit regulatory subunits of PKAII to the cytoplasmic surface of mitochondria. *J Biol Chem* **272**, 15247-15257 (1997).
194 Westphal, R. S., Soderling, S. H., Alto, N. M., Langeberg, L. K. & Scott, J. D. Scar/WAVE-1, a Wiskott-Aldrich syndrome protein, assembles an actin-associated multi-kinase scaffold. *EMBO J* **19**, 4589-4600, doi:10.1093/emboj/19.17.4589 (2000).
195 Affaitati, A. *et al.* Essential role of A-kinase anchor protein 121 for cAMP signaling to mitochondria. *J Biol Chem* **278**, 4286-4294, doi:10.1074/jbc.M209941200 (2003).
196 Jahani-Asl, A. & Slack, R. S. The phosphorylation state of Drp1 determines cell fate. *EMBO Rep* **8**, 912-913, doi:10.1038/sj.embor.7401077 (2007).
197 Cribbs, J. T. & Strack, S. Reversible phosphorylation of Drp1 by cyclic AMP-dependent protein kinase and calcineurin regulates mitochondrial fission and cell death. *EMBO Rep* **8**, 939-944, doi:10.1038/sj.embor.7401062 (2007).
198 Chang, C. R. & Blackstone, C. Cyclic AMP-dependent protein kinase phosphorylation of Drp1 regulates its GTPase activity and mitochondrial morphology. *J Biol Chem* **282**, 21583-21587, doi:10.1074/jbc.C700083200 (2007).
199 Li, J. *et al.* Mitochondrial elongation-mediated glucose metabolism reprogramming is essential for tumour cell survival during energy stress. *Oncogene* **36**, 4901-4912, doi:10.1038/onc.2017.98 (2017).
200 Gomes, L. C., Di Benedetto, G. & Scorrano, L. During autophagy mitochondria elongate, are spared from degradation and sustain cell viability. *Nat Cell Biol* **13**, 589-598, doi:10.1038/ncb2220 (2011).
201 Merrill, R. A. *et al.* Mechanism of neuroprotective mitochondrial remodeling by PKA/AKAP1. *PLoS Biol* **9**, e1000612, doi:10.1371/journal.pbio.1000612 (2011).
202 Martinou, J. C. & Youle, R. J. Mitochondria in apoptosis: Bcl-2 family members and mitochondrial dynamics. *Dev Cell* **21**, 92-101, doi:10.1016/j.devcel.2011.06.017 (2011).
203 Pavlides, S. *et al.* The reverse Warburg effect: aerobic glycolysis in cancer associated fibroblasts and the tumor stroma. *Cell Cycle* **8**, 3984-4001, doi:10.4161/cc.8.23.10238 (2009).
204 Hoppins, S. The regulation of mitochondrial dynamics. *Curr Opin Cell Biol* **29**, 46-52, doi:10.1016/j.ceb.2014.03.005 (2014).
205 Ran, Q. *et al.* Extramitochondrial localization of mortalin/mthsp70/PBP74/GRP75. *Biochem Biophys Res Commun* **275**, 174-179, doi:10.1006/bbrc.2000.3237 (2000).
206 Wadhwa, R., Ando, H., Kawasaki, H., Taira, K. & Kaul, S. C. Targeting mortalin using conventional and RNA-helicase-coupled hammerhead ribozymes. *EMBO Rep* **4**, 595-601, doi:10.1038/sj.embor.embor855 (2003).
207 Barmore, W. & Hughes, J. Physiology, Urea Cycle. *StatPearls*. (2018).

208 Lu, L. *et al.* Aurora kinase A mediates c-Myc's oncogenic effects in hepatocellular carcinoma. *Mol Carcinog* **54**, 1467-1479, doi:10.1002/mc.22223 (2015).
209 Nilsson, J. A. *et al.* Targeting ornithine decarboxylase in Myc-induced lymphomagenesis prevents tumor formation. *Cancer Cell* **7**, 433-444, doi:10.1016/j.ccr.2005.03.036 (2005).
210 Kim, J. W., Tchernyshyov, I., Semenza, G. L. & Dang, C. V. HIF-1-mediated expression of pyruvate dehydrogenase kinase: a metabolic switch required for cellular adaptation to hypoxia. *Cell Metab* **3**, 177-185, doi:10.1016/j.cmet.2006.02.002 (2006).
211 Tsoukalas, N. *et al.* Advanced small cell lung cancer (SCLC): new challenges and new expectations. *Ann Transl Med* **6**, 145, doi:10.21037/atm.2018.03.31 (2018).
212 Elbachiri, M. *et al.* Adult-type granulosa cell tumor of the testis: report of a case and review of literature. *Pan Afr Med J* **26**, 198, doi:10.11604/pamj.2017.26.198.11523 (2017).
213 Kushner, B. H. *et al.* Ifosfamide, carboplatin, and etoposide for neuroblastoma: a high-dose salvage regimen and review of the literature. *Cancer* **119**, 665-671, doi:10.1002/cncr.27783 (2013).
214 Bozkaya, Y. *et al.* Effectiveness of low-dose oral etoposide treatment in patients with recurrent and platinum-resistant epithelial ovarian cancer. *J Obstet Gynaecol* **37**, 649-654, doi:10.1080/01443615.2017.1290056 (2017).
215 Anastassiadis, T., Deacon, S. W., Devarajan, K., Ma, H. & Peterson, J. R. Comprehensive assay of kinase catalytic activity reveals features of kinase inhibitor selectivity. *Nat Biotechnol* **29**, 1039-1045, doi:10.1038/nbt.2017 (2011).
216 Lou, P. H. *et al.* Mitochondrial uncouplers with an extraordinary dynamic range. *Biochem J* **407**, 129-140, doi:10.1042/BJ20070606 (2007).
217 Ran, F. A. *et al.* Genome engineering using the CRISPR-Cas9 system. *Nat Protoc* **8**, 2281-2308, doi:10.1038/nprot.2013.143 (2013).
218 Dunham, W. H., Mullin, M. & Gingras, A. C. Affinity-purification coupled to mass spectrometry: basic principles and strategies. *Proteomics* **12**, 1576-1590, doi:10.1002/pmic.201100523 (2012).
219 Whiting, J. L. *et al.* Protein Kinase A Opposes the Phosphorylation-dependent Recruitment of Glycogen Synthase Kinase 3beta to A-kinase Anchoring Protein 220. *J Biol Chem* **290**, 19445-19457, doi:10.1074/jbc.M115.654822 (2015).
220 Golkowski, M., Shimizu-Albergine, M., Suh, H. W., Beavo, J. A. & Ong, S. E. Studying mechanisms of cAMP and cyclic nucleotide phosphodiesterase signaling in Leydig cell function with phosphoproteomics. *Cell Signal* **28**, 764-778, doi:10.1016/j.cellsig.2015.11.014 (2016).
221 Villen, J. & Gygi, S. P. The SCX/IMAC enrichment approach for global phosphorylation analysis by mass spectrometry. *Nat Protoc* **3**, 1630-1638, doi:10.1038/nprot.2008.150 (2008).
222 Ficarro, S. B. *et al.* Magnetic bead processor for rapid evaluation and optimization of parameters for phosphopeptide enrichment. *Anal Chem* **81**, 4566-4575, doi:10.1021/ac9004452 (2009).
223 Rappsilber, J., Mann, M. & Ishihama, Y. Protocol for micro-purification, enrichment, pre-fractionation and storage of peptides for proteomics using StageTips. *Nat Protoc* **2**, 1896-1906, doi:10.1038/nprot.2007.261 (2007).
224 Golkowski, M. *et al.* Kinobead and Single-Shot LC-MS Profiling Identifies Selective PKD Inhibitors. *J Proteome Res* **16**, 1216-1227, doi:10.1021/acs.jproteome.6b00817 (2017).
225 Cox, J. *et al.* Andromeda: a peptide search engine integrated into the MaxQuant environment. *J Proteome Res* **10**, 1794-1805, doi:10.1021/pr101065j (2011).
226 Tyanova, S. *et al.* The Perseus computational platform for comprehensive analysis of (prote)omics data. *Nat Methods* **13**, 731-740, doi:10.1038/nmeth.3901 (2016).

Vita

Rigney Elizabeth Turnham was born and raised in Edgewood, New Mexico. After graduating high school, she attended New Mexico State University where she earned a Bachelor of Science in Biochemistry. During her undergraduate degree, Rigney worked in the laboratory of Dr. Avis James and Dr. William Boecklen at New Mexico State University researching *Wolbachia* infections in *D. simulans*. A summer internship with Dr. Andrew J. McCammon in the Department of Pharmacology at the University of California, San Diego set her off on a career path focused on drug discovery and disease. In 2012, she joined the University of Washington Department of Pharmacology as a graduate research associate, and earned a Doctor of Philosophy in 2018.